

**THE ASSESSMENT OF HYDROFLUOROCARBONS AS NOVEL MEDIA
FOR SUPERCRITICAL PROCESSING**

Thesis submitted for the degree of
Doctor of Philosophy
at the University of Leicester

by

Christopher Alan Eardley B.Sc. (Leicester)
Department of Chemistry
University of Leicester

August 1999

UMI Number: U536566

All rights reserved

INFORMATION TO ALL USERS

The quality of this reproduction is dependent upon the quality of the copy submitted.

In the unlikely event that the author did not send a complete manuscript and there are missing pages, these will be noted. Also, if material had to be removed, a note will indicate the deletion.



UMI U536566

Published by ProQuest LLC 2013. Copyright in the Dissertation held by the Author.
Microform Edition © ProQuest LLC.

All rights reserved. This work is protected against
unauthorized copying under Title 17, United States Code.



ProQuest LLC
789 East Eisenhower Parkway
P.O. Box 1346
Ann Arbor, MI 48106-1346

THE ASSESSMENT OF HYDROFLUOROCARBONS AS NOVEL MEDIA FOR SUPERCRITICAL PROCESSING

CHRISTOPHER ALAN EARDLEY
UNIVERSITY OF LEICESTER
1999

ABSTRACT

The solvent properties of 1,1,1,2-tetrafluoroethane (HFC 134a), difluoromethane (HFC 32) and pentafluoroethane (HFC 125) are measured in both the liquid and supercritical phases. The relative permittivity, ϵ , of these fluids is presented as a function of pressure and temperature, and is fitted to the reduced density using the function $(\epsilon - 1)/(2\epsilon + 1)$. The dipole moments of the hydrofluorocarbons in the condensed phase are calculated. The dipolarity/polarizability parameter, π^* , is also reported as a function of temperature and pressure for the three hydrofluorocarbons. The change in dipolarity/polarizability with reduced density is explained in terms of local density augmentation in the supercritical phase. A mean sphere approximation model (MSA) is applied to the π^* data and is found to produce an excellent fit for each liquid and supercritical solvent.

The electrical conductivity of a tetrabutylammonium tetrafluoroborate electrolyte in both liquid HFC 134a and liquid and supercritical HFC 32 is reported as a function of pressure. The relative permittivity of the solvent is found to be the major factor affecting the conductivity, through its effect on ion association. The unprecedented wide potential window of HFC 134a is demonstrated and utilized in a variety of novel oxidation processes. Voltammetry is used to study the oxidation of ferrocene at a platinum microelectrode surface in both liquid and supercritical HFC 32. Deviations from Nernstian behaviour are observed in the supercritical phase at pressures close to that of the critical point. These deviations are ascribed to a change in the electrical double layer structure, as confirmed by double layer capacitance measurements.

The electroreduction of carbon dioxide in supercritical CO₂/HFC 134a mixtures is studied at both platinum and lead electrodes. It is demonstrated that oxalate can be produced at a platinum electrode at higher yields than commonly observed in liquid media.

Acknowledgements

My initial thanks go to my supervisor, Dr. Andrew Abbott. His never-ending optimism and support have served as an inspiration over three years of highly enjoyable postgraduate research.

I would also like to express my gratitude to Gill Lonergan, otherwise known as unofficial councilor to the students of R33. I am also most grateful to Keith Wilkinson and John Weale, who always found time to promptly repair high pressure apparatus under even the most severely undermanned working conditions. Thanks also go to Roy Batchen, Gerry Butler and Mick Lee, if not just for their unique sense of humour.

Special thanks go to my father, Alan, and my grandparents, Gwen and Harry, who have provided both moral and financial support throughout my university education. My final thanks are reserved for my fiancée, Britte. For her unrivalled source of encouragement and stability I owe her dearly.

'What is research, but a blind date with knowledge.'

William Henry

CONTENTS

CHAPTER I INTRODUCTION	1
1.1 Introduction	2
1.2 Supercritical Fluids	2
1.3 Electrochemistry in Supercritical Media	11
1.4 Solvent Potential Windows	16
1.5 References	20
CHAPTER II EXPERIMENTAL	27
2.1 Materials	28
2.1.1 Solvents	28
2.1.2 Electrolytes	28
2.1.3 Electroactive Species	28
2.2 Instrumentation	29
2.2.1 High Pressure Apparatus	29
2.2.2 Solvatochromic Shift Measurement	31
2.2.3 High Pressure Bulk Electrolysis	31
2.3 Electrochemical Methods	34
2.3.1 Voltammetry	34
2.3.2 Microelectrodes	34
2.3.3 Relative Permittivity Measurements	37
2.3.4 Double Layer Capacitance Measurements	38
2.3.5 Conductivity Measurements	38
2.4 References	41
CHAPTER III THE SOLVENT PROPERTIES OF LIQUID AND SUPERCRITICAL HYDROFLUOROCARBONS	42
3.1 Introduction	43
3.1.1 Relative Permittivity	43
3.1.2 Solvatochromism and the π^* Scale of Solvent Dipolarity/Polarizability	45
3.1.3 Solvation in Supercritical Fluids	49
3.2 Results and Discussion	58
3.2.1 The Relative Permittivity of Liquid and Supercritical Hydrofluorocarbons	58
3.2.2 Solvatochromic Shifts in Liquid and Supercritical Hydrofluorocarbons	66
3.2.3 Modelling Solvation in Supercritical Fluids through the Mean Sphere Approximation	83

3.3 Conclusions	97
3.4 References	98
CHAPTER IV ELECTROCHEMISTRY IN LIQUID AND SUPERCRITICAL HYDROFLUOROCARBONS	104
4.1 Introduction	105
4.1.1 Electrical Conductivity in Media of Low Relative Permittivity	105
4.1.2 Electrical Conductivity Measurements in Supercritical Media	108
4.1.3 The Electrical Double Layer	111
4.1.4 Measurement of the Double Layer Capacitance via AC methods	116
4.2 Results and Discussion	121
4.2.1 Electrical Conductivity of Liquid and Supercritical Hydrofluorocarbons	121
4.2.2 The Potential Windows of HFC 134a and HFC 32	141
4.2.3 Oxidation Electrochemistry at Extremely Positive Potentials	147
4.2.4 Voltammetry of Ferrocene in Liquid and Supercritical HFC 32	149
4.2.5 Double Layer Structure in Liquid and Supercritical Hydrofluorocarbons	157
4.3 Conclusion	163
4.4 References	164
CHAPTER V THE ELECTROCHEMICAL REDUCTION OF CARBON DIOXIDE IN CARBON DIOXIDE/1,1,1,2-TETRAFLUOROMETHANE	168
5.1 Introduction	169
5.1.1 The Electrochemical Reduction of Carbon Dioxide	169
5.1.2 The Mechanism of CO ₂ Electroreduction	173
5.1.3 Reduction of CO ₂ at Non-ambient Conditions	177
5.2 Results and Discussion	180
5.2.1 Voltammetric Measurements	180
5.2.2 Bulk Electrolysis in Supercritical Carbon Dioxide/1,1,1,2-Tetrafluoroethane Mixtures	184
5.3 Conclusions	188
5.4 References	189
CHAPTER VI SUMMARY AND FUTURE WORK	193
6.1 Summary	194
6.1.1 Solvent Properties	194

6.1.2 Conductivity, Electrochemistry and Double Layer Structure	195
6.1.3 Electrochemical Reduction of Carbon Dioxide	196
6.2 Future Work	197
6.2.1 Solvation in Supercritical Media	198
6.2.2 Electrochemistry and Double Layer Structure	198
6.2.3 Bulk Electrolysis of Carbon Dioxide at Supercritical Conditions	198
APPENDIX	199

CHAPTER I

INTRODUCTION

1.1 Introduction

1.2 Supercritical Fluids

1.3 Electrochemistry in Supercritical Media

1.4 Solvent Potential Windows

1.5 References

1.1 Introduction

The choice of solvent is of the utmost importance in chemical and electrochemical processes because it can affect both the mechanism and kinetics of a reaction.¹ In either application the solvent should ideally be:

- (i) sufficiently concentrated in the desired solute(s)
- (ii) highly chemically and electrochemically stable
- (iii) easy to handle
- (iv) of the optimum viscosity to allow the required mass transport
- (v) cheap
- (vi) non-toxic and acceptable environmentally

In electrochemical applications the solvent should also exhibit high conductivity upon dissolution of an appropriate supporting electrolyte.

This work assesses the suitability of a number of hydrofluorocarbons (HFCs) as solvents for use in supercritical processing. In particular, the solvent properties of supercritical 1,1,1,2-tetrafluoroethane (HFC 134a), difluoromethane (HFC 32) and pentafluoroethane (HFC 125) will be investigated. The feasibility of performing both chemical and electrochemical processes in these supercritical media will be addressed.

1.2 Supercritical Fluids

A substance can not form a liquid above its critical temperature, T_c .² If the temperature and pressure simultaneously exceed that of the critical point, a supercritical fluid is formed.³ Figure 1.2.1 shows a typical phase diagram, where p_c is the critical pressure of the substance.

A supercritical fluid has properties intermediate between those of a gas and a

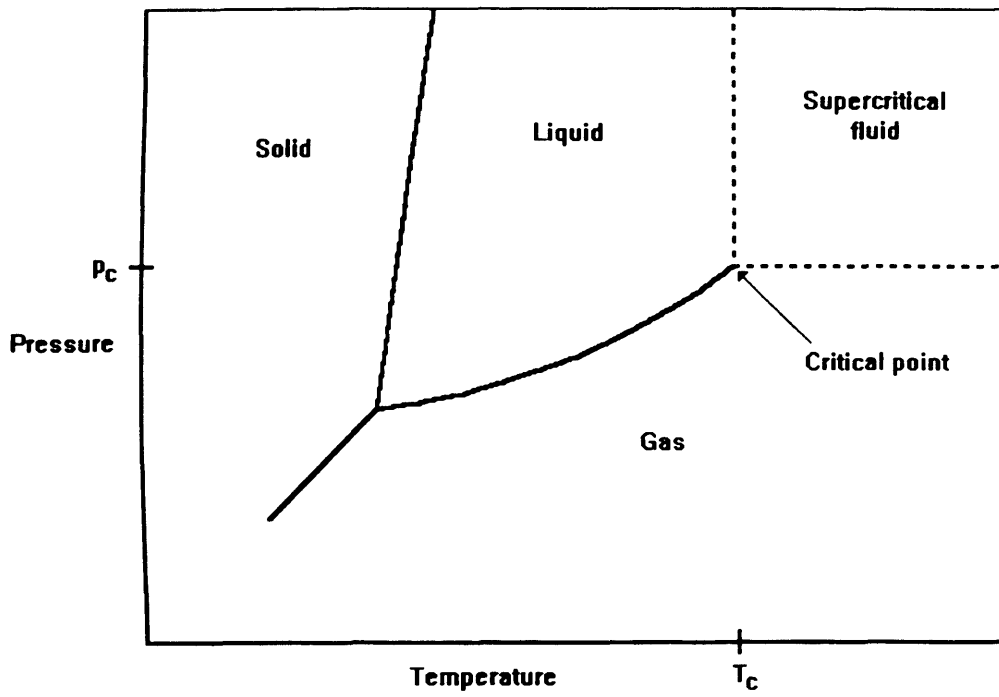


Figure 1.2.1 The phase diagram of a typical substance

liquid. Typical values of a selection of physical properties of a supercritical fluid are compared to those of a gas and liquid in table 1.2.1.⁴

	Gas	SCF	Liquid
Density/g cm ⁻³	10 ⁻³	0.1-1	1
Viscosity/g cm ⁻¹ s ⁻¹	10 ⁻⁴	10 ⁻³ -10 ⁻⁴	10 ⁻²
Diffusivity/cm ² s ⁻¹	10 ⁻¹	10 ⁻³ -10 ⁻⁴	<10 ⁻⁵

Table 1.2.1 Typical physical properties of a gas, supercritical fluid (SCF) and a liquid⁴

Over recent years, supercritical fluids have been of great interest because the fluid density is a highly tuneable function of pressure. Density-dependent solvent properties such as viscosity and relative permittivity can, therefore, be changed by up to an order of magnitude at temperatures close to that of the critical point simply by altering the pressure. With environmental legislation consistently demanding a reduction in the use of industrial toxic organic solvents, supercritical media are expected to be increasingly used as replacements for solvents such as the chlorofluorocarbons (CFCs), aromatics and CCl₄.^{5,6}

Generally the greater the polarity of a substance, the higher its critical temperature.⁷ Water ($T_c = 374.2$ °C, $p_c = 220.5$ bar)² unfortunately has a critical temperature that makes it impractical for widespread use in industrial applications. Supercritical water (sc H₂O) has also been shown to be a highly corrosive medium.^{8,9} Supercritical CO₂ (sc CO₂; $T_c = 31.4$ °C, $p_c = 72.3$ bar),¹⁰ however, has received the

most widespread attention because it is a non-flammable and non-toxic solvent with a very accessible critical temperature.

The problem encountered with sc CO₂ and many other commonly used supercritical fluids, such as SF₆, ethane and xenon, is that the low polarity precludes the dissolution of many polar solutes. Halogenated aliphatic compounds have been investigated as an alternative supercritical solvent class because they are slightly more polar but still have readily accessible critical constants. The solvent properties have so far only been measured for a limited number of fluids^{11,12} such as CF₃H ($\epsilon_c = 3.5$; $T_c = 25.6$ °C; $p_c = 47.8$ bar) and CCl₃F ($T_c = 28.9$ °C; $p_c = 37.7$ bar).

Olsen and Tallman suggested that the hydrofluorocarbons are a particularly promising class of supercritical solvents because they can be polar and yet still exhibit relatively low critical constants.¹³ HFC 134a, HFC 32 and HFC 125 all have critical temperatures below 102 °C,^{14,16} but gaseous dipole moments larger than 1.5 D,^{17,18} as shown in table 1.2.2. These three HFCs are employed as environmentally friendly alternatives to CFC refrigerants.¹⁹⁻²² Their non-toxic and inert nature also makes them suitable for use as supercritical solvents.

Hydrofluorocarbon	Abbreviation	T_c/K	p_c/bar	$\rho_c/\text{kg m}^{-3}$	μ/D
1,1,1,2-Tetrafluoroethane	HFC 134a	374.21	40.59	511.90	2.058
Difluoromethane	HFC 32	351.26	57.82	424.00	1.987
Pentafluoroethane	HFC 125	339.33	36.29	571.30	1.563

Table 1.2.2 The critical constants and dipole moments of HFC 134a, HFC 32 and HFC 125, where ρ_c is the critical density

The unique solvent properties of supercritical fluids has led to their use in applications such as extraction, chromatography and chemical synthesis. In supercritical fluid extraction,^{5,23} the solvent properties can be tuned to maximise the solubility of the extractant. Supercritical CO₂ is used industrially to decaffeinate coffee beans.^{23,24} In this process a flow of sc CO₂ over coffee beans successfully extracts the highly soluble caffeine. As the solubility of caffeine is density dependent, a decrease in the pressure of the CO₂ carrier gas causes solute precipitation. Consequently, the largest production plants can now process coffee at a rate of over 50 million lb/yr. Prior to this process, carcinogenic CCl₄ was used to decaffeinate coffee. Tea can also be decaffeinated by a similar supercritical process.²³

Supercritical CO₂ is also used on an industrial scale in many other extraction processes, including those involving nicotine, hops and flavours.⁵ There has also been considerable interest in the development of novel supercritical fluid extraction processes, such as the extraction of cholesterol from butter and unsaturated fatty acids from fish oils.²⁵

In the 1960s it was recognised that supercritical mobile phases could be employed in chromatographic analysis.²⁶ The supercritical eluent can be tuned to yield maximum efficiency for the analysis of a specific solute. Furthermore, in supercritical fluids high molecular mass compounds can be dissolved and efficiently separated at relatively low temperatures because of the enhanced mass transport of the solute in such media.^{27,28} It was not until 1986, however, and the introduction of the first capillary supercritical chromatograph, that the full capabilities of supercritical fluid chromatography were realised.²⁹ This instrument was promoted as an alternative to gas chromatography.³⁰ Supercritical carbon dioxide, the most commonly employed

supercritical mobile phase, was shown to offer the advantage of solvating the analyte at relatively low temperatures. This is in contrast to typical mobile gas phases which do not solvate the analyte in gas chromatography. Gas chromatography also requires the vaporisation of the injected analyte, which prevents the analysis of many samples. In supercritical chromatography, compounds that are non-volatile or too thermally labile for gas chromatography can be injected. A comparison with liquid chromatography has also shown that faster analysis, lower detection limits and higher injection-to-injection reproducibility are observed with packed column supercritical fluid chromatography.^{31,32} Unfortunately the development of supercritical fluid chromatography has been hindered by the lack of information on the mobile phase. Studies have, therefore, been conducted to relate the polarities of supercritical fluids to those of common liquids,³³⁻³⁵ so that the solvent strength of the supercritical mobile phase can be assessed.

Studies of reactions at supercritical conditions over the last decade have presented researchers with unexpected rates, mechanisms and reaction products.^{7,36-41} Several factors account for the unusual reactivity in supercritical fluids. Firstly supercritical reactions are usually performed at high temperatures, where the relative rates of competing reaction steps are changed exponentially, in accordance with the Arrhenius expression¹

$$\frac{k_1}{k_2} \propto \exp\left[\frac{\Delta G_2^\ddagger - \Delta G_1^\ddagger}{RT}\right] \quad (1.2.1)$$

where k_1/k_2 is the ratio of the rate constants of the competing reactions whose activation energy barriers are ΔG_1^\ddagger and ΔG_2^\ddagger respectively, and R is the gas constant. If $\Delta G_1^\ddagger - \Delta G_2^\ddagger$ is equal to 6 kJ mol^{-1} at room temperature, then the corresponding rates of

reaction will vary by over an order of magnitude. In a supercritical system such as water ($T_c = 374.2$ °C), however, the two rates will only differ by a factor of three at the critical point.

The low viscosity of supercritical fluids (see table 1.2.1) enables diffusion controlled reactions to proceed at higher rates. Consequently, many free-radical and catalysed reactions should proceed faster, as shown by Russell *et al.* in the case of a enzyme-catalysed reaction performed in sc CO₂.⁴² In addition to enzyme-catalysed reactions, heterogeneous catalytic processes are now being performed at supercritical conditions. Examples include isomerization reactions^{43,44} and the Fischer-Tropsch synthesis.⁴⁵ Franck and co-workers demonstrated the low viscosity of sc H₂O to dramatic effect.⁴⁶ Employing a supercritical mixture of 70 % water and 30 % methane they were able to produce flames on injection of pure oxygen. Rapid diffusion is a characteristic of sc H₂O, and consequently typical diffusion flame structures were observed.

When performing reactions at supercritical conditions, the solvent properties can be tuned to give maximum product selectivity or yield. The relative permittivity, viscosity and density can all be selected by temperature and pressure adjustment. For example, the polarity of water decreases dramatically on becoming supercritical because the hydrogen-bonded structure of the liquid phase breaks down.⁴⁷ The relative permittivity of water, however, increases from a non-polar value of 2 to a more polar value of 10 following a pressure increase from 210 to 270 bar at 374 °C.⁴⁸ Thus free-radical or ionic chemistry can be performed in sc H₂O, depending on the conditions of the reaction.³⁶ If there is a change in polarity along the reaction coordinate, the relative permittivity of the solvent can also affect the reaction rate.¹ Hypothetically,

supercritical solvent tuneability implies that a multistep synthesis could be performed in one supercritical solvent at a number of different thermodynamic conditions set by the temperature and pressure.

The unique solubility effects of substances in supercritical fluids also holds important ramifications for supercritical reactions. Gases, such as H₂ and N₂, are miscible with supercritical fluids in all proportions,⁴⁹ whereas in liquids they are only sparingly soluble. In organometallic chemistry, where reactions with gases are frequently performed, the enhanced solubility of such reagents can lead to accelerated reaction rates.^{50,51} Gas miscibility in supercritical fluids has also led to the synthesis of novel organometallic compounds, including dihydrogen and dinitrogen compounds such as $\eta^5\text{-C}_5\text{H}_5\text{Mn}(\text{CO})_2(\text{H}_2)$ and $\eta^5\text{-C}_5\text{H}_5\text{Re}(\text{N}_2)_3$.^{52,53} CO₂ and Xe are primarily used as supercritical solvents in organometallic reactions. Xe is transparent to UV, visible and mid-IR radiation and is, therefore, extremely useful for *in situ* spectroscopic studies of organometallic processes.⁵²⁻⁵⁴

The solubility of a compound can also be adjusted by selection of the supercritical conditions. Supercritical water, for example, can act as a non-polar or polar solvent as shown above. At low fluid densities organic molecules are highly soluble in sc H₂O, and because O₂ is completely miscible, organic waste materials can be rapidly and almost completely oxidised (99.99 %) to benign species such as CO₂, H₂O and N₂.^{7,55} Any salts formed from the neutralisation of acids simply precipitate out of the non-polar solution. The first commercial supercritical water oxidation (SCWO) plant was introduced in 1994 in order to treat industrial wastewater,⁵⁶ and at present there are over ten pilot SCWO plants operating in Germany and the US.

The supercritical solvent can also act as a reactant. In sc CO₂, formic acid can be produced from the reaction of H₂ and CO₂ employing a ruthenium-based catalyst.^{50,57} The reaction rate for this homogeneously catalysed process is eight times greater than that for the same process in liquid tetrahydrofuran at the same conditions. Although CO₂ is relatively unreactive, sc CO₂ has also been shown to react with hex-3-yne to yield cyclic esters.⁵⁸

In addition to the chemical reactions outlined above, supercritical fluids have been successfully applied as media for Diels-Alder reactions, fuel processing, biomass utilization, polymerisation and materials synthesis. Diels-Alder reactions, in which the cycloaddition of a conjugated diene to an alkene or alkyne takes place, have been well characterised in liquid solvents. These reactions are very suitable for probing the effects of supercritical solvents on reaction kinetics because the bimolecular mechanism for the cycloaddition is independent of the fluid phase of the supporting medium.^{7,38,59,60}

In fuel processing, the conversion of heavy hydrocarbons to liquid or gaseous fuels can be achieved with the aid of supercritical solvents or reactants.⁷ For example, the pyrolysis and hydrolysis of oil shale can be achieved when using supercritical toluene or tetralin as the reaction medium.⁶¹ As a result, over 95 % of this organic carbon can be converted to oil. Coal processing is also possible,^{7,62} and commonly employs supercritical CO₂/water or toluene systems to extract and liquefy coal.

Supercritical fluids have successfully been applied as solvation media in the conversion and treatment of biomass in fields such as the delignification and pretreatment of wood,^{63,64} and the liquefaction and degradation of biomass.^{7,43}

Recent work has focused on polymerisation reactions at supercritical conditions.^{7,65-67} Addition polymerisation reactions typically exhibit a negative intrinsic activation volume and so are favoured at high pressure. The solubility of a polymer of a specific molecular weight can be controlled by tuning the supercritical solvent properties, enabling the selection of the molecular weight distribution by changes in the operating temperature and pressure. The synthesis of low-density polyethylene remains the most successful supercritical polymerisation, where supercritical ethylene is employed at pressures as high as 2760 bar.⁷

Supercritical conditions can also be employed in the synthesis of non-polymeric substances, such as fine metal oxide powders.⁶⁸⁻⁷¹ The synthesis of Fe₂O₃, ZrO₂ or TiO₂ in sc H₂O, for example,^{70,71} is an attractive alternative to the sol-gel process because particle morphology and size can be fine tuned by the adjustment of temperature and pressure.

1.3 Electrochemistry in Supercritical Media

The unique properties of supercritical fluids inspired several research groups to investigate their applicability as solvents for electrosynthesis in the early 1980s. Electrochemical studies had been previously performed in sc H₂O, but these investigations concentrated on the corrosion of metals.^{8,9,72,73} It was recognised that the low viscosity of supercritical media could lead to enhanced rates of mass transport of an electroactive species to and from the electrode surface. The rates of many electrochemical processes are limited by mass transport, implying that electrosynthesis in supercritical media could lead to increased production efficiency.

In 1981, Silvestri and co-workers performed the first synthetic electrochemical investigations in supercritical solvents, studying media such as supercritical ammonia (sc NH₃; $T_c = 132.5\text{ °C}$; $p_c = 112.8\text{ bar}$) and sc CO₂.⁷⁴ Employing the relatively polar medium, sc NH₃, they were able to achieve the anodic dissolution of silver and iron. They also showed supercritical bromomethane and sc CO₂ to be poor solvents for electrochemistry because of their low conductivity.

Bard and co-workers have performed the most extensive investigation into electrochemistry in supercritical fluids. Employing mainly polar supercritical solvents, such as acetonitrile ($T_c = 274.7\text{ °C}$; $p_c = 48.3\text{ bar}$), NH₃ and H₂O, the thermodynamics and kinetics of a variety of electrochemical reactions were probed in order to assess the validity of electrosynthesis in these media.⁷⁵⁻⁸⁴

Their primary investigations in sc NH₃ focused on the generation and oxidation of solvated electrons, as well as a cyclic voltammetric study of *m*-chloronitrobenzene (MCNB).⁷⁵ The quasi-reversible cyclic voltammograms observed for the reduction of MCNB deviated markedly from Nernstian behaviour⁸⁵ and were ascribed to an undefined electrode surface effect. The diffusion coefficient of MCNB in sc NH₃ was measured by chronocoulometry as a function of pressure and temperature. Mass transport was consequently shown to be enhanced under supercritical conditions.

Subsequent work in sc NH₃ investigated the reduction of nitrogen-containing aromatics and nitrobenzene.^{78,79} Reactions that are reversible in liquid NH₃ at low temperature were shown to be reversible, or near-reversible, under supercritical conditions. Analysis of the measured diffusion coefficients demonstrated that the Stokes-Einstein equation⁸⁶ can be applied in supercritical media. As a result, it was suggested that solvation in liquid and supercritical ammonia is very similar.

Supercritical electrochemistry, however, allows the manipulation of solvent density, viscosity and relative permittivity.

In 1988 Crooks and Bard investigated the dimerization of quinoline and acridine radical anions and dianions in both liquid and sc NH_3 .⁷⁹ A dimerization reaction was selected as it was expected to be sensitive to changes in density and relative permittivity, properties that can be easily tuned in a supercritical fluid. It was shown that no dramatic change in either reaction rate or products occurred when the critical temperature of the solvent was exceeded. This study demonstrated, therefore, that the tuneable properties of the supercritical state can be selected without additional complication.

Supercritical CO_2 has received widespread interest as an electrochemical solvent because of its low critical temperature and cost. Wightman and co-workers studied the voltammetric oxidation of ferrocene in sc CO_2 using microelectrodes.^{87,88} They found the electrolyte tetrahexylammonium hexafluorophosphate to be insoluble in pure sc CO_2 . On addition of water, however, the conductivity of the solution increased to such an extent that the medium was able to support electrochemistry. It was then discovered that a two-phase system had occurred, with CO_2 and ferrocene in the upper phase and the tetrahexylammonium hexafluorophosphate molten salt with ferrocene in the lower phase. At low electrolyte concentrations, the electrode surface was shown to be coated with a conducting molten salt that allowed the oxidation of ferrocene extracted from the sc CO_2 .

Electrochemistry was attempted in pure sc CO_2 by employing microelectrodes coated with a film of poly(ethylene oxide) containing LiCF_3SO_3 .⁸⁹ Without the addition of a polar modifier, however, the voltammograms were poorly defined.

Abbott and Harper subsequently showed that hydrophobic electrolytes, such as tetrakis(decyl)ammonium tetrphenylborate, can dissolve in sc CO₂ yielding conducting media capable of supporting electrochemistry.⁹⁰ Voltammetry could, therefore, be performed at a platinum macroelectrode in an unmodified sc CO₂ solvent. Poorly defined voltammograms, obscured by electrolyte adsorption, were obtained for the charged species bis(tetradodecylammonium)nickel maleonitrile.

Supercritical water has been thoroughly investigated as an electrochemical solvent, because both organic molecules and salts display relatively high solubility in this medium.^{76,77,83,84} The problems encountered with supporting electrolyte solubility in sc CO₂ are, therefore, absent in sc H₂O. Electroorganic synthesis in this fluid is also an attractive alternative to that in toxic, expensive organic solvents. Bard and co-workers successfully applied electrochemical methods, including chronoamperometry and voltammetry, to study redox couples such as Br⁻/Br₂ and hydroquinone/benzoquinone.^{77,84} As a result, both thermodynamic and kinetic data were collected and the viability of electroorganic synthesis in sc H₂O demonstrated. The measured diffusion coefficients were generally described by the Stokes-Einstein equation. Deviations from Stokes-Einstein behaviour observed at temperatures above 375 °C were ascribed to a change in the solvated ion hydrodynamic diameter. In the case of hydroquinone, it was suggested that the hydrogen bonds between hydroquinone and water break down under these supercritical conditions.

By investigating the pressure dependence of the electrochemical half-reaction I₂/I⁻ in sc H₂O at 385 °C, Flarsheim *et al.* were able to calculate the partial molar volume change of reduction as a function of pressure.⁸³ It was consequently shown that

electrochemical methods can be used to probe the local solvent environment of an ion in a supercritical fluid.

Although it has been demonstrated that polar supercritical fluids such as water, ammonia and acetonitrile are feasible solvents for electrochemistry, they are impractical for use on a large scale. Their high critical temperatures and pressures, in addition to the highly corrosive nature of sc H₂O,⁸⁴ necessitate the investigation of viable polar alternatives.

Olsen and Tallman recently demonstrated that polar halogenated solvents can be used for electrochemical investigations in both the liquid and supercritical states.^{13,91} Their main objective was to demonstrate that electrochemical detection, without the addition of liquid polar modifiers⁹² or the utilisation of modified electrodes,^{89,93-97} can be a very sensitive analytical technique for use in supercritical fluid chromatography. Electrochemical detection is already employed in liquid chromatography because of its sensitivity and selectivity. The current observed at a microelectrode detector is directly proportional to the diffusion coefficient of the electroactive species in the case of a kinetically reversible electron transfer.⁸⁵ Hence the enhanced rates of mass transfer observed in supercritical fluids leads to improved analytical sensitivity in chromatography.

As a result, Olsen and Tallman showed that both supercritical chlorodifluoromethane (CDFM; $T_c = 96.2$ °C; $p_c = 49.7$ bar) and the slightly more polarizable solvent trifluoromethane ($T_c = 25.1$ °C; $p_c = 47.5$ bar) could be made conducting via the dissolution of tetrabutylammonium tetrafluoroborate. While the relative permittivity at the critical point of CDFM (2.31) is higher than that of CO₂ (1.18) it is still relatively modest and leads to problems of solubility, ion association

and electrolyte adsorption on the electrode surface. The studies also discovered that problems with ohmic distortion were even observed using microelectrodes in supercritical CDFM.

Several fluorinated aliphatic compounds, including HFC 134a, HFC 32 and HFC 125, display similar critical constants to those of CDFM and trifluoromethane, but exhibit larger dipole moments.^{17,18} Such hydrofluorocarbon solvents are extremely promising candidates for use in supercritical electrochemistry.

1.4 Solvent Potential Windows

In electrochemistry, the nature of the solvent-electrolyte-electrode system determines the limits of potential that can be used to study an electron transfer process. This potential range, or 'window', is commonly limited by the electrochemical activity of the solvent or electrolyte. Although the most commonly used solvent in electrochemistry, water is highly electrochemically active, as shown by the standard electrode potentials for its oxidation and reduction at 298 K in table 1.4.1.⁸⁵

Half reaction	$E^{\circ}/V(\text{vs. NHE})$
$\text{H}_2\text{O} + \text{e}^- \rightarrow 1/2\text{H}_2 + \text{OH}^-$	-0.8277
$2\text{H}^+ + 1/2\text{O}_2 + 2\text{e}^- \rightarrow \text{H}_2\text{O}$	+1.229

Table 1.4.1 Half reactions for the reduction and oxidation of water at 298 K (NHE = normal hydrogen electrode)

Aqueous systems, therefore, exhibit usable potential ranges of approximately 1.5 ± 0.5 V, depending on the electrolyte and particularly the electrode material used.

In organic electrosynthesis,⁹⁸ polar organic solvents such as acetonitrile, dimethylsulphoxide and propylene carbonate are commonly employed because of their wide usable potential ranges (around 3 to 4 V)⁸⁵ and the high solubility of organic compounds. Although these solvents tend to have convenient liquid ranges, problems are encountered with dryness.

Non-polar organic solvents such as benzene, anisole, toluene, xylene and naphthalene can be employed in electrochemistry without interference from the problems associated with adventitious water. More importantly this class of aromatic and polyaromatic solvents are extremely inert. As a result they display potential windows around 4 V, and in many cases this range is limited by the stability of the supporting electrolyte.^{99,100} The solvent stability results from the large energy difference between the HOMO and LUMO of the molecules. The conductivity of electrolytes in such media, however, is very low because of the non-polar nature of the solvents and the resulting high degree of ionic association.^{101,102}

Further extension of the aforementioned potential limits will allow the investigation of novel electrode processes. For cathodic solution reactions the most negative potential limit is expected to be close to that of an electron in a vacuum, e_{vac}^- (approximately -4.4 V vs. NHE).¹⁰³ Solvents such as liquid helium may allow the application of more negative potentials, but are impractical for use in electrochemical investigations. The electrogeneration of solvated electrons can already be performed in solvents such as liquid ammonia,^{104,105} where the negative potential limit of -2.3 V versus the silver pseudo-reference electrode (Ag^+/Ag) at -50 °C differs from e_{vac}^- by

the free energy of solvation. Thus the practical cathodic potential limit has probably been attained. It should also be noted that although liquid ammonia has a large negative potential limit, its actual potential window extends over only approximately 3 V at most.⁸⁵

The positive potential limit for anodic reactions is attributed to either the oxidation of the electrode material or supporting electrolyte, or the formation of a solvated hole (h^+_{solv}) in the solvent. The potential of formation of the latter is close to that of the solvent cation radical.¹⁰³

The recent development of microelectrodes has permitted electrochemical studies in solvent systems that are too resistive for investigations employing macroelectrodes.¹⁰⁶⁻¹¹⁰ Microelectrodes also allow the use of low concentrations of supporting electrolyte. Pons and co-workers have shown that by employing platinum ultramicroelectrodes, with diameters as low as 0.6 μm , electrochemistry can be performed in acetonitrile without the addition of a supporting electrolyte.^{111,112} As a result, the anodic oxidation limit was extended from about +2.5 V vs. Ag^+/Ag at a macroelectrode with 0.1 M tetrabutylammonium tetrafluoroborate to approximately +3.5 V at a platinum microelectrode with no supporting electrolyte added. Hence, the oxidation of species with very high ionisation potentials was studied, including rare gases and oxygen. The electro-oxidation of such substances occurred around 4-4.5 V vs. Ag^+/Ag . Unfortunately, the reported oxidation potentials are higher than the anodic potential limit of the solvent. It was postulated that at very high potentials the platinum electrode is passivated by a polymeric surface film following the oxidation of acetonitrile. It was suggested that although this film prevents the bulk electrolysis of

the solvent, it is permeable to small molecules such as Xe and O₂ investigated in their work.

Bard and co-workers also used microelectrodes to extend the anodic potential limit of the electrochemical system. Employing liquid SO₂ as the solvent at -70 °C, a range of electrode processes were studied at highly positive potentials.¹¹³⁻¹¹⁸ Using tetrabutylammonium hexafluoroarsenate as the supporting electrolyte, an anodic potential limit of +4.0 V vs. Ag⁺/Ag was achieved. Hence, species such as the ferrocinium cation¹¹⁴ and aliphatic hydrocarbons¹¹⁵ could be oxidised in this electrochemical system.

Unfortunately the cathodic potential limit for liquid SO₂ under such conditions is only -0.7 V vs. Ag⁺/Ag, leading to a potential window of 4.7 V. It is hoped that the discovery of novel inert solvent/electrolyte systems can provide an extension to both the anodic potential limit and usable potential range of liquid SO₂. This work will study the electrochemical stability of HFC fluids and their applicability to oxidation processes that require extremely positive potentials.

1.5 References

- 1) Laidler, K. J. *Chemical kinetics*, 3rd ed.; HarperCollinsPublishers: New York, 1987.
- 2) Reid, R. C.; Prausnitz, J. M.; Poling, B. E. *The Properties of Gases and Liquids*, 4th ed.; McGraw-Hill: New York, 1987.
- 3) Stanley, H. E. *Phase Transitions and Critical Phenomena*; Clarendon Press: Oxford, 1987.
- 4) van Wasen, U.; Swaid, I., Schneider, G. M. *Angew. Chem. Int. Ed. Engl.* **1980**, *19*, 575.
- 5) Taylor, L. T. *Supercritical Fluid Extraction*; John Wiley & Son: New York, 1996.
- 6) Johnston, K. P. *Nature*. **1994**, *368*, 187.
- 7) Savage, P. E.; Gopalan, S.; Mizan, T. I.; Martino, C. J.; Brock, E. E. *AIChE J.* **1995**, *41*, 1723.
- 8) Berry, W. E. *Int. Corros. Conf. Ser.* **1976**, *NACE-4*, 48.
- 9) Vermilyea, D. A.; Indig, M. E. *J. Electrochem. Soc.* **1972**, *119*, 39.
- 10) Gouw, T.; Jentoft, R. J. *J. Chromatogr. Sci.* **1986**, *68*, 303.
- 11) Yonker, C. R.; Frye, S. L.; Kalkwarf, D. R.; Smith, R. D. *J. Phys. Chem.* **1986**, *90*, 3022.
- 12) Kajimoto, O.; Futakami, M.; Kobayashi, T.; Yamasaki, K. *J. Phys. Chem.* **1988**, *92*, 1347.
- 13) Olsen, S. A.; Tallman, D. E. *Anal. Chem.* **1996**, *68*, 2054.
- 14) Tillner-Roth, R.; Baehr, H. D. *J. Phys. Chem. Ref. Data.* **1994**, *23*, 657.
- 15) Outcalt, S. L.; McLinden, M. O. *Int. J. Thermophys.* **1995**, *16*, 79.
- 16) Tillner-Roth, R.; Yokozeki, A. *J. Phys. Chem. Ref. Data.* **1997**, *26*, 1273.

- 17) Meyer, C. W.; Morrison, G. J. *Chem. Eng. Data.* **1991**, *36*, 409.
- 18) Meyer, C. W.; Morrison, G. J. *Phys. Chem.* **1991**, *95*, 3860.
- 19) Preisegger, E.; Henrici, R. *Int. J. Refrig.* **1992**, *15*, 326.
- 20) Pannock, J.; Didion, D. A.; Radermacher, R. *Proc. Int. Refrig. Conf. Energy Effic. New Refrig. Purdue University.* **1992**, 25.
- 21) Shiflett, M. B.; Yokoseki, A.; Bivens, D. B. *Proc. Int. Refrig. Conf. Energy Effic. New Refrig. Purdue University.* **1992**, 35.
- 22) Kuijpers, L.; Miner, S. M. *Status of CFCs-Refrigeration Systems and Refrigerant Properties*; IIR: Paris, **1988**, 291.
- 23) McHugh, M.; Krukoni, V. J. *Supercritical Fluid Extraction*, 2nd ed.; Butterworth-Heinemann: Boston, 1994.
- 24) Katz, S. N.; Spence, J. E.; O'Brien, M. J.; Skiff, R. H.; Vogel, G. J.; Prasad, R. *Method for Decaffeinating Coffee with a Supercritical Fluid*, U.S. Patent 4911537, 1990.
- 25) Krukoni, V. J. *ACS Symp. Ser.* **1988**, *366*, 30.
- 26) Klesper, E.; Corwin, A. H.; Turner, D. A. *J. Org. Chem.* **1962**, *27*, 700.
- 27) Conaway, J. E.; Graham, J. A.; Rogers, L. B. *J. Chromatogr. Sci.* **1978**, *16*, 102.
- 28) Smith, R. M. *Supercritical Fluid Chromatography*; Royal Society of Chemistry: London, 1988.
- 29) McNally, M. E.; Bright, F. V. *ACS Symp. Ser.* **1992**, *488*, 1.
- 30) Berry, V. *LC-GC Mag. Liq. Gas Chromatogr.* **1986**, *4*, 471.
- 31) Wheeler, J. R.; McNally, M. E. *J. Chromatogr.* **1987**, *410*, 343.
- 32) Schwartz, H. E.; *LC-GC Mag. Liq. Gas Chromatogr.* **1987**, *5*, 14.
- 33) Levy, J. M.; Ritchey, W. M. *J. Chromatogr. Sci.* **1986**, *24*, 242.

- 34) Levy, J. M.; Ritchey, W. M. *HRC & CC, J. High Res. Chromatogr. & Chromatogr. Comm.* **1987**, *10*, 493.
- 35) Deye, J. F.; Berger, T. A.; Anderson, A. G. *Anal. Chem.* **1990**, *62*, 615.
- 36) Antal, M. J., Jr.; Brittain, A.; DeAlmeida, C.; Ramayya, S.; Roy, J. C. In *Supercritical Fluids*; ACS Symposium Series 329; Squires, T. G., Paulaitis, M. E., Eds.; American Chemical Society: Washington, 1987.
- 37) Johnston, K. P.; Haynes, C. *AIChE J.* **1987**, *33*, 2017.
- 38) Paulaitis, M. E., Alexander, G. C.; *Pure Appl. Chem.* **1987**, *59*, 61.
- 39) Klein, M. T.; Mentha, Y. G.; Torry, L. A. *Ind. Eng. Chem. Res.* **1992**, *31*, 182.
- 40) Randolph, T. W.; Carlier, C. *J. Phys. Chem.* **1992**, *96*, 5146.
- 41) Jessop, P. G.; Ikariya, T.; Noyori, R. *Science* **1995**, *269*, 1065.
- 42) Russell, A. J.; Beckman, E. J. *Enzyme Microb. Technol.*, **1991**, *13*, 1007.
- 43) Subramaniam, B.; McHugh, M. A. *Ind. Eng. Chem. Process. Des. Dev.* **1986**, *25*, 1.
- 44) Saim, S., Subramaniam, B. *J. Catal.* **1991**, *131*, 445.
- 45) Fan, L.; Yokota, K.; Fujimoto, K. *AIChE J.* **1992**, *38*, 1639.
- 46) Schilling, W.; Franck, E. U. *Ber. Bunsenges. Phys. Chem.* **1988**, *92*, 631.
- 47) Buback, M.; Crerar, D.; Koplitz, L. M. In Ulmer, G.; Barnes, H., Eds. *Hydrothermal Experimental Techniques*; Wiley: New York, 1987.
- 48) Haar, L.; Gallagher, J. S.; Kell, G. S. *NBS/NRC Steam Tables*; Hemisphere: Washington, DC, 1984.
- 49) Tsang, C. Y.; Streett, W. B. *Chem. Eng. Sci.* **1981**, *36*, 993.
- 50) Jessop, P. G.; Ikariya, T.; Noyori, R. *Nature.* **1994**, *368*, 231.
- 51) Rathke, J. W.; Klinger, R. J.; Krause, T. R. *Organometallics*, **1991**, *10*, 1350.

- 52) Howdle, S. M.; Poliakoff, M. *J. Chem. Soc., Chem. Comm.* **1989**, 1099.
- 53) Howdle, S. M.; Grebenik, P.; Perutz, R. N.; Poliakoff, M. *J. Chem. Soc., Chem. Comm.* **1989**, 1517.
- 54) Howdle, S. M.; Healey, M. A.; Poliakoff, M. *J. Am. Chem. Soc.* **1990**, *112*, 4804.
- 55) Ding, Z. Y.; Frisch, M. A.; Li, L.; Gloyna, E. F. *Ind. Eng. Chem. Res.* **1996**, *35*, 3257.
- 56) Svensson, P. *Chem. Technol. Eur.* **1995**, *2*, 16.
- 57) Jessop, P. G.; Hsiao, Y.; Ikariya, T.; Noyori, R.; *J. Am. Chem. Soc.* **1996**, *118*, 344.
- 58) Reetz, M. T.; Könen, W.; Strack, T.; *Chimia.* **1993**, *47*, 493.
- 59) Kim, S.; Johnston, K. P. *ACS Symp. Ser.* **1987**, *329*, 42.
- 60) Ikushima, Y.; Saito, N.; Arai, M. *J. Phys. Chem.* **1992**, *96*, 2293.
- 61) Funazukuri, T.; Yokoi, S.; Wakao, N. *Fuel.* **1988**, *67*, 10.
- 62) Kershaw, J. R. *J. Supercritic. Fluids.* **1989**, *2*, 35.
- 63) Li, L.; Kiran, E. *Ind. Eng. Chem. Res.* **1988**, *27*, 1301.
- 64) Bludworth, J.; Knopf, F. C.; *J. Supercrit. Fluids.* **1993**, *6*, 249.
- 65) Scholsky, K. M. *J. Supercrit. Fluids*, **1993**, *6*, 103.
- 66) Kumar, S. K.; Suter, U. W. *Poly. Prep.* **1987**, *28*, 286.
- 67) Kiran, E.; Saraf, V. P. *J. Supercrit. Fluids.* **1990**, *3*, 198.
- 68) Pommier, C.; Chhor, K.; Bocquet J. F.; Barj, M. *Mat. Res. Bull.* **1990**, *25*, 213.
- 69) Chhor, K.; Bocquet, J. F.; Pommier, C. *Mat. Chem. Phys.* **1992**, *32*, 249.
- 70) Adschiri, T.; Kanazawa, K.; Arai, K. *J. Amer. Ceram. Soc.* **1992**, *75*, 1019.
- 71) Adschiri, T.; Kanazawa, K.; Arai, K. *J. Amer. Ceram. Soc.* **1992**, *75*, 2615.
- 72) MacDonald, D. D.; *Corrosion.* **1978**. *34*, 75.
- 73) MacDonald, D. D.; Scott, A. C.; Wentreck, P. *J. Electrochem. Soc.* **1981**, *128*, 250.

- 74) Silvestri, G.; Gambino, S.; Filardo, G.; Cuccia, C.; Guarino, E. *Angew. Chem. Int. Ed. Eng.* **1981**, *20*, 101.
- 75) Crooks, R. M.; Fan, F. F.; Bard, A. J. *J. Am. Chem. Soc.* **1984**, *106*, 6851.
- 76) McDonald, A. C.; Fan, F. F.; Bard, A. J. *J. Phys. Chem.* **1986**, *90*, 196.
- 77) Flarsheim, W. M.; Tsou, Y.; Trachtenberg, I.; Johnston, K. P.; Bard, A. J. *J. Phys. Chem.* **1986**, *90*, 3857.
- 78) Crooks, R. M.; Bard, A. J. *J. Phys. Chem.* **1987**, *91*, 1274.
- 79) Crooks, R. M.; Bard, A. J. *J. Electroanal. Chem.* **1988**, *240*, 253.
- 80) Crooks, R. M.; Bard, A. J. *J. Electroanal. Chem.* **1988**, *243*, 117.
- 81) Cabrera, C. R.; Garcia, E.; Bard, A. J. *J. Electroanal. Chem.* **1989**, *260*, 457.
- 82) Cabrera, C. R.; Bard, A. J. *J. Electroanal. Chem.* **1989**, *273*, 147.
- 83) Flarsheim, W. M.; Bard, A. J.; Johnston, K. P. *J. Phys. Chem.* **1989**, *93*, 4234.
- 84) Liu, C.; Snyder, S. R.; Bard, A. J. *J. Phys. Chem. B* **1997**, *101*, 1180.
- 85) Bard, A. J.; Faulkner, L. R. *Electrochemical Methods*; Wiley: New York, 1980.
- 86) Atkins, P. W. *Physical Chemistry*, 5th ed.; Oxford University Press: Oxford, 1994.
- 87) Philips, M. E.; Deakin, M. R.; Novotny, M. V.; Wightman, R. M. *J. Phys. Chem.* **1987**, *91*, 3934.
- 88) Niehaus, D.; Philips, M. E.; Michael, A.; Wightman, R. M. *J. Phys. Chem.* **1989**, *93*, 6232.
- 89) Sullenberger, E. F.; Michael, A. C. *Anal. Chem.* **1993**, *65*, 2304.
- 90) Abbott, A. P.; Harper, J. C.; *J. Chem. Soc., Faraday Trans.* **1996**, *92*, 3895.
- 91) Olsen, S. A.; Tallman, D. E. *Anal. Chem.* **1994**, *66*, 503.
- 92) Almquist, S. R.; Nyholm, L.; Markides, K. E. *J. Microl. Sep.* **1994**, *6*, 495.
- 93) Michael, A. C.; Wightman, R. M. *Anal. Chem.* **1989**, *61*, 270.

- 94) Michael, A. C.; Wightman, R. M. *Anal. Chem.* **1989**, *61*, 2193.
- 95) Niehaus, D. E.; Wightman, R. M.; Flowers, P. A. *Anal. Chem.* **1991**, *63*, 1728.
- 96) Sullenberger, E. F.; Michael, A. C. *Anal. Chem.* **1993**, *65*, 3417.
- 97) Sullenberger, E. F.; Dressman, S. F.; Michael, A. C. *J. Phys. Chem.* **1994**, *98*, 5347.
- 98) Hamann, C. H.; Hamnett, A.; Vielstich, W. *Electrochemistry*; Wiley-VCH: Weinheim, 1998.
- 99) Sternberg, H. W.; Markby, R. E.; Wender, I.; Mohilner, D. M.; *J. Electrochem. Soc.* **1966**, *113*, 1060.
- 100) Honda, K.; Nakabayashi, S.; Fujishima, A. *J. Electrochem. Soc.* **1980**, *111*, 391.
- 101) Heath, G. A.; Campbell, R. H.; Hefter, G. T.; McQueen, R. C. S. *J. Chem. Soc., Chem. Comm.* **1983**, 1123.
- 102) Abbott, A. P. *Chem. Soc. Rev.* **1993**, *22*, 435.
- 103) Bard, A. J. *Pure & Appl. Chem.* **1992**, *64*, 185.
- 104) Bard, A. J.; Itaya, K.; Malpas, R. E.; Teherani, T. *J. Phys. Chem.* **1980**, *84*, 1262.
- 105) Uribe, F. A.; Sharp, P. R.; Bard, A. J. *J. Electroanal. Chem.* **1983**, *152*, 173.
- 106) Lines, R.; Parker, V. D. *Acta. Chem. Scand.* **1977**, *B31*, 369.
- 107) Howell, J. O.; Wightman, R. M. *Anal. Chem.* **1984**, *56*, 524.
- 108) Howell, J. O.; Wightman, R. M. *Anal. Chem.* **1984**, *88*, 3915.
- 109) Bond, A. M.; Fleischmann, M.; Khoo, S. B.; Pons.; Robinson, J. *Indian J. Technol.* **1986**, *24*, 492.
- 110) Bond, A. M.; Mann, T. F. *Electrochim. Acta.* **1987**, *32*, 8633.
- 111) Cassidy, J.; Khoo, S. B.; Pons, S.; Fleischmann, M. *J. Phys. Chem.* **1985**, *89*, 3933.

- 112) Dibble, T.; Bandyopadhyay, S.; Ghoroghchian, J.; Smith, J. J.; Sarfarazi, F.; Fleischmann, M.; Pons, S. *J. Phys. Chem.* **1986**, *90*, 5275.
- 113) Gaudiello, J. G.; Sharp, P. R.; Bard, A. J.; *J. Am. Chem. Soc.* **1982**, *104*, 6373.
- 114) Sharp, P. R.; Bard, A. J. *J. Inorg. Chem.* **1983**, *22*, 2689.
- 115) Garcia, E.; Kwak, J.; Bard, A. J. *J. Inorg. Chem.* **1988**, *27*, 4377.
- 116) Garcia, E.; Bard, A. J. *J. Electrochem. Soc.* **1990**, *137*, 2752.
- 117) Chlistunoff, J. B.; Bard, A. J. *J. Inorg. Chem.* **1992**, *31*, 4582.
- 118) Chlistunoff, J. B.; Bard, A. J. *J. Inorg. Chem.* **1993**, *32*, 3521.

CHAPTER II

EXPERIMENTAL

2.1 Materials

2.1.1 Solvents

2.1.2 Electrolytes

2.1.3 Electroactive Species

2.2 Instrumentation

2.2.1 High Pressure Apparatus

2.2.2 Solvatochromic Shift Measurement

2.2.3 High Pressure Bulk Electrolysis

2.3 Electrochemical Methods

2.3.1 Voltammetry

2.3.2 Microelectrodes

2.3.3 Relative Permittivity Measurements

2.3.4 Double Layer Capacitance Measurements

2.3.5 Conductivity Measurements

2.4 References

2.1 Materials

2.1.1 Solvents

The hydrofluorocarbon solvents used in this work are presented in table 2.1.1. All three were obtained from ICI Klea and used as received. All CO₂/HFC 134a mixtures (>99.9%) were prepared by ICI Klea and used without further purification.

Solvent	<i>M/g</i> mol ⁻¹	Normal b. pt./K	Purity
1,1,1,2-Tetrafluoroethane	102.03	247.08	>99.9%
Difluoromethane	52.02	221.50	>99.9%
Pentafluoroethane	120.02	225.01	>99.9%

Table 2.1.1 Physical properties¹⁻³ of the hydrofluorocarbons used in this work

2.1.2 Electrolytes

All of the electrolytes used in the present study are listed in table 2.1.2. Each electrolyte was dried *in vacuo* prior to use.

2.1.3 Electroactive Species

Ferrocene (Aldrich, 98 %), xenon (BOC) and krypton (BOC) were all used as received. Cesium (18-crown-6) tetrafluoroborate was prepared by refluxing equimolar concentrations of CsCl (Aldrich) and NaBF₄ (BDH) in triply distilled water for one hour, followed by shaking the cooled solution in dichloromethane containing

Salt	Abbreviation	Source	Purity
Tetrabutylammonium tetrafluoroborate	TBABF₄	Fluka	> 99 %
Tetrabutylammonium perchlorate	TBAClO₄	Fluka	≥ 99 %
Tetrabutylammonium hexafluorophosphate	TBAPF₆	Aldrich	98 %
Tetrabutylammonium nitrate	TBANO₃	Fluka	~ 97 %

Table 2.1.2 The tetraalkylammonium-based electrolytes used in this work

18-crown-6 (Avocado chemicals) at a concentration of $3 \times 10^{-3} \text{ mol dm}^{-3}$. The organic layer was then removed and evaporated to dryness to yield a white precipitate. This was recrystallised from ethyl acetate and dried *in vacuo*. Rubidium (18-crown-6) tetrafluoroborate was prepared by the same synthetic route, using RbCl (99.8 %, Aldrich) instead of CsCl. In both cases the product identity was confirmed using mass spectrometry.

2.2 Instrumentation

2.2.1 High Pressure Apparatus

A schematic of the high pressure apparatus is shown in figure 2.2.1. Prior to each experiment the reaction vessel was purged with the appropriate HFC gas at reduced pressure. Pressure was then applied using a model 10-600 pump (Hydraulic Engineering Corp., Los Angeles, CA), driven by compressed air. The temperature of the high pressure cell was measured using an iron/constantan thermocouple, the tip of which was in contact with the solvent close to the cell centre, and retained at a given value ($\pm 0.5 \text{ K}$) using a CAL 9900-controlled heater. The pressure was monitored

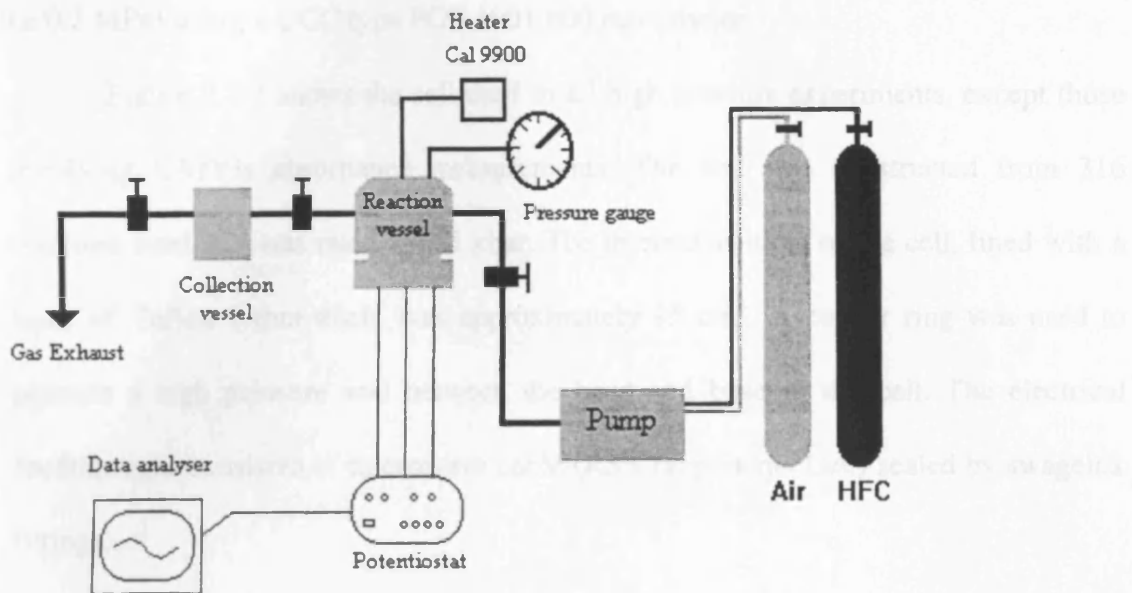


Figure 2.2.1 Schematic of the high pressure apparatus

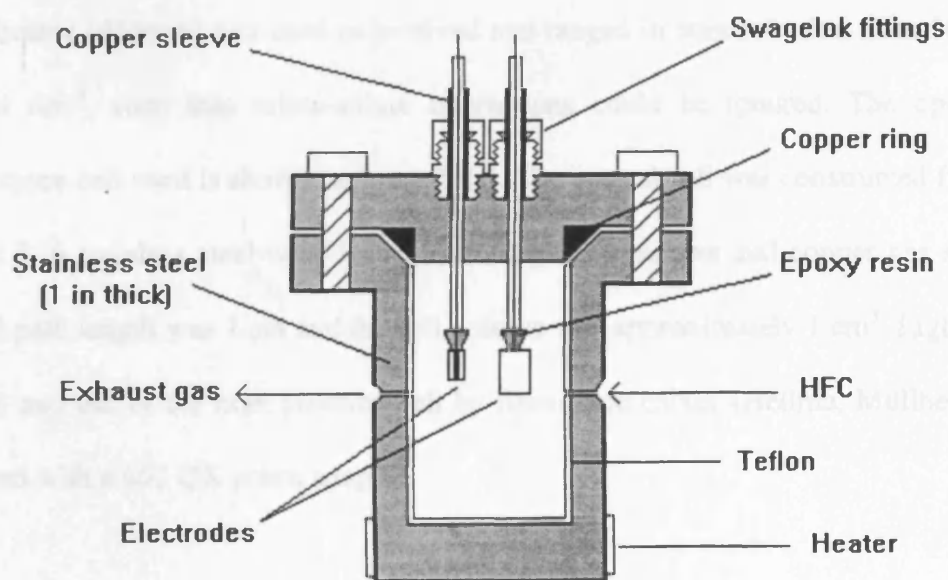


Figure 2.2.2 The high pressure cell

(± 0.2 MPa) using a UCC type PGE 1001.600 manometer.

Figure 2.2.2 shows the cell used in all high pressure experiments, except those involving UV/Vis absorbance measurements. The cell was constructed from 316 stainless steel and was rated to 1.5 kbar. The internal volume of the cell, lined with a layer of Teflon 1 mm thick, was approximately 15 cm^3 . A copper ring was used to provide a high pressure seal between the head and base of the cell. The electrical feedthroughs consisted of microwave cable (RS Components Ltd.) sealed by swagelok fittings.

2.2.2 Solvatochromic Shift Measurement

A Beckman Model DU 650 spectrophotometer was used to measure the solvatochromic shift of Nile Red in the visible absorbance spectrum. The Nile Red indicator (Aldrich) was used as received and ranged in concentration from 10^{-4} to $10^{-6} \text{ mol dm}^{-3}$, such that solute-solute interactions could be ignored. The optical high pressure cell used is shown in figure 2.2.3. The optical cell was constructed from brass and 316 stainless steel with 1 cm thick sapphire windows and copper gas seals. The cell path length was 1 cm and the cell volume was approximately 1 cm^3 . Light was fed into and out of the high pressure cell by fibre-optic cables (Hellma, Müllheim, FRG) fitted with a 662 QX prism adapter.

2.2.3 High Pressure Bulk Electrolysis

A concentric cylindrical two electrode configuration, with an electrode separation of 2 mm, was used in all bulk electrolyses. The outer stainless steel

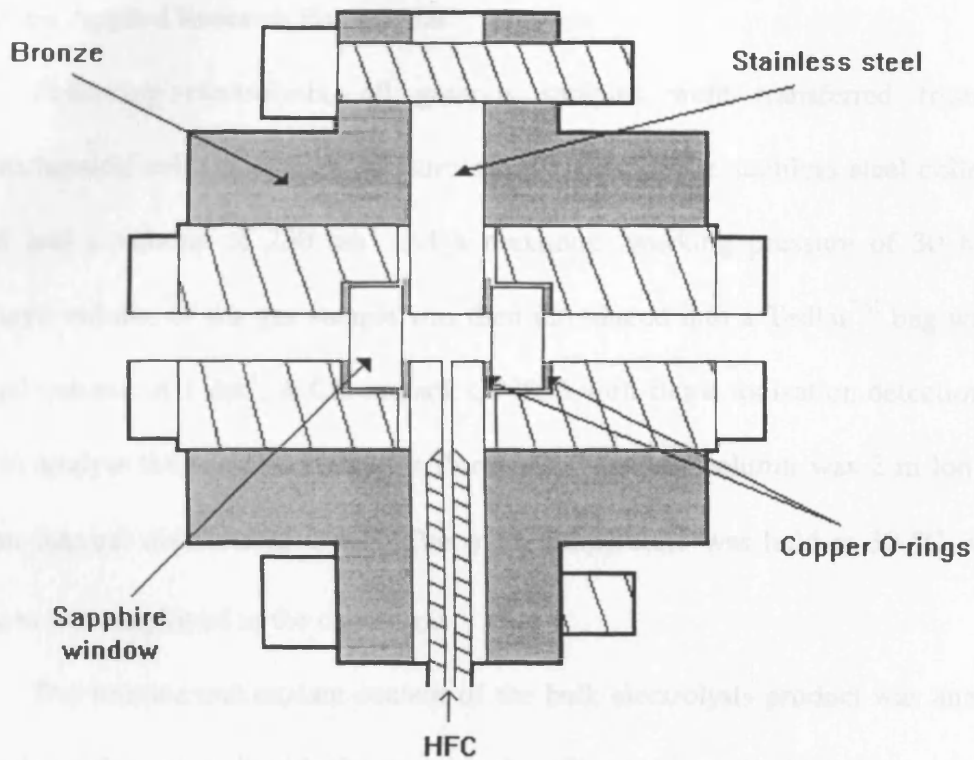


Figure 2.2.3 The high pressure optical cell

cylinder formed the anode, and was platinised by the standard technique.⁴ The inner cathodic cylinder was formed from either platinum black on stainless steel or lead. The electrode areas of the anode and cathode were 45.4 cm² and 38.6 cm² respectively. Each electrolysis was performed under potentiometric control, employing an EG & G Princeton Applied Research Potentiostat.

Following electrolysis, all gaseous samples were transferred from the electrochemical cell into a high pressure sample vessel. The stainless steel collection vessel had a volume of 250 cm³ and a maximum working pressure of 30 bar. A measured volume of the gas sample was then introduced into a TedlarTM bag with an internal volume of 1 dm³. A Chrompack CP9000 with flame ionisation detection was used to analyse the sample, where the Poropack Q-packed column was 2 m long and had an internal diameter of 4 mm. The oven temperature was held at 30 °C, whilst nitrogen was employed as the carrier gas.

The formate and oxalate content of the bulk electrolysis product was analysed by high performance liquid chromatography. The recovered electrolyte was first dissolved in 0.1 M H₂SO₄(aq) to ensure protonation of any formate and oxalate anions. Following filtration through a 20 µm glass sinter, the solutions were analysed via a Hewlett Packard 164 high performance liquid chromatograph. A Whatman Partisphere C18 reverse phase column was used to detect both formic and oxalic acids. The mobile phase consisted of 10 mM H₃PO₄(aq), where the flow rate was maintained at 1 ml min⁻¹ and the sample injection volume was 20 µl. The products were detected by UV absorbance, employing a fixed wavelength of 210 nm.

2.3 Electrochemical Methods

2.3.1 Voltammetry

All voltammetric measurements were performed with a PGSTAT 20 potentiostat (Ecochemie, Holland), computer controlled via GPES software. At high pressure the working macroelectrode was a 1 mm diameter platinum disc electrode sealed in glass and the counter electrode a platinum flag, unless stated otherwise. Each platinum working electrode was polished with both 1 μm and 0.3 μm alumina before cycling in 0.1 M sulphuric acid prior to experiment. All potentials are quoted versus a silver (Ag^+/Ag) pseudo-reference electrode. All electrical feedthrough connections were insulated with Torrseal epoxy resin (Varian).

Electrochemical investigations carried out at atmospheric pressure were performed at $-78\text{ }^\circ\text{C}$, cooled by a dry ice/acetone mixture. These solutions were thoroughly deoxygenated with nitrogen gas prior to experiment. The same three-electrode array as mentioned above was employed.

All microelectrodes utilised were 10 μm diameter platinum discs sealed in glass capillaries. In the high pressure cell, the electrical feedthrough connection to the microelectrode was first surrounded by a glass cylinder containing silicone rubber (RS Components). The glass tube was then coated with Torrseal epoxy resin to ensure the complete electrical isolation of the microelectrode tip.

2.3.2 Microelectrodes

Microelectrodes have at least one electrode dimension in the micron range by definition. As a result, the properties of these electrodes are dependent on their size. Although originally developed for *in vivo* electrochemical investigations in biological

cells,^{5,6} microelectrodes are now employed in a variety of systems. Microelectrode geometries such as discs, rings and lines have been utilised, but in the current work only microdiscs have been used. The popularity of microelectrodes can be attributed to several important properties:

- (i) Extremely low currents pass through the electrochemical cell, often in the range of a few nanoamperes. Problems encountered with ohmic distortion at macroelectrodes, therefore, can be dramatically reduced. Microelectrodes have thus been used to study poorly conducting solutions, such as media of low relative permittivity⁷⁻⁹ and solvents with little or even no added supporting electrolyte.¹⁰⁻¹² Voltammetry can also be performed in solutions with a high concentration of an electroactive species and at very high potential sweep rates as a consequence of the low ohmic drop in solution.
- (ii) Increasing the time of measurement results in a transition from linear to spherical diffusion. Consequently, at long times of measurement, a hemispherical diffusion field surrounds the microdisc electrode surface leading to improved rates of mass transport and stationary diffusion. The enhanced mass transport conditions allow the facile investigation of both fast electron transfer processes and fast coupled chemical reactions. The detection limits in electroanalytical measurements can also be improved with the utilisation of microelectrodes because of the high rates of reactant diffusion to the electrode surface.
- (iii) The extremely small surface area of a microelectrode leads to a very low interfacial capacitance. The ratio of faradaic to non-faradaic current, therefore, is much improved because of the significant reduction in double layer charging

currents. This provides a large improvement in the data acquired from short timescale transient techniques such as cyclic voltammetry at high potential sweep rates.

When kinetically reversible redox couples are studied by voltammetry at slow potential scan rates using microelectrodes, steady state voltammograms are obtained. The shape of the current-potential curve in such cases is described by equation (2.3.1)¹³

$$E = E^{o'} + \frac{RT}{nF} \ln \frac{D_R^{1/2}}{D_O^{1/2}} + \frac{RT}{nF} \ln \frac{i_d - i}{i} \quad (2.3.1)$$

where E is the applied potential, $E^{o'}$ is the formal potential, R is the gas constant ($8.3145 \text{ J K}^{-1} \text{ mol}^{-1}$), T is the temperature, n is the number of electrons transferred, F is Faraday's constant (96485 C mol^{-1}), D_R and D_O are the diffusion coefficients of the reduced and oxidised species respectively, i is the measured current and i_d is the diffusion-controlled current limit.

When $i = i_d/2$ the third term on the right hand side of equation (2.3.1) is equal to zero. At such conditions the potential is known as the half wave potential, $E_{1/2}$:

$$E_{1/2} = E^{o'} + \frac{RT}{nF} \ln \frac{D_R^{1/2}}{D_O^{1/2}} \quad (2.3.2)$$

Hence, equation (2.3.1) can be modified to

$$E = E_{1/2} + \frac{RT}{nF} \ln \frac{i_d - i}{i} \quad (2.3.3)$$

If the redox couple behaves reversibly, therefore, a plot of E versus $\log[(i_d - i)/i]$ for the voltammetric wave will yield a line with a slope equal to $2.303RT/nF$.

Following a potential step from a potential where the current is zero to a value where the electron transfer kinetics are sufficiently fast that the electrode reaction is diffusion controlled, the current at a microdisc electrode is given by equation (2.3.4)¹⁴

$$i = \frac{nFD^{1/2}c\pi^{1/2}r^2}{t^{1/2}} + 4nFDcr \quad (2.3.4)$$

where c is the concentration of the electroactive species, r is the radius of the microdisc and t is the time. At long times the second term on the right hand side of equation (2.3.4) dominates. Hence, under steady state conditions the diffusion-controlled current is given by equation (2.3.5).

$$i_d = 4nFDcr \quad (2.3.5)$$

The diffusion coefficient of an electroactive species, therefore, can easily be calculated by measurement of the diffusion-limited steady state current using voltammetry.

2.3.3 Relative Permittivity Measurements

Capacitance measurements were performed using a pair of nickel electrodes, each with an area of 7.5 cm², and with a 1 mm gap between the rectangular plates. The relative permittivity, ϵ , was measured in the capacitance cell with capacitance C_0 such that the measured capacitance was given by

$$C = \epsilon C_0 \quad (2.3.6)$$

Cell capacitances were measured at 65 kHz with a 20 mV ac voltage amplitude using a 1254 frequency response analyser and a 1286 potentiostat (both Solartron Instruments). The cell geometrical capacitance was 6.6 pF. The uncertainty of each capacitance measurement was 40 fF. The equipment was tested with several pure solvents of known ϵ , including dichloroethane, toluene and acetonitrile. In each case

the measured ϵ varied from the literature value by no more than 1 %. The relative permittivity was calculated from the average cell capacitance obtained from ten experimental runs.

2.3.4 Double Layer Capacitance Measurements

A novel electrochemical cell design was required due to the low capacitance of the electrolyte solutions in the liquid and supercritical phase. A schematic of the novel three-electrode array employed is shown in figure 2.3.1. Two rectangular stainless steel plates ($24 \times 11 \times 0.5$ mm) were held in a parallel-plate design by Teflon spacers. The separation between the two electrodes was 4 mm. Both plates were coated with a layer of platinum black, electrodeposited by the standard technique.⁴ These plates formed the working and counter electrodes of the cell. The pseudo-reference electrode was a length of silver wire run through parallel holes in the Teflon spacers. Hence, the pseudo-reference electrode was a silver grill lying centrally between the working and counter electrodes.

An ac impedance method was used to measure the capacitances, employing a 1286 potentiostat and a 1254 frequency response analyser (both Solartron Instruments) controlled by ZPLOT software. A 20 mV ac amplitude was used to record impedance spectra in the frequency range 65000 to 1 Hz. The acquired data were analysed using ZVIEW software.

2.3.5 Conductivity Measurements

The capacitance cell shown in figure 2.3.1 was also used to measure solution conductivity. An ac impedance method was applied to measure the solution resistance,

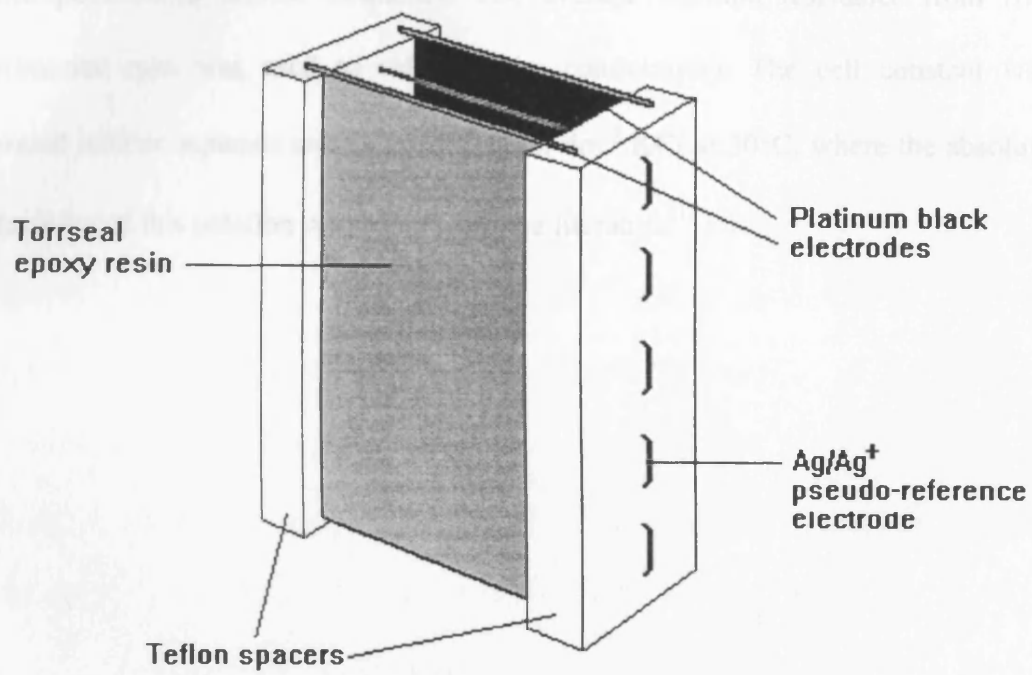


Figure 2.3.1 The double layer capacitance cell

employing a 1286 potentiostat and a 1254 frequency response analyser (both Solartron Instruments) controlled by ZPLOT software. A 20 mV ac amplitude was used to record impedance spectra in the frequency range 65000 to 1000 Hz. The acquired data were analysed using ZVIEW software. The uncompensated solution resistance was obtained by extrapolation to infinite frequency. The average solution resistance from five experimental runs was used to calculate the conductivity. The cell constant was calibrated with an aqueous solution of 0.01 mol dm⁻³ KCl at 30°C, where the absolute conductivity of this solution was taken from the literature.¹⁵

2.4 References

- 1) Tillner-Roth, R.; Baehr, H. D. *J. Phys. Chem. Ref. Data*. **1994**, *23*, 657.
- 2) Tillner-Roth, R.; Yokoseki, A. *J. Phys. Chem. Ref. Data*. **1997**, *26*, 1273.
- 3) Outcalt, S. L.; McLinden, M. O.; *Int. J. Thermophys.* **1995**, *16*, 79.
- 4) Vogel, A. I. *Textbook of Inorganic Analysis*; Longman: London, 1978.
- 5) Whaler, N. J.; Riley, J.; Nair, P. *J. Appl. Physiol.* **1967**, *23*, 798.
- 6) Ferris, C. D. *Introduction to Bioelectrodes*; Plenum Press: New York, 1974.
- 7) Lines, R.; Parker, V. D. *Acta. Chem. Scand.* **1977**, *B31*, 369.
- 8) Howell, O. J.; Wightman, R. M. *J. Phys. Chem.* **1984**, *88*, 3915.
- 9) Bond, A. M.; Mann, T. F. *Electrochim. Acta.* **1987**, *32*, 8633.
- 10) Howell, O. J.; Wightman, R. M. *Anal. Chem.* **1984**, *56*, 524.
- 11) Bond, A. M.; Fleischmann, M.; Robinson, J. J. *Electroanal. Chem.* **1984**, *168*, 299.
- 12) Cassidy, J.; Khoo, S. B.; Pons, S.; Fleischmann, M. *J. Phys. Chem.* **1985**, *89*, 3933.
- 13) Bard, A. J.; Faulkner, L. R. *Electrochemical Methods*; Wiley: New York, 1980.
- 14) Saito, Y. *Rev. Polarogr.* **1968**, *15*, 177.
- 15) Wu, Y. C.; Pratt, K. W.; Koch, W. F. *J. Soln. Chem.* **1989**, *18*, 515.

CHAPTER III

THE SOLVENT PROPERTIES OF LIQUID AND SUPERCRITICAL HYDROFLUOROCARBONS

3.1 Introduction

3.1.1 Relative Permittivity

3.1.2 Solvatochromism and the π^* Scale of Solvent Dipolarity/Polarizability

3.1.3 Solvation in Supercritical Fluids

3.2 Results and Discussion

3.2.1 The Relative Permittivity of Liquid and Supercritical Hydrofluorocarbons

3.2.2 Solvatochromic Shifts in Liquid and Supercritical Hydrofluorocarbons

3.2.3 Modelling Solvation in Supercritical Fluids through the Mean Sphere Approximation

3.3 Conclusions

3.4 References

3.1 Introduction

Before employing a solvent in either a chemical or electrochemical context, a knowledge of its macroscopic electronic properties are required. The relative permittivity is a fundamental property of the bulk solvent, essential to the quantification of solute-solvent and solute-solute interactions. On a microscopic level, solvatochromic shift data provides information on solvation in the cybotactic region of a solute molecule. Solvatochromic shift data can, therefore, be directly correlated with properties such as the free energy of a solute in a given solvent.¹⁻³ Considering that the measurement of solvatochromic shifts at high temperature and pressure can be time consuming, a model that predicts the microscopic solvent properties based on macroscopic electric properties would be particularly useful.

3.1.1 Relative Permittivity

Measurement of the relative permittivity, ϵ , of a liquid or supercritical medium is necessary if its electrical properties are to be studied and interpreted. The dependence of ϵ on temperature and density also allows the application of liquid molecular theories, permitting the calculation of molecular properties.

Consider an electronically non-conducting material, a dielectric, inbetween the plates of a parallel-plate capacitor. The measured capacitance, C , is defined as the charge stored by the capacitor, q , per unit of potential difference, V , between the plates,⁴ i.e.,

$$C = \frac{q}{V} \quad (3.1.1)$$

The relative permittivity of a medium can be measured using the capacitance ratio given in equation (2.3.6). Hence, ϵ is defined by the equation

$$\epsilon = \frac{\epsilon_m}{\epsilon_0} \quad (3.1.2)$$

where ϵ_m is the permittivity of the medium and ϵ_0 is the permittivity of free space ($8.854 \times 10^{-12} \text{ F m}^{-1}$).

In 1936, Onsager defined the local electric field in a liquid assembly of permanent dipoles.⁵ It was approximated that a point dipole occupies a spherical cavity in a dielectric continuum. The local electric field, X_{loc} , operating on the reference point dipole was shown to be equal to the field in the empty cavity, which is the sum of the external electric field, X_{ext} , and the field of the partly oriented surrounding molecules. Hence, X_{loc} was evaluated as follows

$$X_{loc} = \frac{3\epsilon}{2\epsilon + 1} X_{ext} \quad (3.1.3)$$

Kirkwood employed the definition of the Onsager local field to derive the theory of molecular polarizability.⁶ As a result, the relative permittivity of a polar liquid can be related to the apparent dipole moment μ^* through the Kirkwood equation

$$\frac{(\epsilon - 1)(2\epsilon + 1)}{9\epsilon} \left(\frac{M}{\rho} \right) = \frac{N_A}{3} \left(\alpha + \frac{\mu^{*2}}{3\epsilon_0 k_B T} \right) \quad (3.1.4)$$

where M is the relative molecular mass, ρ the liquid density, N_A the Avogadro constant, α the molecular polarizability and k_B is the Boltzmann constant. The apparent dipole moment is given by

$$\mu^* = g^{1/2} \mu \quad (3.1.5)$$

where μ is the dipole moment in the gas phase and g is the Kirkwood correlation parameter. g is a measure of the restriction to rotation caused by the cage of molecules immediately surrounding a central dipole. This parameter was defined by Kirkwood as

$$g = \frac{\mu^{*2}}{\mu^2} = 1 + \sum_{i=1}^{\infty} Z_i \langle \cos \gamma_i \rangle \quad (3.1.6)$$

where Z_i is the number of nearest neighbours to the central molecule in the i th coordination shell and $\langle \cos \gamma_i \rangle$ is the mean cosine angle, γ , formed by the dipole moments of molecules in the i th shell with the central dipole. Both g and μ^* , therefore, depend on the structure of the medium.

3.1.2 Solvatochromism and the π^* Scale of Solvent Dipolarity/Polarizability

The electronic states of a molecule each have a specific energy E and wavefunction ψ related by the Schrödinger equation⁷

$$H\psi = E\psi \quad (3.1.7)$$

where H is the Hamiltonian operator. In the case of an isolated molecule in quantum mechanics, these electronic states are relaxed states corresponding to the most stable nuclear configurations. Immediately following an electronic transition the final state, termed a Franck-Condon state, cannot be relaxed because nuclei require considerably more time (around 10^{-12} s) than electrons (approximately 10^{-16} s) to rearrange to their most stable configuration.^{8,9} Hence, the nuclear configuration in both the initial relaxed and final Franck-Condon states is unchanged.

A radiative electronic transition links the initial relaxed and the final Franck-Condon states in an absorption or emission process. If the molecule is surrounded by a medium, each electronic state is stabilised or destabilised by an amount known as the

solvation energy, E_s . This influence of the solvating medium on the electronic absorption and emission spectra of the solute molecule is defined as solvatochromism.⁸

The solvatochromic shift between two solvents is the difference in solvation energies between the final and initial states, as shown in figure 3.1.1.

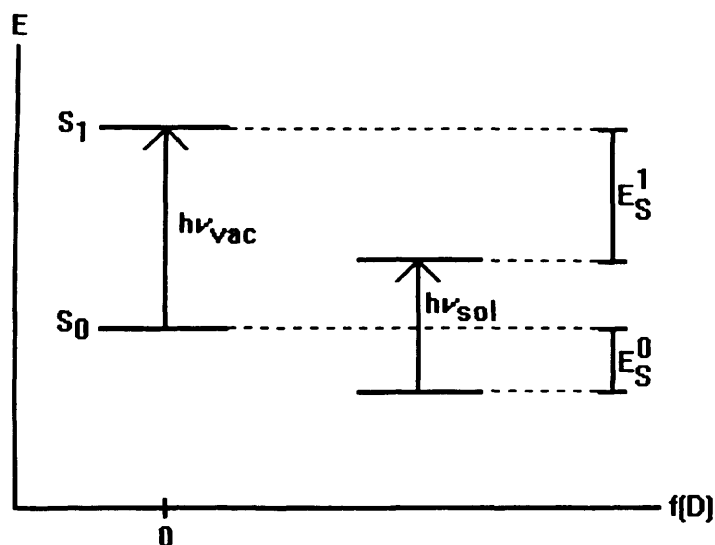


Figure 3.1.1 A solvatochromic shift energy diagram for the case of a vacuum and a solvent. E_s^0 and E_s^1 are the solvation energies of the ground and excited states respectively, and $f(D)$ is the Onsager solvent polarity function $2(\epsilon - 1)/(2\epsilon + 1)$

Consider a neutral solute molecule in a liquid solvent. The multipole moments and polarizability describe the electron distribution of each molecule. The multipole moments are a measure of the permanent intrinsic asymmetry of the electrical charges of a molecule, whereas the polarizability is a measure of the electrical charge displacement in an externally applied electric field. If the solute and solvent both have non-zero dipole moments, then both are said to be 'polar', and more specifically 'dipolar'. Combination of the two molecular properties μ and α results in four major dielectric interactions, as shown in table 3.1.1. These interactions are termed non-

specific because they do not depend on the formation of solute-solvent entities of fixed stoichiometry and geometry as observed with specific interactions such as hydrogen-bonding.

		Solute property	
		μ_M	α_M
Solvent property	μ_S	dipole-dipole	solvent Stark effect
	α_S	dipole-induced dipole	dispersion

Table 3.1.1 Non-specific dielectric interactions between a dipolar solute and a dipolar solvent

Quantitatively solvation is defined as the energy of interaction between a solute and a solvent. Theoretically,^{8,10} the solvation energy of a solute can be expressed as

$$E_{solv} = P\Pi \quad (3.1.8)$$

where P and Π represent the polarity of the solute and solvent respectively. This approach is sufficient in the case of non-specific interactions, but to compensate for the failings of this method when specific interactions occur, several empirical solvent polarity scales have been devised. Commonly employed single parameter scales are the $E_T(30)^{11-13}$ and $Z^{14,15}$ (ref) polarity scales. Such scales 'mix' the non-specific and specific interactions into a single solvent parameter. A more satisfactory approach is to

use a multi-parameter description of the solvent polarity, as in the π^* scale of solvent dipolarity/polarizability.¹⁶⁻²²

The π^* scale relies on a linear solvation energy relationship correlating solvent effects on a solute.^{18,23,24} This relationship has the general form

$$XYZ = XYZ_0 + a\alpha + b\beta + h\delta_H + SPPE \quad (3.1.9)$$

where XYZ represents a property of the system, such as a reaction rate constant or the position of an absorption maximum in an UV/vis, NMR or ESR spectrum. α is a scale of solvent hydrogen-bond donor (HBD) acidities, β is a scale of hydrogen-bond acceptor (HBA) basicities and a and b are the corresponding hydrogen-bonding constants associated with the solute. δ_H is known as the Hildebrand solubility parameter and is a measure of the solvent/solvent interactions that are interrupted in creating a cavity for the solute.^{25,26} $SPPE$ is a parameter based on the solvent polarity-polarizability effects.

Kamlet, Taft and co-workers utilised a linear solvation energy relationship to correlate the peak position of a UV/vis absorption maximum of an indicator solute in a liquid solvent with characteristic values of HBD, HBA and $SPPE$ parameters determined for various solvents.^{17,19} For UV/vis spectral data, Kamlet and Taft showed that the $SPPE$ term can be expressed by the parameter π^* , a measure of solvent dipolarity/polarizability. This parameter is so-named because it is derived from solvatochromic effects on $p \rightarrow \pi^*$ and $\pi \rightarrow \pi^*$ electronic transitions. Hence, an arbitrary π^* scale of solvent polarities has been established, in which for example, non-polar cyclohexane has a π^* value of 0.0 and dimethyl sulphoxide has a π^* value of 1.0. Substitution of the π^* parameter for the $SPPE$ term in equation (3.1.9) leads to

$$XYZ = XYZ_0 + s(\pi^* + d\delta) + a\alpha + b\beta + h\delta_H \quad (3.1.10)$$

where s is the susceptibility of XYZ to changing $SPPE$ and is a constant characteristic of the solute. δ is a polarizability correction term equal to zero for nonhalogenated aliphatics, 0.5 for halogenated aliphatics and 1.0 for aromatic solvents. When the electronic spectrum is shifted bathochromically (to lower frequencies) with increasing solvent dipolarity, d is zero and the δ term can be neglected. The π^* scale was first constructed by averaging the spectral shift data of seven indicators.¹⁶ Currently, over forty spectral indicators have been characterised,¹⁶ where most are nitro-substituted aromatics such as 2-nitroanisole.

In UV/vis absorbance spectroscopy, the ground and electronic excited states of an indicator molecule will generally occupy the same volume in accordance with the Franck-Condon principle. As a result, h is zero in such cases and the δ_H term of equation (3.1.10) can be ignored.¹⁸ If the solute-solvent hydrogen-bonding interactions are minimal and the UV/vis absorbance maximum is shifted bathochromically with increasing solvent dipolarity, equation (3.1.10) can, therefore, be reduced to

$$\nu_{max} = \nu_0 + s\pi^* \quad (3.1.11)$$

where ν_{max} is the wavenumber of maximum absorbance in the UV/vis spectrum and ν_0 is the reference wavenumber of maximum absorbance determined for a standard solvent (cyclohexane).

3.1.3 Solvation in Supercritical Fluids

The isothermal compressibility, κ_T , of a fluid is given by⁷

$$\kappa_T = -\frac{1}{V} \left(\frac{\partial V}{\partial P} \right)_T \quad (3.1.12)$$

where V is the volume and P the pressure. As the critical point of a fluid is approached from above the critical temperature along the scaling axis, the isothermal compressibility diverges (i.e., as $T \rightarrow T_c$ from above, $\kappa_T \rightarrow \infty$).^{27,28} The scaling axis is simply an extension of the gas-liquid phase boundary into the supercritical regime. In the phase diagram, therefore, there is a region with $T > T_c$ where κ_T is large, such that $\kappa_T > \kappa^0$, the compressibility of an ideal gas. This compressible region actually extends much further than the near-critical region, where all fluids behave universally as described by the theory of critical phenomena.^{27,28}

A large compressibility means that substantial changes in supercritical solvent density can easily be achieved. This is because the energetic gain and entropic loss associated with the condensation of dispersed molecules into regions of higher-than-bulk density are almost equal in this region of the phase diagram. Hence, large fluctuations in local solvent densities occur in a pure supercritical solvent, leading to regions of high and low density. At the critical point, the correlation length of these fluctuations, ξ , becomes macroscopic as two phases are formed.^{27,29} If a single solute molecule is then introduced into a supercritical solvent in the compressible regime, its microscopic environment at a particular time will be dependent on the low or high-density region in which it resides.³⁰ Thus the microscopic solvent environment immediately surrounding a solute will differ to that of the macroscopic average. In reality, however, a solute molecule will additionally modify its solvent microenvironment in a compressible supercritical fluid.³¹

In 1983, Eckert and co-workers discovered large negative partial molar volumes for naphthalene in supercritical ethylene.³² Similar partial molar volume measurements and results followed.^{33,34} Large positive partial molar volumes have

been reported for some solutes in supercritical media,³⁵ but this phenomenon is relatively uncommon. It was thus concluded by Eckert *et al.* that there was a solvent density collapse around the solute. Future refinement of this interpretation has shown that the large negative partial molar volumes are an indirect consequence of the solute-solvent interactions.^{36,37}

It is the solvent density fluctuations out to lengths of order ξ from the solute that lead to the large partial molar volumes observed in the compressible regime.^{33,36,37} Consequently, there is an increase in the ensemble average of the surrounding solvent density. These density correlations are also responsible for the regions of high and low density in the pure supercritical solvent. Hence, the partial molar volume of an infinitely dilute solute diverges at the critical point of the solvent, as does the correlation length of the density fluctuations, ξ , showing the effect to be a strictly critical phenomenon. Every infinitely dilute near-critical system exhibits divergence, but its sign is dependent on short-ranged solute-solvent interactions, occurring over distances of a few angstroms.^{31,37} As a result, the large partial molar volume effect only indirectly depends on the solute-solvent interactions.

Debenedetti and Mohamed, employing fluctuation theory, introduced a scheme for the classification of dilute near-critical solvent systems according to the sign of diverging, long-ranged quantities.³⁸ Debenedetti and Petsche³⁷ later reformulated this classification scheme in terms of the direct correlation function, c , by first recognising that

$$\rho \bar{V}_1^{\infty} = \kappa_T \delta \quad (3.1.13)$$

where ρ is the number density of the solvent and \bar{V}_1^∞ is the partial molar volume of the solute at infinite dilution. δ is the rate of change of pressure upon addition of solute in the limit of infinite dilution, such that

$$\delta = \lim_{x_1 \rightarrow 0} \left[N \left(\frac{\partial p}{\partial N_1} \right)_{T, V, N_2} \right] \quad (3.1.14)$$

where subscripts 1 and 2 represent the solute and solvent respectively, x is a mole fraction and N the mass ($N = N_1 + N_2$). From the Kirkwood-Buff fluctuation theory of solutions,³⁹ Debenedetti and Petsche showed that

$$\bar{V}_1^\infty = kT\kappa_T (I - C_{12}^\infty) \quad (3.1.15)$$

where k is the Boltzmann constant and C_{12}^∞ is the solute-solvent direct correlation function integral in the limit of infinite dilution, given by

$$C_{12}^\infty = \rho \int c_{12}^\infty(\mathbf{r}) d\mathbf{r} \quad (3.1.16)$$

where $c_{12}^\infty(\mathbf{r})$ is the solute-solvent direct correlation function at infinite dilution which describes the radial distribution of a solvent molecule around the solute as a consequence of solute-solvent direct interactions. $c_{12}^\infty(\mathbf{r})$ approximately extends over the range of the solute-solvent interaction potential and generally dictates the short-range phenomena in dilute near-critical solutions. Equation (3.1.15) shows that the sign of \bar{V}_1^∞ is determined by the value of C_{12}^∞ . Combining equations (3.1.13) and (3.1.15) gives

$$C_{12}^\infty = I - \frac{\delta}{\rho kT} \quad (3.1.17)$$

which allows the calculation of the solute-solvent direct correlation function integral. Employing a long-ranged fluctuation integral^{40,41} equation (3.1.13) can be written as

$$\rho \bar{V}_1^\infty = \rho k T \kappa_T - \Gamma \quad (3.1.18)$$

where

$$\Gamma = \rho \int (g_{12}^\infty(r) - 1) dr \quad (3.1.19)$$

Γ is the statistical excess number of solvent molecules around an infinitely dilute solute molecule as compared to a uniform distribution at bulk conditions. $g_{12}^\infty(r)$ is the unlike radial distribution function at infinite dilution. This radially averaged pair correlation function represents the probability that there will be a solvent molecule located a distance r away from the solute. At large values of r , the particles 1 and 2 become uncorrelated, $g_{12}(r) \rightarrow 1$ and the solvent has a bulk number density ρ . The function $[g_{12}(r) - 1]$ decreases exponentially as r becomes large²⁸

$$g_{12}(r) - 1 \approx \frac{1}{r} \exp\left(-\frac{r}{\xi}\right) \quad (3.1.20)$$

A combination of equation (3.1.15) and (3.1.18) yields

$$\Gamma = \rho k T \kappa_T C_{12}^\infty \quad (3.1.21)$$

Hence, Γ diverges at the critical point of the solvent, with a sign equal to that of C_{12}^∞ . It has thus been shown that C_{12}^∞ determines the solute behaviour in the near-critical regime, as displayed in table 3.1.2.

In the weakly attractive case, long-range solvent density enhancement about the solute is observed, but it is insufficient to overcome the osmotic effect associated with the introduction of solute molecules into the solvent.³⁸ That is the attractive potential associated with the solute-solvent interaction is smaller in magnitude than the solvent-solvent interaction.

Solute behaviour	C_{12}^{∞}	\bar{V}_1^{∞}	Γ
Repulsive	$C_{12}^{\infty} < 0$	$\bar{V}_1^{\infty} \rightarrow +\infty$	$\Gamma \rightarrow -\infty$
Weakly attractive	$0 \leq C_{12}^{\infty} \leq 1$	$\bar{V}_1^{\infty} \rightarrow +\infty$	$\Gamma \rightarrow +\infty$
Attractive	$C_{12}^{\infty} > 1$	$\bar{V}_1^{\infty} \rightarrow -\infty$	$\Gamma \rightarrow +\infty$

Table 3.1.2 The classification of near-critical supercritical systems^{37,38}

Subsequent to the partial molar volume measurements, many spectroscopic techniques such as infrared⁴²⁻⁴⁴ and fluorescence spectroscopy⁴⁵⁻⁴⁸ have been used to probe the local supercritical solvent environment around a dilute solute. Amongst the spectroscopic techniques utilised, the solvatochromic shift method, commonly employing the dipolarity/polarizability parameter π^* , has been used to quantify the solvent properties of supercritical fluids. The π^* parameter has been shown to increase with solvent density for a supercritical fluid^{43,49,50}. Supercritical systems studied include CO₂, N₂O, CCl₃F, NH₃, Xe, SF₆ and ethane^{51,52}.

The spectroscopic measurements have generally shown that close to the critical temperature and density, the local solvent density around the solute is higher than the actual bulk density. The effect of enhanced solvent density about the solute has been termed 'clustering' or 'local density augmentation'.⁵³ Less frequently observed is the case of depleted solvent density in the region around the solute due to repulsive solute-solvent interactions.^{35,54-57} These spectroscopically observed solvent density effects are a direct consequence of short-range solute-solvent potential interactions.^{36,58} In contrast to the indirect effects representative of critical phenomena described above,

such as the large partial molar volumes of infinitely dilute solutes, the direct effects are nondivergent as the critical point is approached. As solvation is primarily determined by the solute's microenvironment,^{36,58-60} local solvent density enhancements largely control solubility. Conversely, the indirect effects of solute-solvent interactions only weakly effect solvation because they primarily control the range of solvent density enhancement about a solute on the approach of the critical point.³¹

When considering short-range near-critical solvation phenomena, the number of solvent molecules around a solute can be described by the clustering number, N_{clus} .⁶¹ Integration of the radial distribution function $g_{12}(r)$ within the range defining the solvation shell, r_1 to r_2 , allows the estimation of N_{clus}

$$N_{clus} = 4\pi\rho \int_{r_1}^{r_2} g_{12}(r) r^2 dr = 4\pi\rho \int_{r_1}^{r_2} (1 + h_{12}(r)) r^2 dr \quad (3.1.22)$$

The contributions to N_{clus} can then be divided into two parts,

$$N_{clus}^1 = 4\pi\rho \int_{r_1}^{r_2} r^2 dr \quad (3.1.23)$$

$$N_{clus}^2 = 4\pi\rho \int_{r_1}^{r_2} h_{12}(r) r^2 dr \cong 4\pi\rho \int_{r_1}^{r_2} c_{12}(r) r^2 dr \quad (3.1.24)$$

N_{clus}^1 is simply the bulk fluid density multiplied by the volume of the solvation shell.

This contribution, therefore, increases linearly with increasing bulk density. The second contribution, N_{clus}^2 , describes the increment in the number of solvent molecules in the solvation shell as a consequence of direct solute-solvent interactions. At short distances $h_{12}(r)$ is approximately equal to the direct correlation function $c_{12}(r)$, thus allowing the substitution of $c_{12}(r)$ into equation (3.1.22). As a result, N_{clus}^2 generally reaches a maximum value around the critical density, because at higher densities solute-solvent repulsion dominates and $c_{12}(r)$ becomes negative.³⁶ Local density augmentation effects are, therefore, usually most prominent around the critical density.

As the temperature of the dilute supercritical system is increased, the effect of local density augmentation diminishes. The magnitude of the solute-solvent attractive interactions and the temperature to which high fluid compressibility persists in the supercritical medium will determine the temperature range in which local density enhancements are observed. Generally, local density enhancements are observed in the temperature range $1 \leq T_r \leq 1.04$, although cases have been reported at temperatures above $T_r = 1.10$.^{53,62-64} Local density augmentations at extremely high reduced temperatures are usually a consequence of strongly attractive solutes, such as multivalent ions in supercritical water.^{65,66}

The extent of local density augmentation in supercritical solutions is generally calculated by either computer simulation,^{67,70} integral equation formulations^{29,33,71,72} or compressible electrostatic continuum methods.⁷³⁻⁷⁶ Although computer simulation can be used to evaluate solvation energies in an infinitely dilute supercritical system, to calculate the total correlation function $g_{12}(r) - 1$ close to the critical point costly simulations on very large systems are required. The total correlation function describes the combined effects of direct and indirect solvent density enhancements.⁶¹

Under a set of approximations known as closures,²⁹ integral equation methods yield similar information to computer simulation. The validity of various closures, which are basically approximations to the correlation functions, has been assessed in near-critical fluids.^{33,71,72}

Compressible electrostatic continuum models have recently been used to compute average density inhomogeneities in supercritical solutions.⁷³⁻⁷⁶ Here the solvent is represented as a continuous dielectric medium with characteristic density-dependent compressibility and relative permittivity functions. The solute is taken to be

a charge distribution in a cavity. Here both the size and relative permittivity of the enhanced solvent density region must be known prior to calculation of the average density inhomogeneities. These models, which are numerical solutions to Poisson's equation,⁷⁷ have provided reasonable free energies of solvation and solvent density distributions for dilute supercritical fluids. The models, however, tend to predict relative rather than absolute solvation energies.⁷⁸ Nevertheless, these models are a significant improvement over incompressible continuum methods where there are two regions of solvent relative permittivity: higher-than-bulk in the region of enhanced solvent density and bulk value relative permittivity outside this region.^{79,80} Note that the compressible electrostatic continuum model evaluates density enhancements entirely from direct interactions between the continuum solvent and the potential field of the solute, hence yielding no information on the indirect effects.

In this work, relative permittivity measurements above 30 °C for liquid and supercritical HFC 134a, HFC 32 and HFC 125 are reported for the first time. As a result, the dipole moment is calculated for each HFC fluid. The dipolarity/polarizability parameter, π^* , is also reported for the above solvents as a function of temperature and pressure, to cover the liquid and supercritical states over the range 30 to 130 °C and 40 to 300 bar. Consequently, the local solvent environment of a dilute polar solute in each supercritical HFC solvent is probed. The π^* parameter and relative permittivity of these solvents are correlated through a hard sphere approximation model.

3.2 Results and Discussion

3.2.1 The Relative Permittivity of Liquid and Supercritical Hydrofluorocarbons

Figures 3.2.1, 3.2.2 and 3.2.3 show the relative permittivity, ϵ , of HFC 134a, HFC 32 and HFC 125 respectively, as a function of pressure over a range of temperatures compiled from the data given in tables 1-15 of the appendix. As stated earlier the uncertainty of each pressure measurement is ± 2 bar. For HFC 134a the uncertainty of each density is no more than $\pm 2 \text{ kg m}^{-3}$ at 303 K, rising to a maximum of $\pm 16 \text{ kg m}^{-3}$ at 403 K. HFC 32 has a density uncertainty maximum of $\pm 2 \text{ kg m}^{-3}$ at 303 K and $\pm 10 \text{ kg m}^{-3}$ at 363 K. For HFC 125 the density uncertainty is no more than $\pm 3 \text{ kg m}^{-3}$ at 303 K and $\pm 21 \text{ kg m}^{-3}$ at 353 K. The relative permittivity values were obtained with an uncertainty of $\pm 1 \%$. The HFC 134a ϵ values at 303 K measured here are slightly higher than those previously reported;⁸¹ however, the difference lies within the experimental uncertainty in ϵ ($< 1\%$ deviation). The relative permittivity increases with increasing pressure and decreases with increasing temperature in both liquid and supercritical phases for each solvent. Hence, the isothermal density dependence of the dielectric constant $(\delta\epsilon/\delta\rho)_T$ is always positive. For all solvents ϵ increases roughly linearly with applied pressure in the liquid state. Above the critical temperature the increase in ϵ is also approximately linear with pressure at high pressures (> 200 bar), but decreases more rapidly as the pressure approaches the critical value corresponding to the region of high fluid compressibility.

The relative permittivity data were fitted to the equation

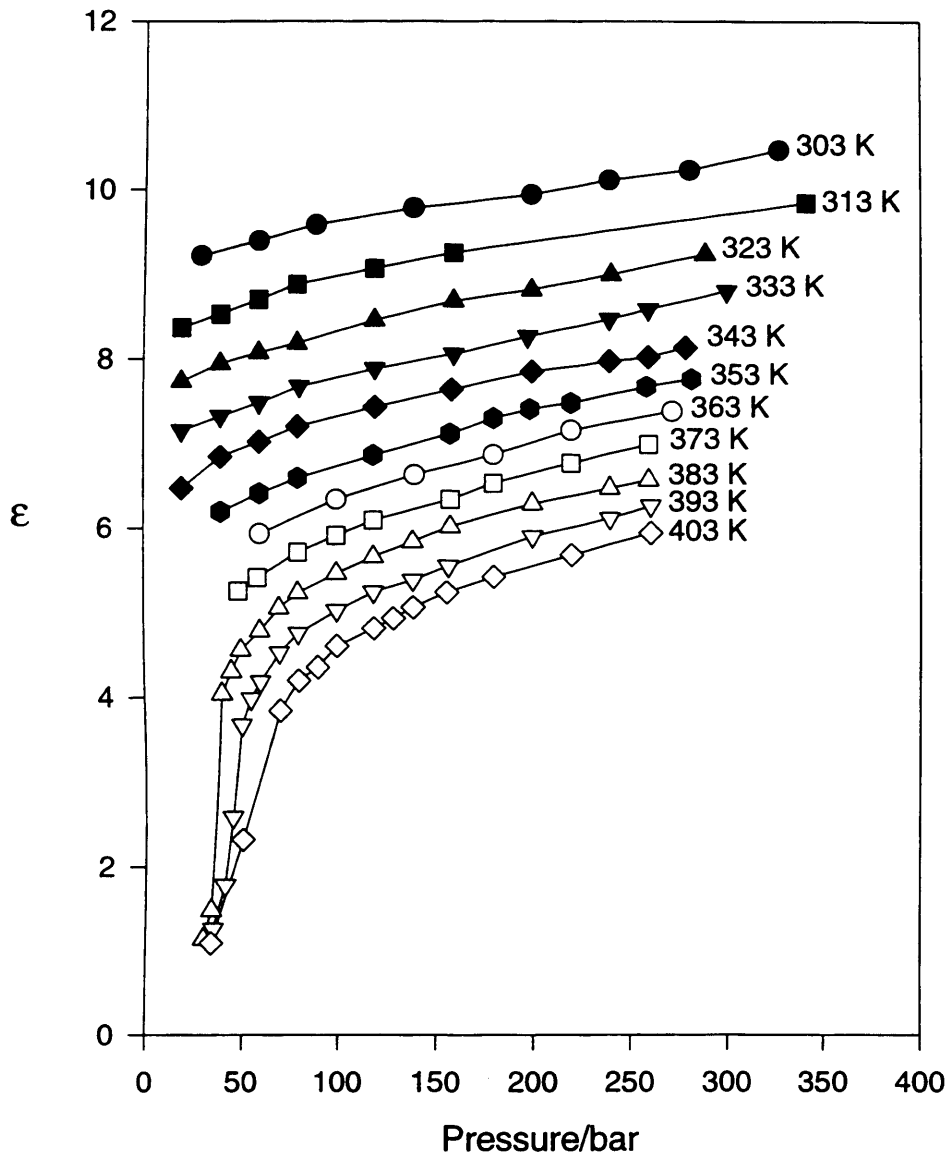


Figure 3.2.1 Pressure dependence of the relative permittivity of HFC 134a at various temperatures

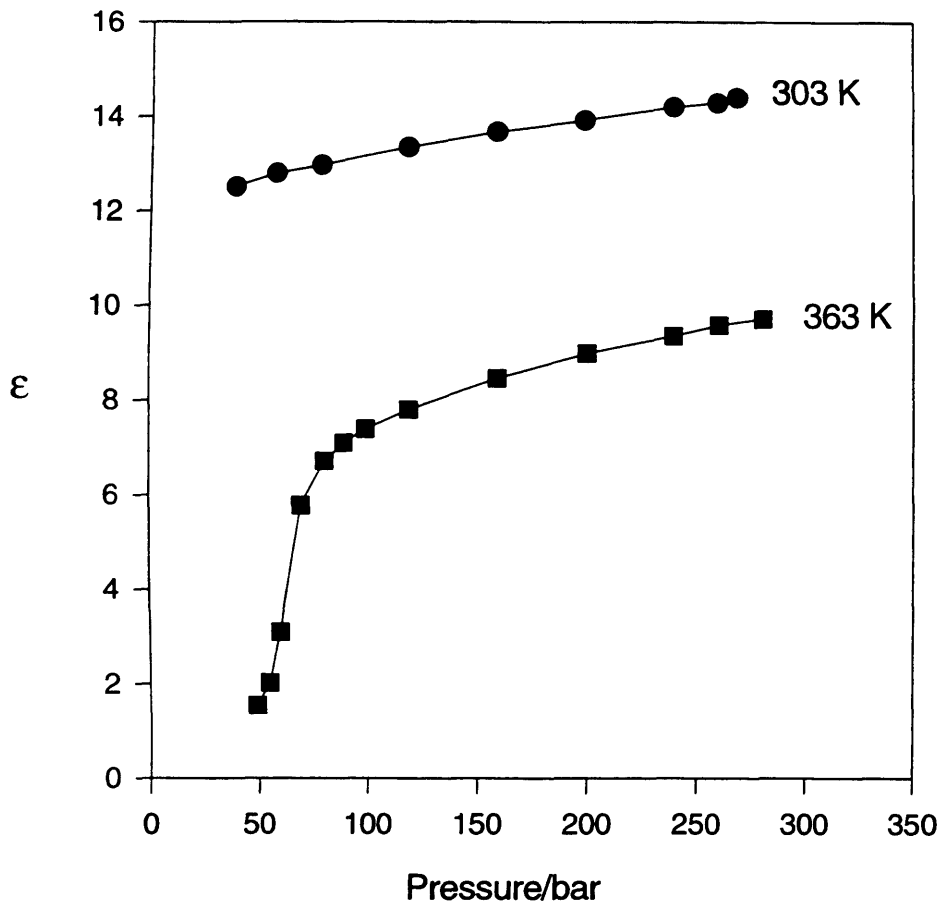


Figure 3.2.2 Pressure dependence of the relative permittivity of HFC 32 at various temperatures

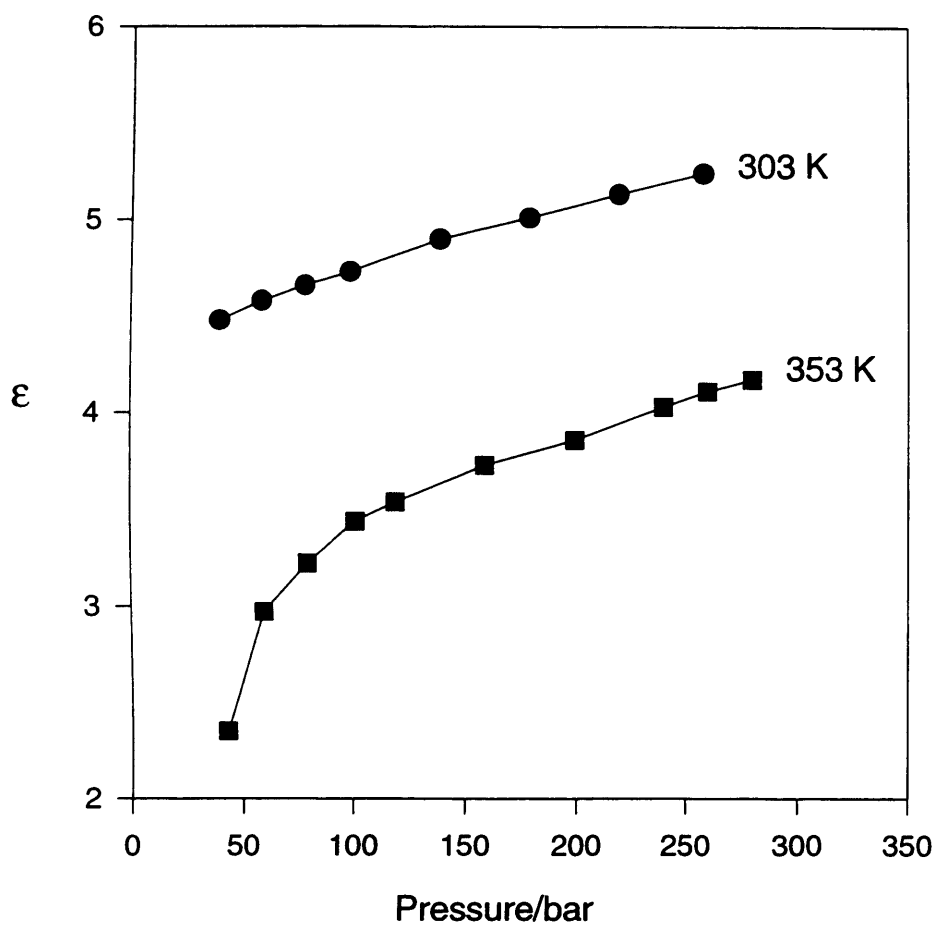


Figure 3.2.3 Pressure dependence of the relative permittivity of HFC 125 at various temperatures

$$\left[\frac{\epsilon - 1}{(2\epsilon + 1)} = A + B\rho_r \right]_T \quad (3.2.1)$$

where ρ_r is the reduced density and A and B are constants at a given temperature.

Figure 3.2.4 shows a plot of $\epsilon - 1/(2\epsilon + 1)$ against ρ_r for HFC 134a. Clearly $\epsilon - 1/(2\epsilon + 1)$ is linearly related to the isothermal reduced density. Figures 3.2.5 and 3.2.6 show that the constants of proportionality vary linearly with temperature and fit well to the equations

$$A = 0.471 - (5.1 \times 10^{-4} T) \quad (r = 0.964) \quad (3.2.2)$$

$$B = 9.5 \times 10^{-4} + (1.5 \times 10^{-4} T) \quad (r = 0.970) \quad (3.2.3)$$

where T is the temperature in Kelvin. Equation (3.2.1) also holds for HFC 32 and HFC 125, with the appropriate constants given in table 3.2.1.

	HFC 32	HFC 125
A	0.541 - (5.6 × 10⁻⁴T)	0.392 - (6.5 × 10⁻⁴T)
B	2.0 × 10⁻⁴T - 0.0303	0.0151 + (1.9 × 10⁻⁴T)

Table 3.2.1 A and B values for HFC 32 and HFC 125, where T is the temperature in K

Kirkwood's theory of molecular polarizability,⁶ employing the definition of the Onsager local field in a liquid assembly of permanent dipoles,⁵ is assumed the most appropriate for the three HFCs studied. The relative permittivity of a polar liquid can be related to the apparent dipole moment μ^* through equation (3.1.4).

By performing a linear regression of the Kirkwood function as a function of $1/T$, the value of μ^* can be determined. For each fluid and temperature the Kirkwood

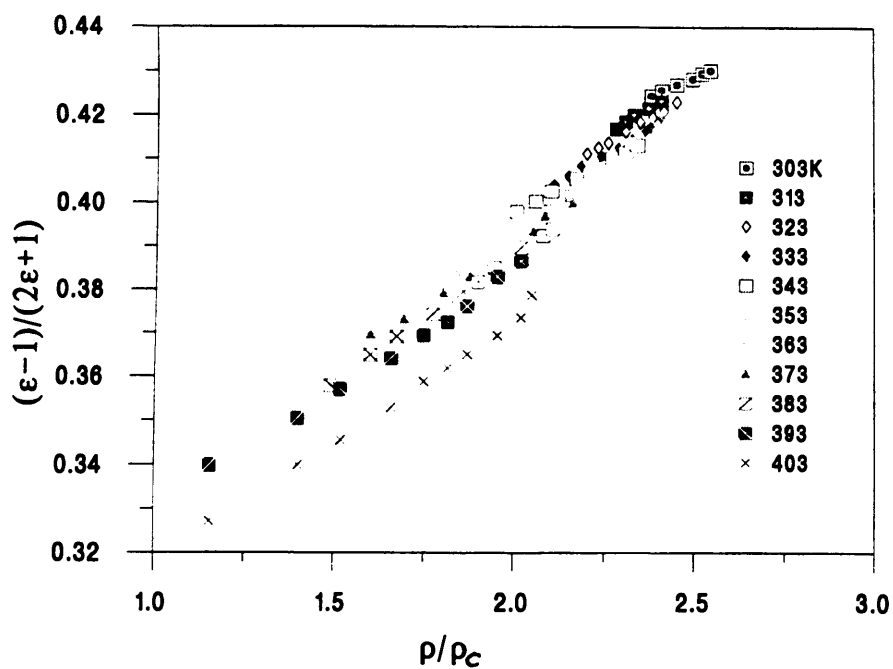


Figure 3.2.4 $(\epsilon - 1)/(2\epsilon + 1)$ as a function of reduced density (ρ/ρ_c) for HFC 134a

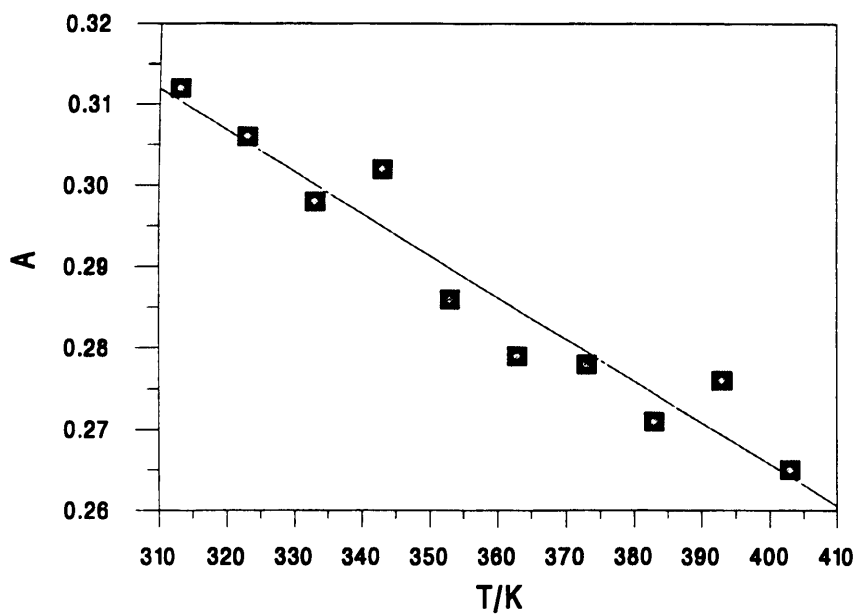


Figure 3.2.5 A as a function of temperature for HFC 134a

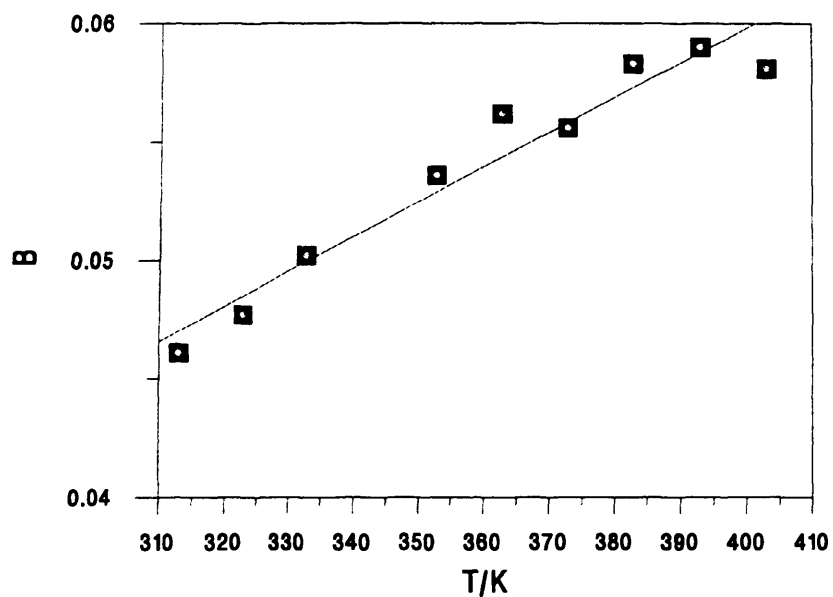


Figure 3.2.6 B as a function of temperature for HFC 134a

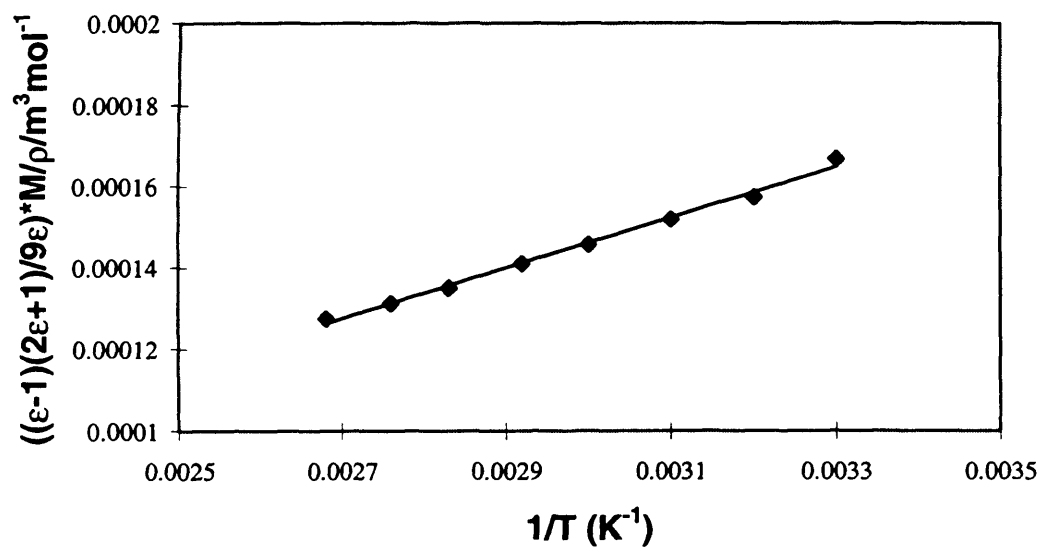


Figure 3.2.7 Determination of the dipole moment of HFC 134a in the liquid phase by the Kirkwood representation

function was approximately independent of density. In figure 3.2.7 the mean Kirkwood function at each temperature is plotted against $1/T$ for HFC 134a, yielding a dipole moment in the liquid phase of $\mu^* = (3.20 \pm 0.36) \text{ D}$ ($r = 0.997$). The large uncertainty is a consequence of the error associated with each density calculation. This measurement agrees with the previously obtained value of $\mu^* = (3.54 \pm 0.01) \text{ D}^{81}$ within experimental uncertainties.

Application of equation (3.1.4) to HFC 32 and HFC 125 yields the apparent dipole moments listed in table 3.2.2. The apparent dipole moments of the three HFCs follow the order of the gaseous dipole moments, that is HFC 134a > HFC 32 > HFC 125. Although HFC 134a and HFC 32 display extremely similar values of μ^* , HFC 125 has a much lower apparent dipole moment.

Fluid	$\mu/D^{82,83}$	μ^*/D	g
HFC 134a	2.058	3.20	2.42
HFC 32	1.978	3.06	2.39
HFC 125	1.563	2.14	1.88

Table 3.2.2 Dipole moments and Kirkwood correlation factors for HFC 134a, HFC 32 and HFC 125

Calculation of the Kirkwood correlation parameter, g , via equation (3.1.5) shows the difference in μ^* to partially arise from the lower g value of HFC 125, as shown in table 3.2.2. The g values in table 3.2.2 suggest that the HFC 125 molecule

has the greatest mobility of the three fluids, whereas the HFC 134a and HFC 32 molecules experience restrictions to rotation of a similar magnitude. The values of g determined for the three fluids given here are similar to those previously calculated for HFC media.^{84,85}

The relative permittivity of HFC 134a and HFC 32 is more sensitive to changes in density and temperature than HFC 125 because of the correspondingly higher μ^* values, in accordance with equation (3.1.4). Consequently, HFC 134a and HFC 32 may prove to be more useful solvents in supercritical processing.

3.2.2 Solvatochromic Shifts in Liquid and Supercritical Hydrofluorocarbons

The values of π^* were calculated from equation (3.1.11). Nile Red ($s = -2300$ cm^{-1} and $\nu_o = 20.51 \times 10^3$ cm^{-1})⁸⁶ was chosen as an indicator solute as it has previously been shown to be suitable for studies of supercritical fluids and gives a higher resolution than most other solutes. The structure of the Nile Red molecule is shown in figure 3.2.8. Figure 3.2.9 shows the values of π^* for HFC 134a as a function of temperature and pressure. At 30 °C and 10 bar the π^* value is 0.45 which is comparable with solvents such as ethyl acetate, butylamine and p-xylene.⁵ As expected the π^* value in the liquid region increases roughly linearly with increasing pressure in the liquid state. There is a marked decrease in the value of π^* at temperatures above 100 °C and below 60 bar.

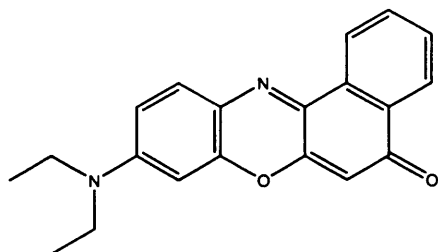


Figure 3.2.8 The structure of Nile Red

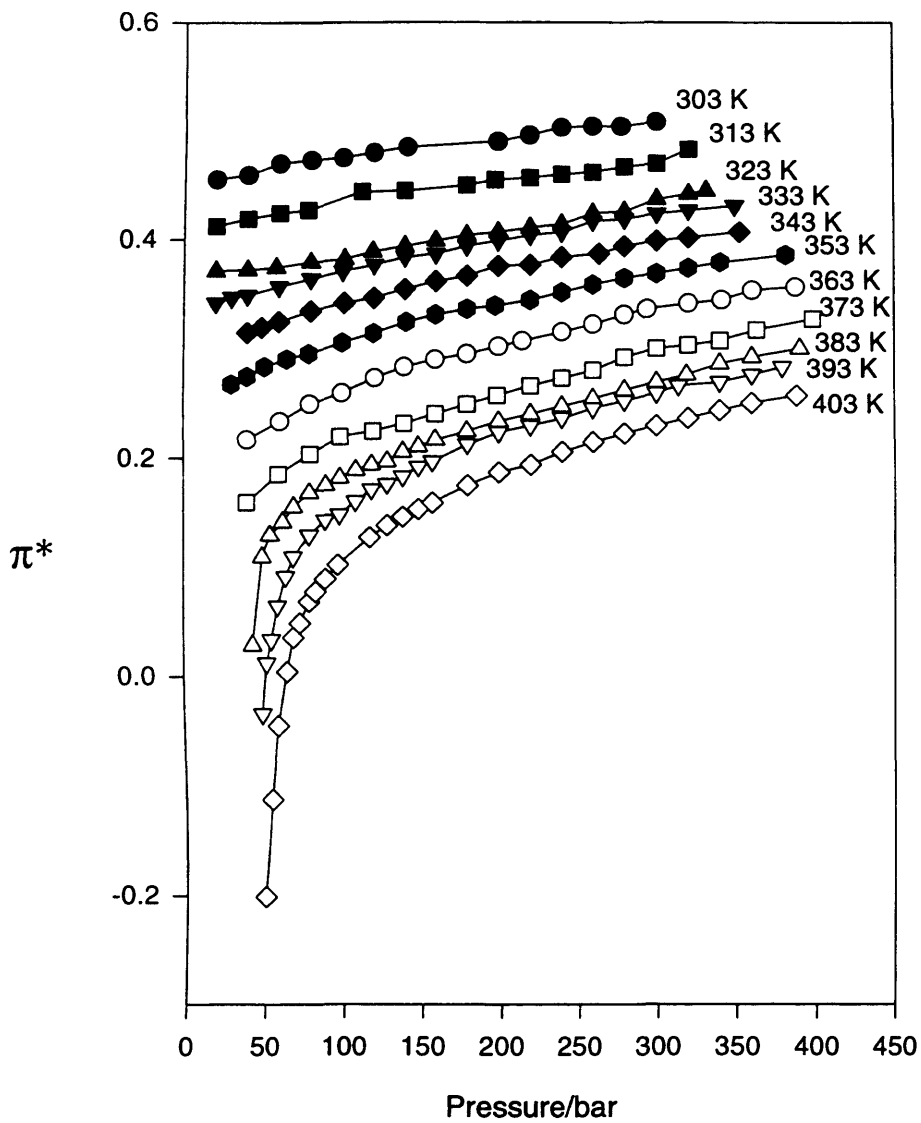


Figure 3.2.9 Dipolarity/polarizability parameter π^* for HFC 134a as a function of pressure and temperature

Figures 3.2.10 and 3.2.11 show similar plots for HFC 32 and HFC 125 respectively. As observed previously for HFC 134a, only at temperatures close to and above T_c is there a more marked decrease in π^* as the pressure decreases towards p_c . Note that the π^* values of these HFC solvents are smaller than those of the chlorinated analogues at ambient temperatures.¹⁸ The π^* values of HFC 134a, HFC 32 and HFC 125 in the supercritical state, however, are much higher than most solvents commonly used for supercritical fluid extraction, such as CO₂ and ethane.^{43,49,52} The increased polarity of these media coupled with the accessible critical conditions and inertness makes them ideal candidates for extraction solvents.

It is interesting to note that π^* of the HFC fluids is not directly correlated to the dipole moment of the solvent molecules. At any given reduced density $\pi^*_{\text{HFC 32}} > \pi^*_{\text{HFC 134a}} > \pi^*_{\text{HFC 125}}$, whereas the dipole moment decreases in the order HFC 134a > HFC 32 > HFC 125 (Table 3.2.2). This difference must result from an increased packing density of the smaller HFC 32 molecules around the solute.

For this work to be useful, π^* must be an accurate guide to solvent properties. Jackson *et al.* recently studied the solubility of water in HFC 134a and found a correlation between log solubility and density, although deviations occurred at high density.⁸⁷ Figure 3.2.12 shows the linear correlation between log solubility and π^* for the same data at 383 K. An improved correlation is observed between π^* and log solubility ($r = 0.994$) over density and log solubility ($r = 0.968$) as reported by Jackson *et al.*

Other groups that have studied the effect of temperature and pressure on the solvent properties of supercritical fluids have found that there are three density regions

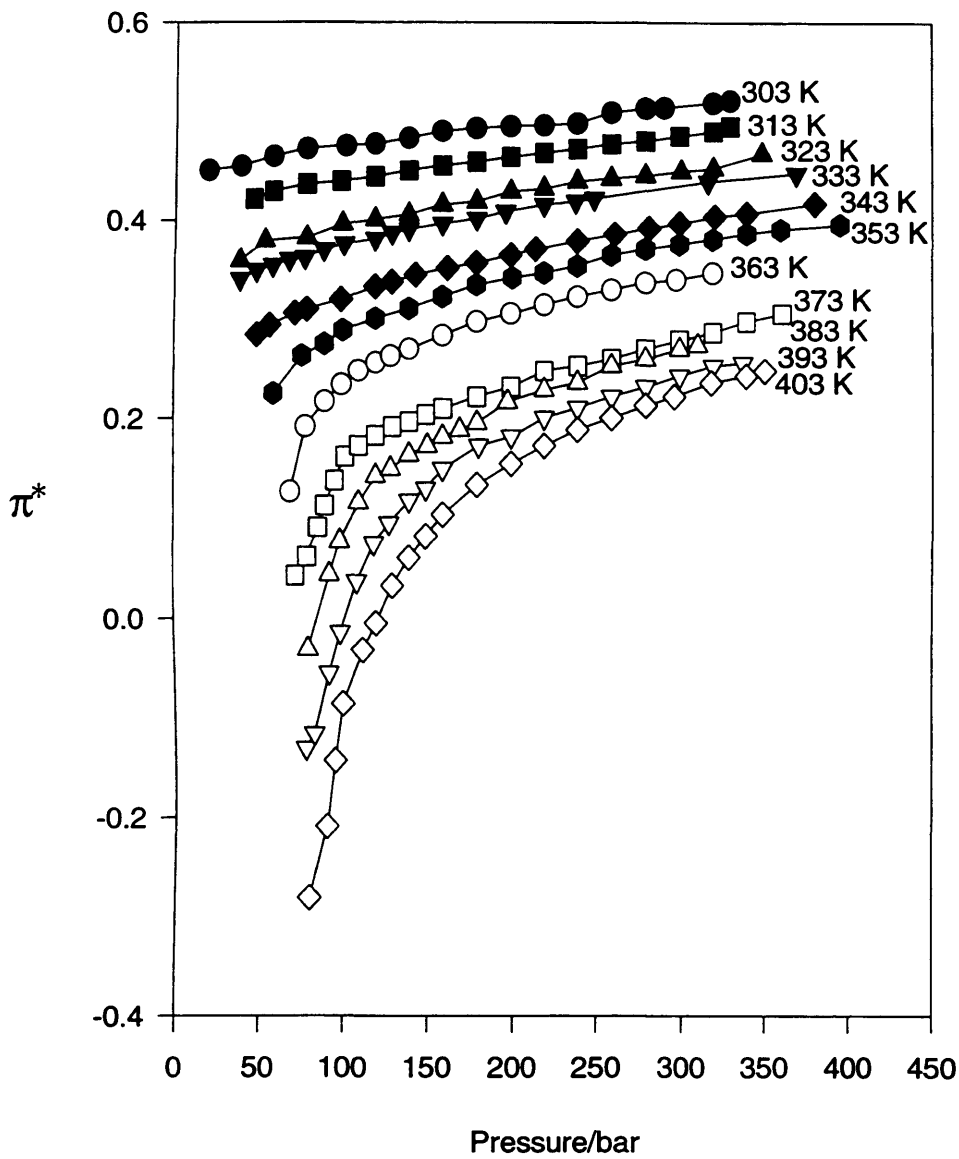


Figure 3.2.10 Dipolarity/polarizability parameter π^* for HFC 32 as a function of pressure and temperature

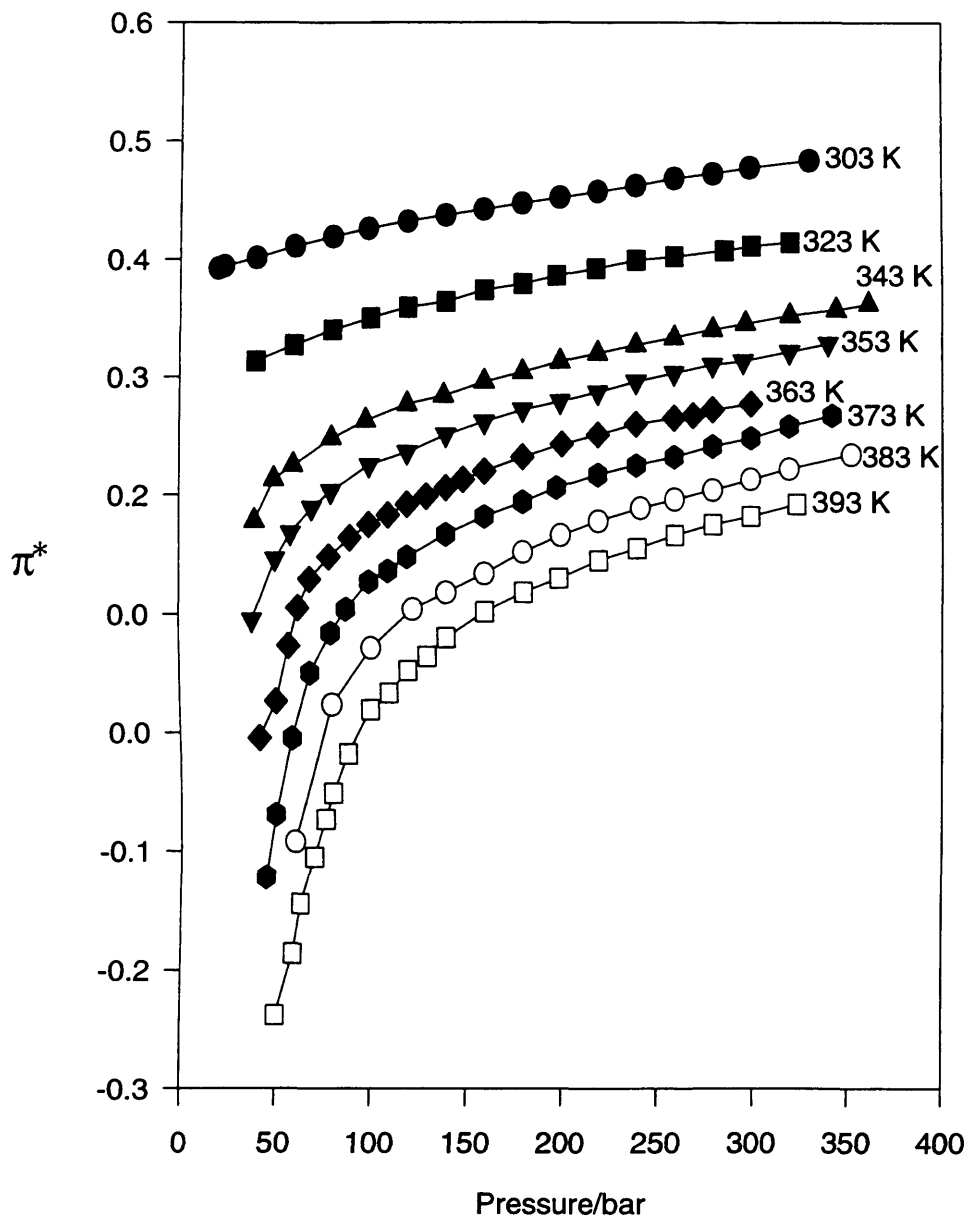


Figure 3.2.11 Dipolarity/polarizability parameter π^* for HFC 125 as a function of pressure and temperature

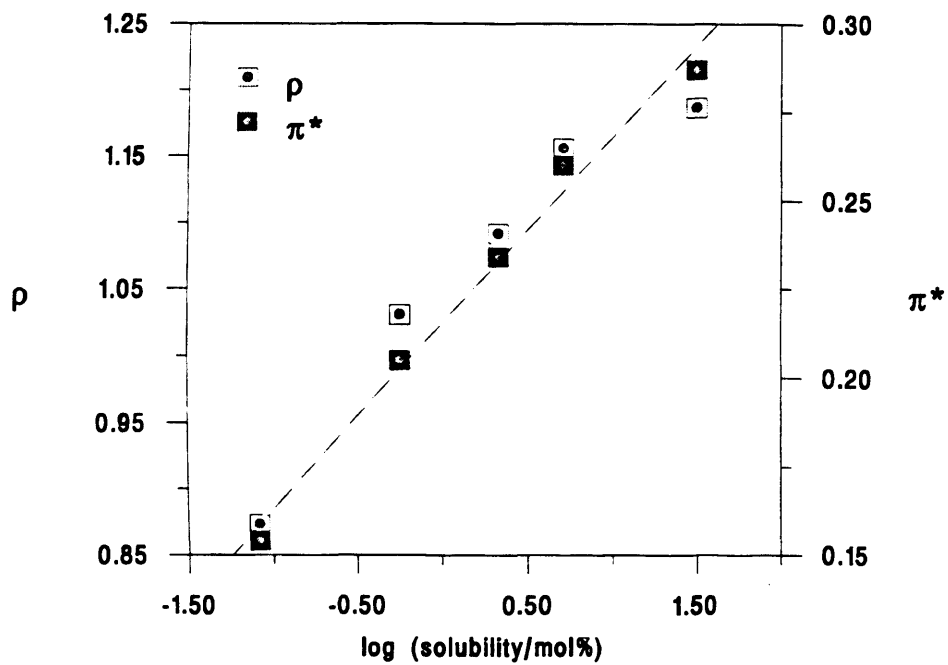


Figure 3.2.12 Correlation between the solubility of water in HFC 134a at 383 K with π^* and solvent density (in grams per cubic centimetre)

with distinctly different solvent properties.^{31,61} Previous studies in solvents such as CO₂, SF₆ and C₂H₆ have shown 3 distinct density regions with marked changes occurring in solvent properties at reduced densities, ρ_r , of approximately 1 and 2. These changes have been ascribed to local density augmentation as outlined above. The present study is, however, the first to investigate the properties of a variety of solvents over such a wide range of temperatures and pressures. The solvents studied are also interesting because they fill the polarity gap between non-polar solvents such as CO₂ and ethane^{51,52} and aqueous solutions.⁸⁸

Figure 3.2.13 shows the dependence of π^* on reduced density ($\rho_r = \rho/\rho_c$; for HFC 134a $\rho_c = 515.25 \text{ kg m}^{-3}$) for HFC 134a over the range 30 to 130 °C and 40 to 300 bar. Three distinct density regions can be observed with boundaries at reduced densities of approximately 1 and 2, yielding a shape indicative of local density augmentation.^{31,61} The liquid-like region ($\rho_r > 2$) has a steep slope. For dilute supercritical fluid solutions in this region, the bulk fluid density and local solvent density about the indicator solute have been shown to be very similar. The slope is less steep in the near-critical region ($1 < \rho_r < 2$) where the local solvent density about the solute is believed to be considerably higher than the bulk value due to clustering. This is caused by direct attractive potential interactions between Nile Red and HFC 134a. The free volume and compressibility are much larger in this region. Hence, the molecules can move into more energetically favourable positions with less resistance than in an incompressible liquid. In the gas-like region ($\rho_r < 1$) the slope again increases, suggesting that the local density is approaching that of the bulk as ρ_r tends to zero.

These regions are less clearly defined than those observed for π^* and other

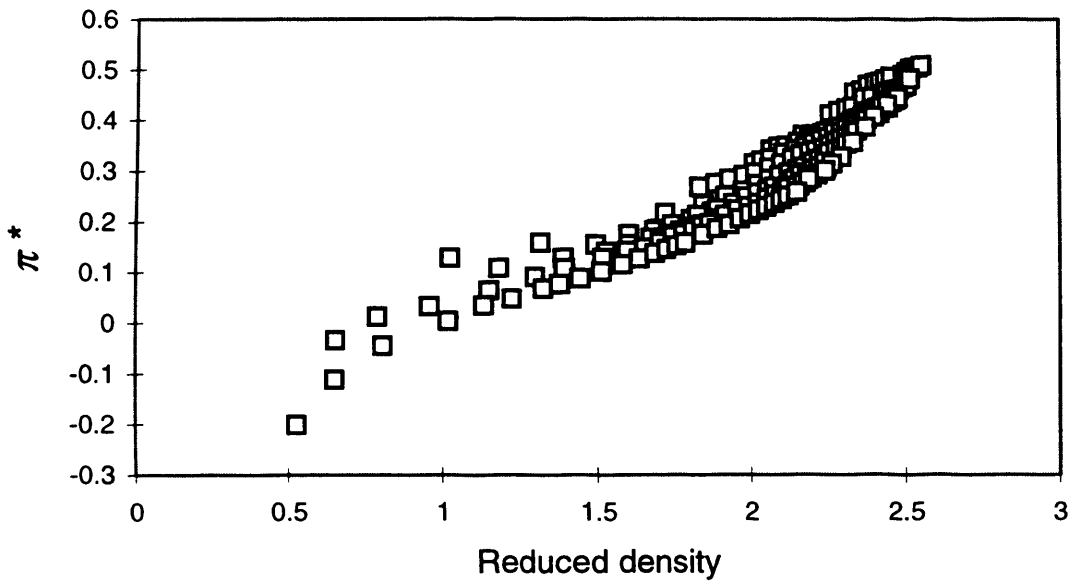


Figure 3.2.13 Effect of reduced density on π^* for HFC 134a

solvent parameters in CO₂, Xe and ethane.^{46,52} This is probably because HFC 134a is a more polar molecule and the solvent-solvent interactions are larger than in less polar solvents. In NH₃, no discontinuous changes in π^* were observed with reduced density⁵² suggesting that the solvent-solute interactions are similar in magnitude to the solvent-solvent interactions.

The forms of the isotherms displayed in figure 3.2.9 are similar to those observed in figure 3.2.1 in the case of the bulk relative permittivity of HFC 134a. Figure 3.2.14 shows that these two parameters are not directly proportional to each other. Figure 3.2.15 shows that there are no distinct changes in relative permittivity with density as observed with π^* . This is as expected, because relative permittivity is a bulk property of the solvent, whereas π^* is determined by local solute-solvent interactions.

Figures 3.2.16 and 3.2.17 show π^* as a function of reduced density for HFC 125 and HFC 32 respectively for the supercritical data. Figure 3.2.18 is redrawn for comparison from the data presented in figure 3.2.13 to show just the supercritical region and include the full pressure range measured. The shape of the plots indicates that local density augmentation occurs in each of the three solvents, and the effect becomes more pronounced as $T \rightarrow T_c$ from above. It is useful to study the different solvation characteristics of these solutions by considering the solvent-solvent-solute interactions. This has been modelled in a number of ways,⁸⁹⁻⁹¹ but the van der Waals approach used by Debenedetti *et al.*^{37,38} is the most appropriate for the rigid solute used in this study. Attractive forces between the solvent and solute dominate at a given reduced temperature T_r , when

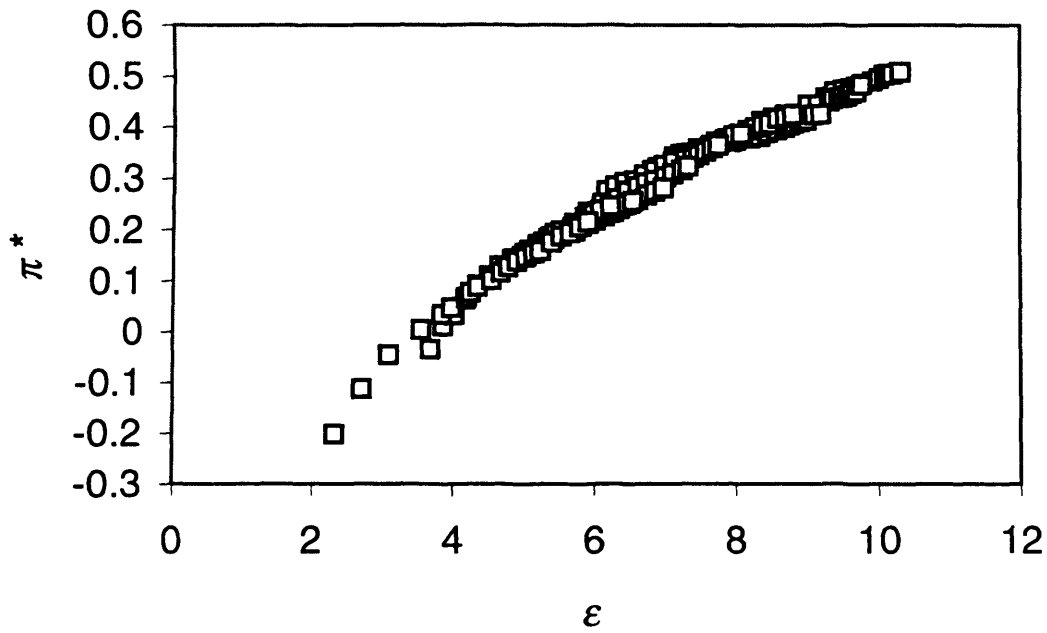


Figure 3.2.14 π^* as a function of bulk relative permittivity for HFC 134a

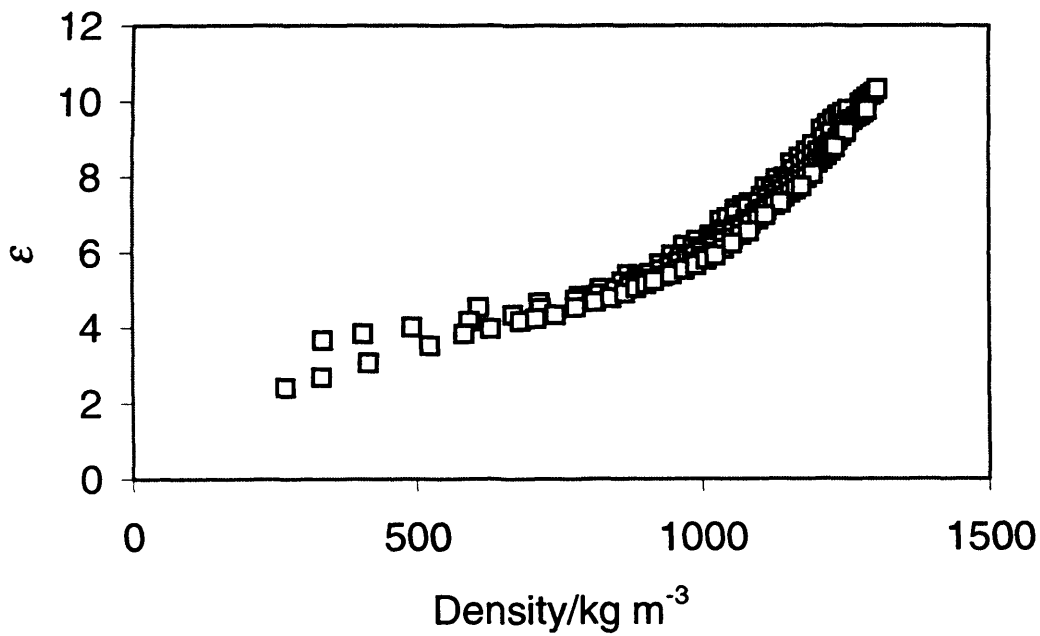


Figure 3.2.15 Bulk relative permittivity of HFC 134a as a function of density

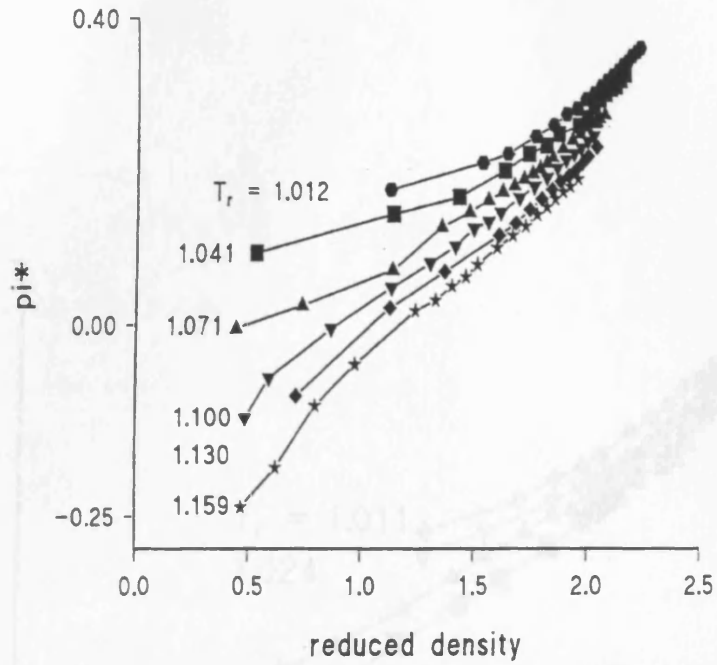


Figure 3.2.16 π^* as a function of reduced density for HFC 125 for the supercritical data presented in figure 3.2.11

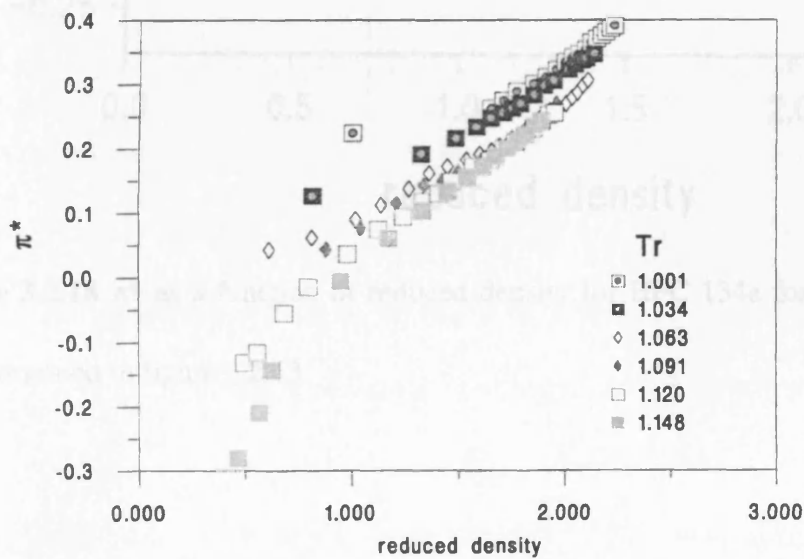


Figure 3.2.17 π^* as a function of reduced density for HFC 32 for the supercritical data presented in figure 3.2.10

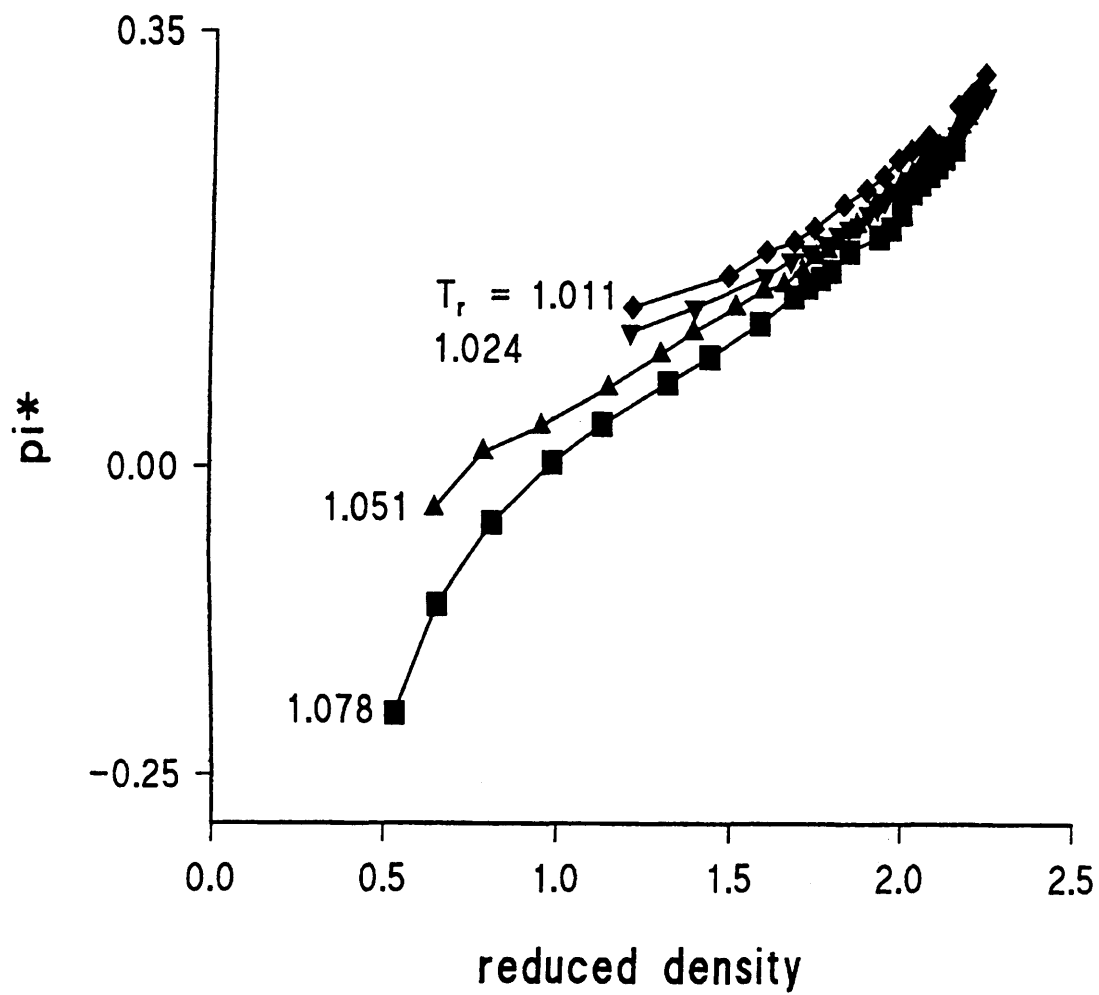


Figure 3.2.18 π^* as a function of reduced density for HFC 134a for the supercritical data presented in figure 3.2.13

$$\frac{3\rho_r \alpha^{1/2} (3 - \rho_r)^2}{4[3 + \rho_r(\gamma - 1)]} > T_r \quad (3.2.4)$$

where $\gamma = (\sigma_1 / \sigma_2)^3$ and $\alpha = \gamma(\epsilon_1 / \epsilon_2)$. Subscripts 1 and 2 denote the solute and solvent respectively, σ is the diameter of the species and ϵ is the interactive energy.

Similarly repulsive behaviour is observed when

$$\frac{9\alpha^{1/2} (3 - \rho_r)^2}{4[3(\gamma + 1) - \rho_r]} < T_r \quad (3.2.5)$$

Between these two limits there are weak interactions between the solvent and solute. Figure 3.2.19 shows the boundaries between the three regimes for a van der Waals representation of Nile Red with HFC 32, 134a and 125. For all of the solvents studied π^* increases linearly with reduced density in the region where repulsive solvent-solute interactions dominate. This is logical as the local density around the solute will increase linearly with the bulk reduced density. It is interesting to note that the change in π^* with reduced density is approximately constant over the range of reduced temperatures studied. What is more surprising is that $d\pi^*/d\rho_r$ is roughly similar for all of the HFC solvents studied (0.264 ± 0.0196). While this approach suggests the approximate reduced densities at which the solvent properties should change it does not give an indication of the magnitude of the solvent-solvent-solute interactions.

As the reduced density is decreased the solvent and solute will have weak interactions and the solvent-solvent interactions will be strong. At lower T_r the solvent-solute interactions will be larger and the local density around the solute will increase leading to a decrease in $d\pi^*/d\rho_r$. This is observed for all solvents at all reduced

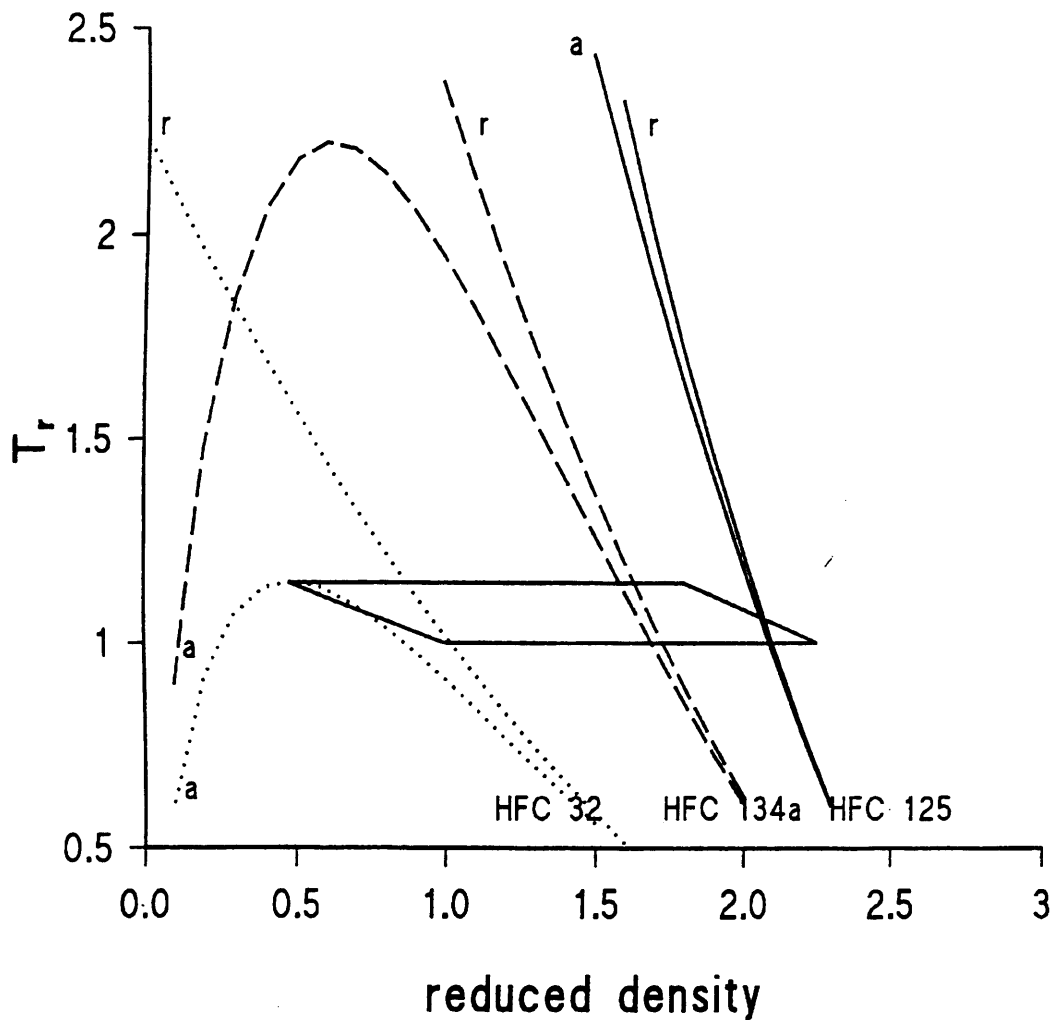


Figure 3.2.19 Boundaries between the three regimes for a van der Waals representation of Nile Red with HFC 32, HFC 134a and HFC 125 (calculated using equations (3.2.4) and (3.2.5) (a = attractive forces dominate, r = repulsive forces dominate))

temperatures studied. If the linear region at high reduced density is extrapolated to lower reduced density then a baseline is obtained of how π^* should change if the local density was equal to the bulk density. Extrapolation of the measured π^* value to this baseline will give the local solvent density around the solute. A similar approach has also been used by Johnston *et al.*⁹²

Figure 3.2.20 shows the ratio of the local to bulk densities as a function of the bulk fluid density for HFC 134a. At T close to T_c there is a sharp increase in the fluid density surrounding the solute. The local densities are similar to those observed from fluorescence and EPR studies in CF_3H ,^{93,94} CO_2 ⁵³ and ethane⁵⁸ and theoretical calculations in aqueous systems.⁷³ Figure 3.2.21 and 3.2.22 shows the comparison of the data for all of the HFC solvents at comparable T_r values. As can clearly be seen the ratio of local to bulk densities at $T_r \approx 1.01$ (Figure 3.2.21) is the same irrespective of the solvent. This is a remarkable observation considering the marked differences in dipole moment and size of the solvent molecules and the temperature and pressure differences in the measurements. It should also be appreciated that the HFC 125 and 134a data are extensively in the region where attractive forces dominate, whereas the HFC 32 data are dominated by repulsive solvent-solute interactions. Direct comparison at higher T_r was not possible, but Figure 3.2.22 shows data at $T_r \approx 1.1$ and while the data are not identical, they are remarkably similar and the trend is correct with the small change in T_r . Such maxima have been observed previously.^{58,93,94} The ratio of local to bulk density as a function of reduced density for di-*tert*-butylnitroxide in supercritical ethane⁵⁸ and pyrene in sc CO_2 ⁹⁵ is comparable with Nile Red in HFC fluids at the corresponding T_r showing a commonality to all of these systems *i.e.*, the solvation is controlled extensively by the reduced temperature at any

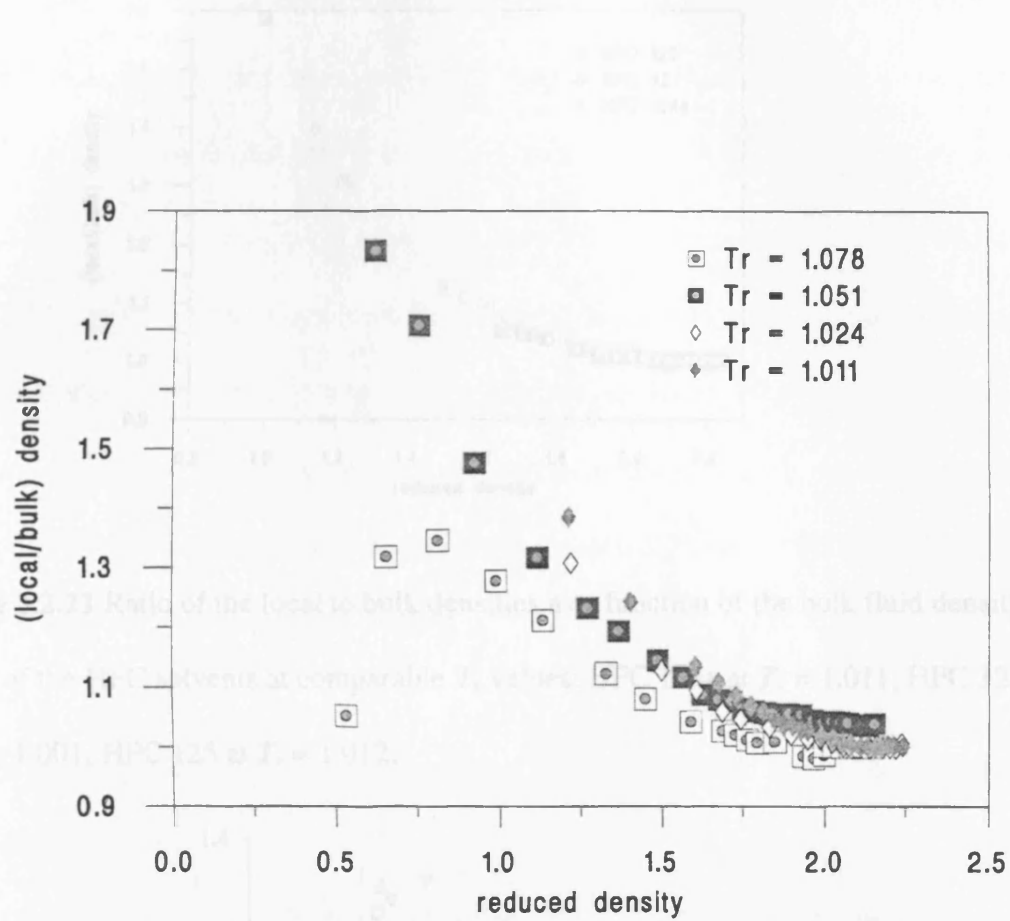


Figure 3.2.20 Ratio of the local to bulk densities as a function of the bulk fluid density for HFC 134a

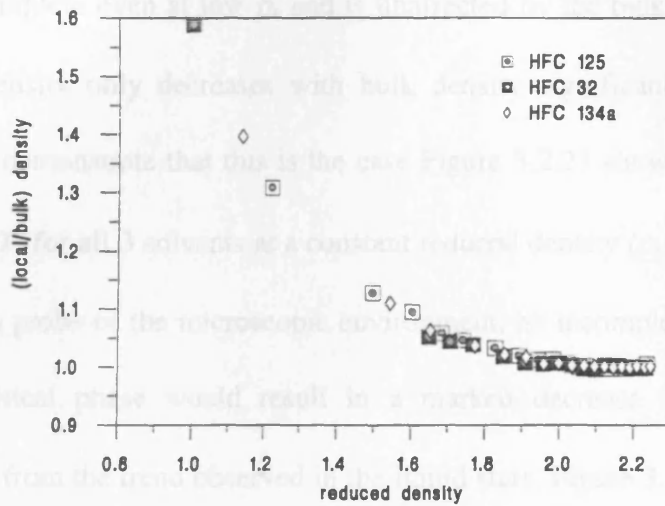


Figure 3.2.21 Ratio of the local to bulk densities as a function of the bulk fluid density for all of the HFC solvents at comparable T_r values: HFC 134a at $T_r = 1.011$; HFC 32 at $T_r = 1.001$; HFC 125 at $T_r = 1.012$;

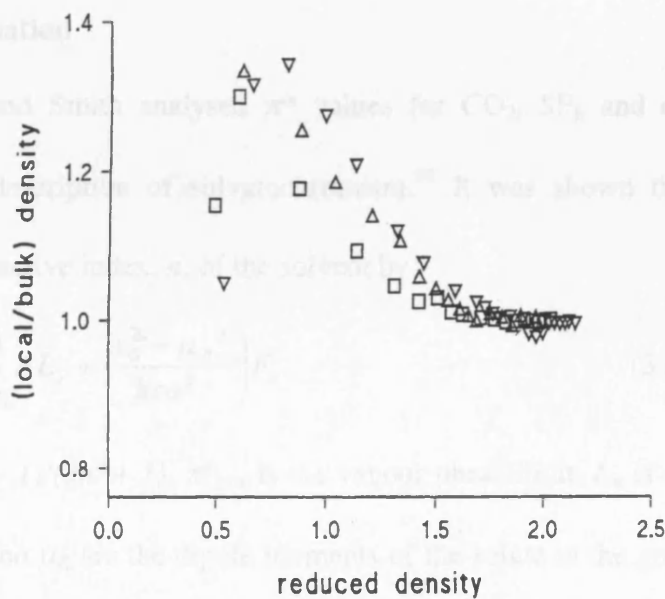


Figure 3.2.22 Ratio of the local to bulk densities as a function of the bulk fluid density for all of the HFC solvents at comparable T_r values: HFC 134a at $T_r = 1.078$ (∇); HFC 32 at $T_r = 1.091$ (Δ); HFC 125 at $T_r = 1.100$ (\square);

given reduced density. Figures 3.2.21 and 3.2.22 suggest that at $T_r \approx T_c$ the solvation sheath is complete even at low ρ_r and is unaffected by the bulk density. At higher T_r , the local density only decreases with bulk density significantly below the critical density. To demonstrate that this is the case Figure 3.2.23 shows the reduced π^* as a function of T_r for all 3 solvents at a constant reduced density ($\rho_r = 1.65$). Since π^* can be used as a probe of the microscopic environment, an incomplete solvation sheath in the supercritical phase would result in a marked decrease in π^* , at the critical temperature from the trend observed in the liquid state. Figure 3.2.23, therefore, shows that the primary solvation sheath remains intact as each HFC is heated from liquid to supercritical conditions at constant density.

3.2.3 Modelling Solvation in Supercritical Fluids through the Mean Sphere Approximation

Yonker and Smith analysed π^* values for CO₂, SF₆ and ethane using the McRae-Bayliss description of solvatochromism.⁹⁶ It was shown that π^* could be related to the refractive index, n , of the solvent by

$$\pi^* = \pi^*_{gas} + \frac{1}{2s} \left(AL_o + \frac{\mu_G^2 - \mu_E^2}{hca^3} \right) F_o \quad (3.2.6)$$

where $F_o = 2(n^2 - 1)/(2n^2 + 1)$, π^*_{gas} is the vapour phase limit, L_o is a weighted mean wavelength, μ_G and μ_E are the dipole moments of the solute in the ground and excited states, c is the speed of light in a vacuum, a is the radius of the cavity occupied by the solute, h is Planck's constant and A is the polarizability effect constant. A plot of π^* versus F_o showed that two regions of solvation were present in the supercritical state.

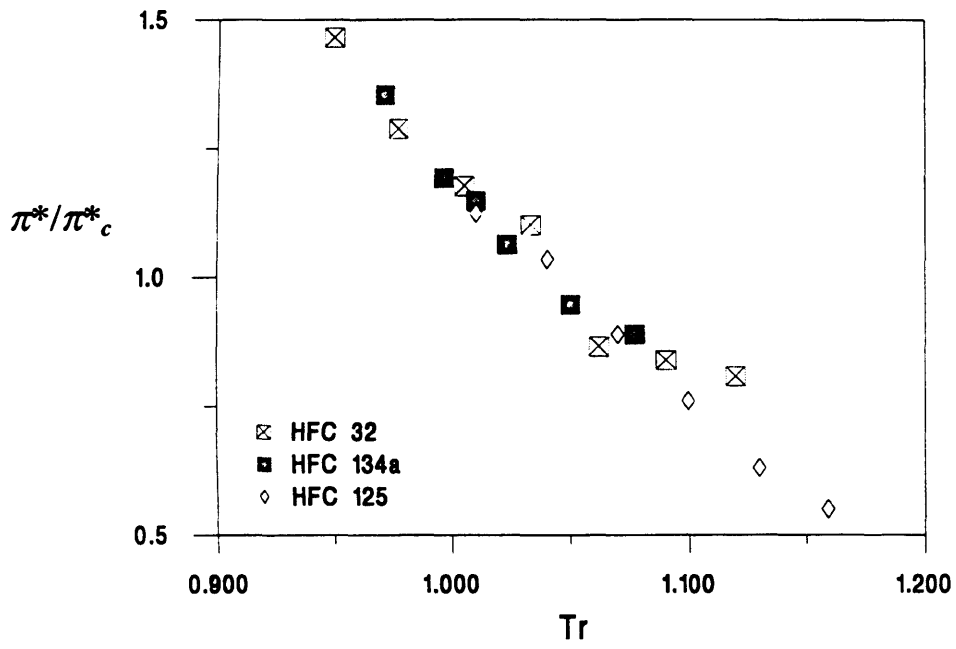


Figure 3.2.23 π^*_r as a function of T_r for all of the HFC solvents at constant ρ_r (1.65)

The slopes of these plots were also shown to be at variance to those measured in the liquid state. The break in slope was proposed to originate from cluster formation of the solvent around the solute and hence a transition from gas-like to liquid-like behaviour.

It has been shown⁹⁷ that the reaction field, R , created by an electrostatic field of polar molecules surrounding a solute is given by

$$R = \frac{2(\epsilon - 1) \mu_G}{(2\epsilon + 1) a^3} \quad (3.2.7)$$

If the reaction field is responsible for the stabilisation of the excited state of the indicator solute then π^* should be correlated to the Kirkwood function, $(\epsilon - 1)/(2\epsilon + 1)$.

Figure 3.2.24 shows that there is a good correlation between these two parameters for fluids with $\rho_r > 1.3$. This includes data from both the liquid and supercritical states.

The breakdown of this simple model at low reduced densities is probably caused by local solvent density augmentation. π^* is only strongly correlated to the Kirkwood function at high ρ_r where both the local and bulk solvent density are roughly equal.

Another cause of the failure of this model at low ρ_r could be an increase in the average solvent-solute separation distance i.e., the cavity size increases. If the latter case is accurate then the radius of the cavity will be given by

$$a^3 = M/N_A\rho \quad (3.2.8)$$

where M is the molar mass and N_A is the Avogadro constant. Hence, π^* will be proportional to the Kirkwood parameter multiplied by the reduced density. Figure 3.2.24 shows that the linear correlation between π^* and this modified parameter ($r = 0.984$) is worse than that for π^* and the simple Kirkwood parameter ($r = 0.993$). This

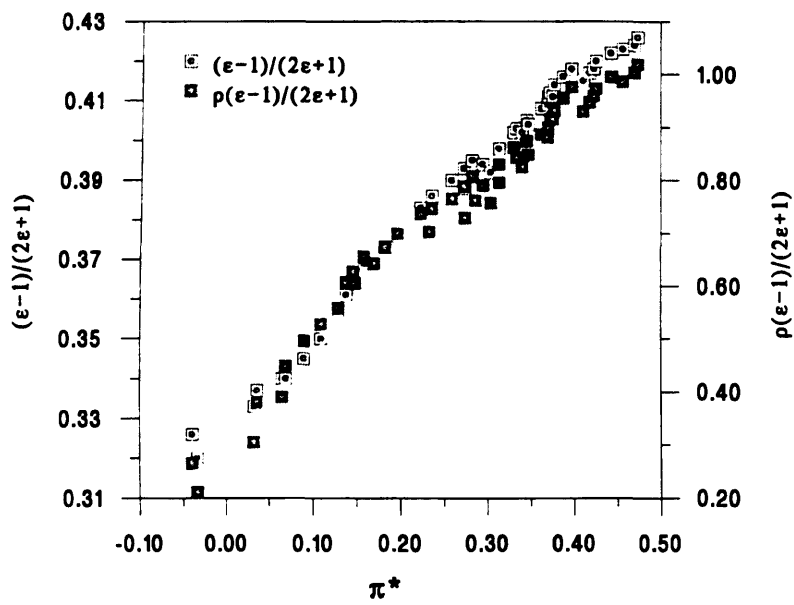


Figure 3.2.24 Plot of $(\epsilon - 1)/(2\epsilon + 1)$ (white squares with black dots) and $(\epsilon - 1)/(2\epsilon + 1)\rho_r$ (shaded squares) versus π^* for HFC 134a for the data shown in figure 3.2.9

suggests that these deviations are due to solvent clustering and not expansion of the solvation cavity.

A more complex model is thus required to simulate the behaviour of fluids close to the critical point. The properties of supercritical fluids have also been correlated to Dimroth's E_T and E'_T polarity scales⁹⁸ and this has given similar results to the π^* findings. This is not surprising as both scales are based upon the same principle and a strong correlation between the two has previously been demonstrated.^{44,99} Recent work by Streck and Richert⁹⁸ has shown that E_T thermochromic shifts in liquid 2-methyl-tetrahydrofuran can be modelled using a mean sphere approximation (MSA). This is a model developed by Wertheim¹⁰⁰ and used in many different forms to model solvent properties. In the form used by Streck and Richert the Gibbs energy of solvation is characterised using the hard sphere radius of the solvent, d , and the relative permittivity of the solvent, ϵ . It can be shown that the absorption maximum of the solute in the solvent can be related to a complex function of the solution relative permittivity, $\alpha(\epsilon)$ by:

$$v_{max} = v_{gas} + \frac{2\alpha(\epsilon)\mu_G(\mu_G - \mu_E)}{4\pi\epsilon_0 chD^3} \quad (3.2.9)$$

where v_{gas} is the absorption maximum of the solute in a vacuum, D is the radius of the solute and ϵ_0 is the permittivity of free space. The function $\alpha(\epsilon)$ is given by

$$\alpha(\epsilon) = \frac{8(\epsilon - 1)}{2uR^3\rho^3 + 2\epsilon[1 + R(1 - 2u)]^3 + [1 + R\rho]^3} \quad (3.2.10)$$

where

$$R = d / D$$

$$\rho = \frac{(1-u)}{(1-2u)}$$

$$u = \frac{3\xi}{(1+4\xi)}$$

$$\xi = \frac{1}{2} \left[1 - \frac{9}{4 + f^{1/3} + f^{-1/3}} \right]$$

$$f = 1 + 54\varepsilon^{1/2} \left[1 - \left[1 + \frac{1}{27\varepsilon^{1/2}} \right]^{1/2} \right]$$

Hence, for a given solute in a specific solvent π^* should be proportional to $\alpha(\varepsilon)$.

Combining equations (3.2.9) and (3.1.11) it can be seen that

$$\pi^* = \pi^*_{gas} + \frac{2\alpha(\varepsilon)\mu_G(\mu_G - \mu_E)}{s4\pi\varepsilon_0 chD^3} \quad (3.2.11)$$

In section 3.2.2 it was shown that the solute has a complete solvation sheath in the supercritical phase. A hard sphere approximation model such as the MSA, therefore, should accurately predict π^* in both the liquid and supercritical states. According to equation (3.2.11) a plot of π^* vs. $\alpha(\varepsilon)$ should have the same slope and intercept irrespective of the solvent. Figure 3.2.25 is a test of equation (3.2.11) for the data shown in figures 3.2.9, 3.2.10 and 3.2.11. Here the radius of the solute was calculated to be 4.72 Å from the van der Waals volume. The radii of the HFC molecules were also calculated from van der Waals volumes and are 2.59 Å, 2.14 Å and 2.64 Å for HFC 134a, HFC 32 and HFC 125 respectively. The ground state and excited state dipole moments of Nile Red were taken from the literature as 7.0 D and 18.6 D respectively.¹⁰¹

As can clearly be seen from figure 3.2.25, all of the solvents show excellent fits to the hard sphere approximation model. This is a remarkable observation considering

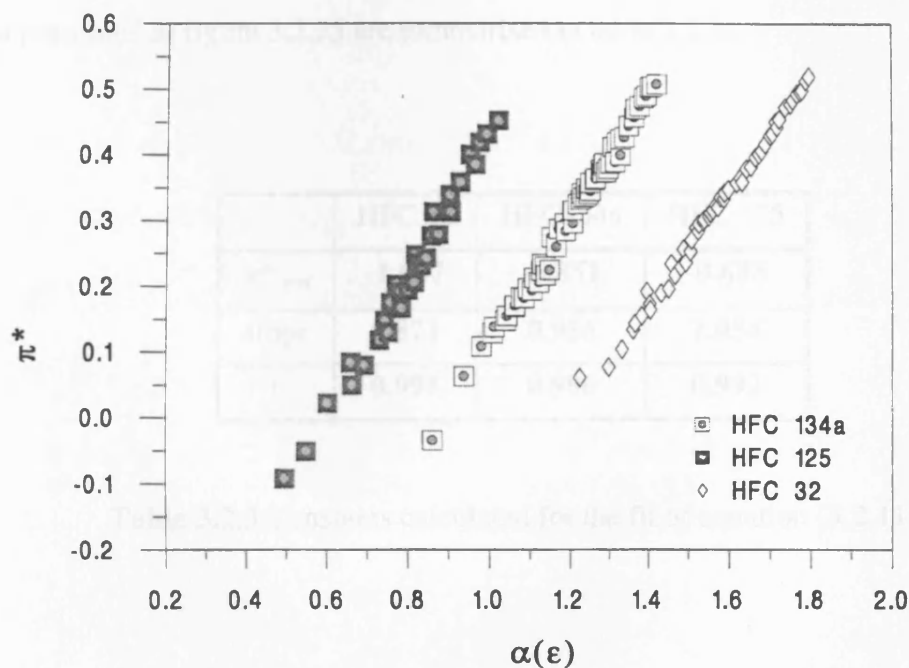


Figure 3.2.25 Plot of π^* versus $\alpha(\epsilon)$ for the data shown in figures 3.2.9, 3.2.10 and 3.2.11

the wide range of densities over which this simple model is applicable and the differences in polarity of the three solvents. It should also be noted that there is no discontinuity for any of the solvents between the dipolarity/polarizability of the solvent medium in the supercritical and in the liquid phase. The slopes and intercepts of the data presented in figure 3.2.25 are summarised in table 3.2.3.

	HFC 32	HFC134a	HFC 125
π^*_{gas}	-1.047	-0.851	-0.633
slope	0.871	0.956	1.054
r	0.996	0.996	0.992

Table 3.2.3 Constants calculated for the fit of equation (3.2.11)

It should be noted that both the solute and solvent were assumed to be spherical. While this assumption is only an approximation, the diameter of the solute and solvent have a relatively small effect on $\alpha(\epsilon)$ and this does not significantly alter the values of the parameters listed in table 3.2.3. The theoretical slope was calculated to be 0.44 but there is a large uncertainty in the dipole moment in the ground state¹⁰¹ and the cavity diameter. All that can be concluded is that the observed slopes were of a similar order of magnitude to that calculated. The slopes listed in table 3.2.3 for HFC 125 and HFC 134a are very similar to each other whereas there is a slight deviation for HFC 32. This may result from other solvent-solute interactions which are not described in equation (3.2.11), namely, the solvent Stark effect, dispersion, and hydrogen bonding. The polarizability of the solute molecule has been ignored in the present

work, but its effect on the solvation energy is apparently small for solute molecules exhibiting a large change in permanent dipole moment upon electronic excitation.³ This is likely to be true for Nile Red, which has a permanent dipole moment increase of 11.6 D following electronic excitation. Nevertheless modification of equation (3.2.11) to account for such effects remains the topic of further work.

The intercept for all 3 solvents should be close to the dipolarity/polarizability of the solute in a vacuum. The π^*_{gas} values are relatively similar for all three solvents and are in accordance with those published for other solutes.^{51,102} The observed differences probably arise from deviation in the virial equation for calculating relative permittivities for the less polar fluids at low reduced densities but may also be indicative of a slight hydrogen bond donor characteristic of the more polar solvents.

Hydrogen bond interactions¹⁹ can be accounted for by modifying equation (3.1.11) to

$$v = v_o + s\pi^* + a\alpha + b\beta \quad (3.2.12)$$

where α and β are measures of the hydrogen bond donor (HBD) acidity and hydrogen bond acceptor (HBA) basicity, respectively, and a , b and s are susceptibility constants. The hydrogen bond acceptor parameter, β , for all of the HFC solvents studied should be zero by analogy with the chlorinated analogues under ambient conditions.² The hydrogen bond donor parameter, α , for pentachloro- and tetrachloroethane is zero while for dichloromethane $\alpha = 0.4$. The literature claims that the hydrogen bond acceptor characteristics of Nile red are insignificant⁸⁶ but does not quantify them.

Analysis of the data in the literature^{2,19} shows that the hydrogen bond donor susceptibility factor is small but significant ($\alpha = -1208 \text{ cm}^{-1}$).

Lagalante and co-workers have measured the Kamlet-Taft parameters, π^* and β , for six liquid and supercritical fluorinated ethane solvents, including HFC 134a and HFC 125.¹⁰³ Figure 3.2.26 compares the π^* values of HFC 134a determined in the current work to those obtained by Lagalante *et al.* using the solvatochromic probe molecule 4-nitroanisole.¹⁰⁴ Comparison of the HFC 125 data was not possible because of the different temperatures employed. The π^* values calculated for HFC 134a using the Nile Red indicator are consistently higher than those determined by Lagalante and colleagues in both the liquid and supercritical phases. The hydrogen bond acceptor properties of 4-nitroanisole are so insignificant that $\alpha \approx 0$ is a reasonable assumption.¹⁶ It is, therefore, implied that the aforementioned difference in π^* results from the neglect of hydrogen bonding interactions between HFC 134a and Nile Red. Similar inconsistencies in π^* , however, have been observed for CO₂ when employing Nile red and nitroanisole solvatochromic probes.¹⁰⁵ It should be noted that CO₂ is known to exhibit little in the way of hydrogen bonding characteristics (α and $\beta \approx 0$).^{43,49}

Lagalante *et al.* showed that HFC 134a is unable to act as a hydrogen bond acceptor, implying that β is equal to zero. If the π^* values determined by Lagalante and co-workers are assumed to be accurate, the hydrogen bond donor parameter of HFC 134a can easily be calculated using equation (3.2.12). Values of ν , ν_0 , s and α corresponding to the Nile Red solvatochromic measurements are used. The Nile red isotherms in figure 3.2.26 were fitted to ninth order polynomials, each with correlation coefficients greater than or equal to 0.999, to facilitate interpolation. The π^* data of

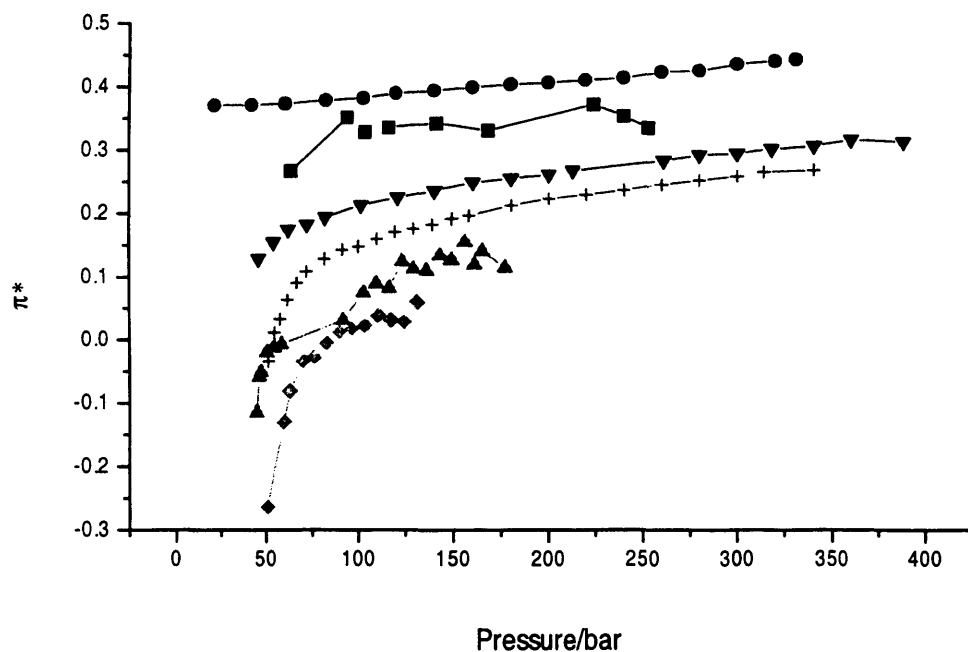


Figure 3.2.26 Comparison of π^* values for HFC 134a determined via the solvatochromic probe molecules Nile red (circles = 323 K; inverted triangles = 378 K; crosses = 393 K) and 4-nitroanisole^{103,104} (squares = 323 K; triangles = 378 K; diamonds = 393 K)

Lagalante and co-workers were then used to calculate α for HFC 134a as a function of temperature and pressure as shown in figure 3.2.27.

Liquid HFC 134a at 323 K has α values that range from approximately 0.05 to 0.2 over the pressure range of approximately 60 to 250 bar, compared to α values of 0.08 and 0.19 for liquid acetone and acetonitrile at 25 °C, respectively.² The large spread in α values can be attributed to the relatively poor accuracy of the 4-nitroanisole solvatochromic measurements. 4-nitroanisole is a comparatively poor solvatochromic probe for use in studies of supercritical media because its electronic transition energy is located in the UV portion of the spectrum where there may be a greater number of closer spaced vibrational bands within the measured peak maximum.¹⁰⁴

Supercritical HFC 134a, at 378 K and 393 K, has α values that lie generally in the range of 0.2 to 0.3 at pressures above 60 bar. In comparison, liquid methylene chloride and nitromethane have α values that lie in this range, at 0.30 and 0.22 respectively at 25 °C.² At pressures below 60 bar, α increases dramatically as the pressure tends towards zero. This pressure region, however, corresponds to the highest experimental uncertainties in π^* . If hydrogen bonding interactions do exist between HFC 134a and Nile Red they are likely to be relatively consistent over the measured temperature and pressure range. Large variations in the hydrogen bond interactions would result in a poor correlation between the polarizability function, $\alpha(\epsilon)$, and π^* . Employing UV/vis spectroscopy, Kim and Johnston characterised the hydrogen bond donor ability of supercritical fluoroform with the solvatochromic probe phenol blue.⁴⁰ It was shown that the hydrogen bond interactions were well developed at the critical density and did not change substantially with pressure up to approximately 350 bar. Bennett and Johnston characterised the hydrogen bond donor strength

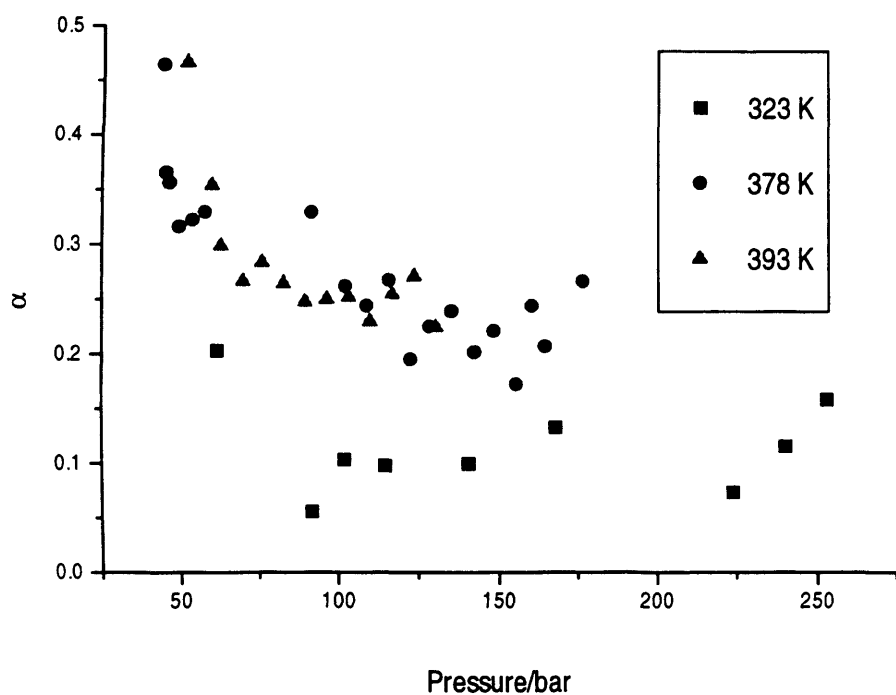


Figure 3.2.27 The hydrogen bond donor parameter, α , for HFC 134a as a function of pressure and temperature, calculated from the data given in figure 3.2.26

of supercritical water with the UV/vis spectroscopic solvatochromic probes acetone and benzophenone.⁸⁸ They also showed that hydrogen bonding can persist in supercritical media at low densities, and specifically as low as 0.1 g cm^{-3} in supercritical water at $380 \text{ }^\circ\text{C}$.

The results displayed in figure 3.2.27 are also inconsistent because α , and hence the hydrogen bond donating ability of HFC 134a, increases as the temperature of the system is raised from liquid to supercritical values. Generally, the hydrogen bond donor strength of a solvent decreases with temperature at a given density.^{40,88}

3.3 Conclusion

The relative permittivity of environmentally acceptable refrigerants HFC 134a, HFC 32 and HFC 125 has been measured at temperatures ranging from 303 to 403 K under pressures from 40 to 300 bar. Under these conditions the isothermal pressure dependence of the relative permittivity $(\delta\epsilon/\delta p)_T$ is always positive, and the isobaric temperature dependence $(\delta\epsilon/\delta T)_p$ always negative in both the liquid and supercritical phases. The relative permittivity has been fitted to the reduced density employing the function $(\epsilon - 1)/(2\epsilon + 1)$ and the HFC fluid phase dipole moments reported.

This work has also shown that HFC 134a, HFC 32 and HFC 125 should be useful fluids for supercritical fluid extraction because of their relatively high dipolarity/polarizability in the supercritical state coupled with their accessible critical conditions. It has been shown that local density augmentation occurs in all of the HFC fluids investigated and that the fluid density around the solute at a given T , varies similarly for a range of solvents. All of the dipolarity/polarizability data measured are found to fit well to the proposed hard sphere approximation model.

3.4 References

- 1) Kamlet, J. M.; Carr, P. W.; Taft, R. W.; Abraham, M. H. *J. Am. Chem. Soc.* **1981**, *103*, 6062.
- 2) Kamlet, J. M.; Abboud, J. M.; Abraham, M. H.; Taft, R. W. *J. Org. Chem.* **1983**, *48*, 2877.
- 3) Richert, R.; Wagener, A. *J. Phys. Chem.* **1993**, *97*, 3146.
- 4) Franco, S. *Electric Circuit Fundamentals*; Saunders College: New York, 1995.
- 5) Onsager, L. *J. Am. Chem. Soc.* **1936**, *58*, 1486.
- 6) Kirkwood, J. G. *J. Chem. Phys.* **1939**, *7*, 911.
- 7) Atkins, P. W. *Physical Chemistry*, 4th edn.; Oxford University Press: Oxford, 1990.
- 8) Suppan, P.; Ghoneim, N. *Solvatochromism*; Royal Society of Chemistry: Cambridge, 1997.
- 9) Hollas, J. M. *Modern Spectroscopy*, 2nd edn.; Wiley: Chichester, 1992.
- 10) Suppan, P. *J. Photochem. and Photobiol, A: Chem.* **1990**, *50*, 293.
- 11) Dimroth, K.; Reichardt, C.; Siepmann, T.; Bohlmann, F. *Lieb. Ann. Chem.* **1963**, *661*, 1.
- 12) Reichardt, C. *Angew. Chem.* **1979**, *91*, 119.
- 13) Reichardt, C. *Chem. Rev.* **1994**, *94*, 2319.
- 14) Kosower, E. M. *J. Am. Chem. Soc.* **1958**, *80*, 3253.
- 15) Kosower, E. M. *J. Chim. Physique.* **1964**, *61*, 230.
- 16) Kamlet, M. J.; Abboud, J.-L. M.; Taft, R. W. *J. Am. Chem. Soc.* **1977**, *99*, 6027.
- 17) Kamlet, M. J.; Abboud, J.-L. M.; Taft, R. W. *Prog. Phys. Org. Chem.* **1981**, *13*, 485.
- 18) Bekárek, V. *J. Phys. Chem.* **1981**, *85*, 722.

- 19) Taft, R. W.; Abboud, J.-L. M.; Kamlet, M. J.; Abraham, M. H. *J. Solution. Chem.* **1985**, *14*, 154.
- 20) Brady, J. E.; Carr, P. W. *J. Phys. Chem.* **1985**, *89*, 1813.
- 21) Nicolet, P.; Laurence, C. *J. Chem. Soc., Perkin Trans.* **1986**, *2*, 1071.
- 22) Laurence, C.; Nicolet, P.; Dalati, M. T.; Abboud J.-L. M.; Notario, R. *J. Phys. Chem.* **1994**, *98*, 5807.
- 23) Taft, R. W.; Murray, J. S. In *Quantitative Treatment of Solute-Solvent Interactions*; Politzer, P., Murray, J. S., Eds.; Elsevier: Amsterdam, 1994.
- 24) Abboud, J.-L. M.; Taft, R. W.; Kamlet, M. J. *J. Chem. Res. (S)* **1984**, 98.
- 25) Hildebrand, J. H.; Scott, R. L. *The Solubility of Nonelectrolytes*, 3rd edn.; Dover Publ: New York, 1964.
- 26) Hildebrand, J. H.; Scott, R. L. *Regular Solutions*; Prentice Hall: Englewood Cliffs, NJ, 1962.
- 27) Stanley, H. E. *Phase Transitions and Critical Phenomena*; Clarendon Press: Oxford, 1987.
- 28) Fisher, M. E. *J. Math. Phys.* **1964**, *5*, 944.
- 29) Hansen, J. P.; McDonald, I. R. *Theory of Simple Liquids*; Academic Press: London, 1986.
- 30) Martinez, H. L.; Ravi, R.; Tucker, S. C. *J. Chem. Phys.* **1996**, *104*, 1067.
- 31) Tucker, S. C.; Maddox, M. W. *J. Phys. Chem. B* **1998**, *102*, 2437.
- 32) Eckert, C. A.; Ziger, D. H.; Johnston, K. P.; Ellison, T. K.; *Fluid Phase Equilib.* **1983**, *14*, 167.
- 33) McGuigan, D. B.; Monson, P. A. *Fluid Phase Equilib.* **1990**, *57*, 227.
- 34) Chimonwitz, E. H., Afrane, G. *Fluid Phase Equilib.* **1996**, *120*, 167.

- 35) Biggerstaff, D. R.; Wood, R. H. *J. Phys. Chem.* **1988**, *92*, 1988.
- 36) Chialvo, A. A.; Cummings, P. T. *AIChE J.* **1994**, *40*, 1558.
- 37) Petsche, I. B.; Debenedetti, P. G. *J. Phys. Chem.* **1991**, *95*, 386.
- 38) Debenedetti, P. G.; Mohamed, R. S. *J. Chem. Phys.* **1989**, *90*, 4528.
- 39) Kirkwood, J. G.; Buff, F. P. *J. Chem. Phys.* **1951**, *19*, 774.
- 40) Kim, S.; Johnston, K. P. *Ind. Eng. Chem. Res.* **1987**, *26*, 1206.
- 41) Debenedetti, P. G. *Chem. Eng. Sci.* **1987**, *42*, 2203.
- 42) Blitz, J. P.; Yonker, C. R.; Smith, R. D. *J. Phys. Chem.* **1989**, *93*, 6661.
- 43) Ikushima, Y.; Saito, N.; Arai, M.; Arai, K. *Bull. Chem. Soc. Jpn.* **1991**, *64*, 2224.
- 44) Ikushima, Y.; Saito, N.; Arai, M. *J. Phys. Chem.* **1992**, *96*, 2293.
- 45) Zagrobelny, J.; Betts, T. A.; Bright, F. V. *J. Am. Chem. Soc.* **1992**, *114*, 5249.
- 46) Sun, Y.; Bunker, C. E.; Hamilton, N. B. *Chem. Phys. Lett.* **1993**, *210*, 111.
- 47) Heitz, M. P.; Bright, F. V.; *J. Phys. Chem.* **1996**, *100*, 6889.
- 48) Brennecke, J. F.; Eckert, C. A.; *Proc. Int. Symp. Supercrit. Fluids (I) Nice, Fr.* **1988**, 263.
- 49) Sigman, M. E.; Lindley S. M.; Leffler, J. E. *J. Am. Chem. Soc.* **1985**, *107*, 1471.
- 50) O' Neill, M.; Kruss, P.; Burk, R. C. *Can. J. Chem.* **1993**, *71*, 1834.
- 51) Yonker, C. R.; Frye, S. L.; Kalkwarf, D. R.; Smith, R. D. *J. Phys. Chem.* **1986**, *90*, 3022.
- 52) Smith, R. D.; Frye, S. L.; Yonker, C. R.; Gale, R. W.. *J. Phys. Chem.* **1987**, *91*, 3059.
- 53) Knutson, B. L.; Tomasko, D. L.; Eckert, C. A.; Debenedetti, P. G.; Chialvo, A. A. In *Supercritical Fluid Technology*; ACS Symposium Series 488; Bright, F. V., McNally, M. E., Eds.; American Chemical Society: Washington, DC, 1992.

- 54) Zeng, X. C.; Shen, J. W.; Tanaka, H.; Nakanishi, K.; Yuan, H. *Fluid Phase Equilib.* **1986**, *116*, 296.
- 55) Petsche, I. B.; Debenedetti, P. G. *J. Chem. Phys.* **1989**, *91*, 7075.
- 56) Cochran, H. D.; Cummings, P. T.; Karaborni, S. *Fluid Phase Equilib.* **1992**, *71*, 1.
- 57) Cummings, P. T.; Chialvo, A. A.; Cochran, H. D. *Chem. Eng. Sci.* **1994**, *49*, 2735.
- 58) Carlier, C.; Randolph, T. W. *AIChE J.* **1993**, *39*, 876.
- 59) Munoz, F.; Chimonwitz, E. H. *Fluid Phase Equilib.* **1992**, *71*, 237.
- 60) Luo, H.; Tucker, S. C. *Theor. Chem. Acc.* **1997**, *96*, 84.
- 61) Kajimoto, O. *Chem. Rev.* **1999**, *99*, 355.
- 62) Betts, T. A.; Zagrobelny, J.; Bright, F. V. *J. Supercrit. Fluids* **1992**, *5*, 48.
- 63) Flanagan, L. W.; Balbuena, P. B.; Johnston, K. P.; Rosky, P. J. *J. Phys. Chem.* **1995**, *99*, 5196.
- 64) Myers, D. J.; Urdahl, R. S.; Cherayil, B. J.; Fayer, M. D. *J. Chem. Phys.* **1997**, *107*, 9741.
- 65) Cui, S. T.; Harris, J. G. *Chem. Eng. Sci.* **1994**, *49*, 2749.
- 66) Wallen, S. L.; Palmer, B. J.; Fulton, J. L. *J. Chem. Phys.* **1998**, *108*, 4039.
- 67) Allen, M. P.; Tildesley, D. J. *Computer Simulation of Liquids*; Oxford University: Oxford, 1989.
- 68) Strauch, J. P.; Cummings, P. T. *J. Chem. Phys.* **1992**, *96*, 864.
- 69) Guissani, Y.; Guillot, B. *J. Chem. Phys.* **1993**, *98*, 8221.
- 70) Kataoka, Y. *J. Chem. Phys.* **1987**, *87*, 589.
- 71) Kovalenk, A.; Pizio, O.; Henderson, D. *J. Phys. Chem. B* **1997**, *101*, 3571.

- 72) Cochran, H. D.; Lee, L. L.; Pfund, D. M. In *International Symposium on Supercritical Fluid Proceedings*; Perrut, M., Ed.; Societe Francaise de Chemie: Nice, 1988.
- 73) Luo, H.; Tucker, S. C. *J. Phys. Chem.* **1996**, *100*, 11165.
- 74) Luo, H.; Tucker, S. C. *J. Am. Chem. Soc.* **1995**, *117*, 11359.
- 75) Wood, R. H.; Quint, J. R.; Grolier, J. -P. E. *J. Phys. Chem.* **1981**, *85*, 3944.
- 76) Wood, R. H.; Quint, J. R. *J. Phys. Chem.* **1989**, *93*, 936.
- 77) Bockris, J. O. M.; Reddy, A. K. N. *Modern Electrochemistry*, 1st ed.; Plenum Press: New York, 1970; Vol. I.
- 78) Luo, H.; Tucker, S. C. *J. Phys. Chem. B* **1997**, *101*, 1063.
- 79) Beveridge, D. L.; Schnuelle, G. W. *J. Phys. Chem.* **1975**, *79*, 2562.
- 80) Johnston, K. P.; Bennett, G. E.; Balbuena, P. B.; Rosky, P. J. *J. Am. Chem. Soc.* **1996**, *118*, 6746.
- 81) Barao, T.; Nieto de Castro, C. A.; Mardolcar, U. V.; Okambawa, R.; St-Arnaud, J. *M. J. Chem. Eng. Data* **1995**, *40*, 1242.
- 82) Meyer, C. W.; Morrison, G. *J. Chem. Eng. Data* **1991**, *36*, 409.
- 83) Meyer, C. W.; Morrison, G. *J. Phys. Chem.* **1991**, *95*, 3860.
- 84) Barao, M. T.; Mardolcar, U. V.; Nieto de Castro, C. A. *Int. J. Thermophys.* **1996**, *17*, 573.
- 85) Barao, M. T.; Nieto de Castro, C. A.; Mardolcar, U. V. *Int. J. Thermophys.* **1997**, *18*, 419.
- 86) Deye, J. F.; Berger, T. A.; Anderson, A. G. *Anal. Chem.* **1990**, *62*, 615.
- 87) Jackson, K.; Bowman, L. E.; Fulton, J. L. *Anal. Chem.* **1995**, *67*, 2368.
- 88) Bennet, G. E.; Johnston, K. P.; *J. Phys. Chem.* **1994**, *98*, 441.

- 89) Panayiotou, C.; Vera, J. H. *Polym. J.* **1982**, *14*, 681.
- 90) Beret, S.; Prausnitz, J. M. *AIChE J.* **1975**, *21*, 1123.
- 91) Donohue, M. D.; Prausnitz, J. M. *AIChE J.* **1978**, *24*, 849.
- 92) Johnston, K. P.; Kim, S.; Combes, J. *ACS Symp. Ser.*, **1989**, *406*, 52.
- 93) Brennecke, J. F.; Tomasko, D. L.; Peshkin, J.; Eckert, C. A. *ACS Symp. Ser.*, **1989**, *406*, 14.
- 94) Betts, T. A.; Zagrobelny, J.; Bright, F. V. *ACS Symp. Ser.*, **1992**, *488*, 48.
- 95) Rice, J. K.; Niemeyer, E. D.; Dunbar, R. A.; Bright, F. V. *J. Am. Chem. Soc.* **1995**, *117*, 5832.
- 96) Yonker, C. R.; Smith, R. D. *J. Phys. Chem.* **1988**, *92*, 235.
- 97) Smith, R. D.; Yonker, C. R. *J. Phys. Chem.* **1989**, *93*, 1261.
- 98) Streck, C.; Richert, R. *Ber. Bunsen-Ges. Phys. Chem.* **1994**, *98*, 619.
- 99) Abboud, J.-L. M.; Kamlet, M. J.; Taft, R. W. *J. Am. Chem. Soc.* **1977**, *98*, 8325.
- 100) Wertheim, M. S. *J. Chem. Phys.* **1971**, *55*, 4291.
- 101) Dutt, G. B.; Doraiswamy, S.; Peraisamy, N.; Venkataraman, B. *J. Chem. Phys.* **1990**, *93*, 8498.
- 102) Essfar, M.; Guiheneuf, G.; Abboud J.-L. M. *J. Am. Chem. Soc.* **1982**, *104*, 6786.
- 103) Lagalante, A. F.; Hall, R. F.; Bruno, T. J. *J. Phys. Chem. B* **1998**, *102*, 6601.
- 104) Lagalante, A. F.; Private communication.
- 105) Abbott, A. P.; Eardley, C. A.; Scheirer, J. E. *J. Phys. Chem.* **1999**. In press.

CHAPTER IV

ELECTROCHEMISTRY IN LIQUID AND SUPERCRITICAL HYDROFLUOROCARBONS

4.1 Introduction

- 4.1.1 Electrical Conductivity in Media of Low Relative Permittivity
- 4.1.2 Electrical Conductivity Measurements in Supercritical Media
- 4.1.3 The Electrical Double Layer
- 4.1.4 Measurement of the Double Layer Capacitance via AC Methods

4.2 Results and discussion

- 4.2.1 Electrical Conductivity of Liquid and Supercritical Hydrofluorocarbons
- 4.2.2 The Potential Windows of HFC 134a and HFC 32
- 4.2.3 Oxidation Electrochemistry at Extremely Positive Potentials
- 4.2.4 Voltammetry of Ferrocene in Liquid and Supercritical HFC 32
- 4.2.5 Double layer Structure in Liquid and Supercritical HFC 32

4.3 Conclusion

4.4 References

4.1 Introduction

If electrochemical investigations are to be performed in a solvent-electrolyte system, the medium must display both suitably high electrical conductivity and electrochemical stability over the potential range of interest. When these criteria are met, the structure of the electrical double layer will strongly influence the process of electron transfer under investigation at the electrode-solution interface.

This work will assess the validity of performing electrochemical processes in both liquid and supercritical hydrofluorocarbons. A comparison of the results from both voltammetric and double layer capacitance measurements will enable the elucidation of electrical double layer structure in both a liquid and supercritical HFC.

4.1.1 Electrical Conductivity in Media of Low Relative Permittivity

The potential energy of interaction, V , between two charges q_1 and q_2 separated by a distance r is given by¹

$$V = \frac{q_1 q_2}{4\pi\epsilon\epsilon_0 r} \quad (4.1.1)$$

where $\epsilon\epsilon_0$ defines the absolute permittivity of the medium. In media of low relative permittivity, the electrostatic energy of ion-ion interactions may be significantly larger than the kinetic energies associated with the thermal motion of ions. As first suggested by Bjerrum,² a pair of oppositely charged ions may then associate in solution to form an ion pair. If the aforementioned electrolyte is symmetrical, the ion pair will be electrically neutral. An uncharged ion pair does not respond to an externally applied electric field and will, therefore, not contribute to the conduction of current.

In media of low relative permittivity ($\epsilon < 15$), the coulombic attraction between ion pair dipoles and free ions may be strong enough to induce triple ion formation, as first proposed by Fuoss and Kraus in the 1930s.³ When the relative permittivity of the medium is below approximately 10, larger ion aggregates such as uncharged quadrupoles can form.⁴

If the molar conductivity of an electrolyte is plotted against the square root of its concentration, three distinct regions are frequently observed in media of low permittivity with concentration ranges dependent on the nature of both the solvent and salt^{3,5-8}

- (i) At very low electrolyte concentrations, there is a sharp decrease in the molar conductivity with increasing electrolyte concentration. This decrease is more dramatic than that described by the Onsager equation,⁹ and can be attributed to the formation of neutral ion pairs.
- (ii) At higher concentrations, triple ion formation becomes significant and the molar conductivity begins to increase after passing through a minimum.
- (iii) There is a subsequent decrease in molar conductivity with increasing electrolyte concentration that can be attributed to the formation of larger, uncharged ion aggregates. This molar conductivity behaviour is, however, usually ascribed to the increasing viscosity of the concentrated electrolyte solution.

Fuoss and Kraus investigated the conductivity of quaternary ammonium salts in dioxane-water mixtures, benzene, anisole and chlorobenzene.^{3,5-7} By considering the equilibria between free ions, ion pairs and triple ions, they were able to devise a mathematical framework in which to calculate the dissociation constants of the ion aggregates involved.³ Solutions of very low electrolyte concentration were considered

so that the activity coefficient, γ , could be assumed to be unity. The following dissociation equilibria were considered in the case of the 1-1 electrolyte, MX,



The ion pairing equilibrium of (4.1.2) is described by the dissociation constant K_P . It was assumed that the MXM^+ and XMX^- triple ions have equal probabilities of formation and, therefore, the dissociation processes of (4.1.3) and (4.1.4) can both be characterised by the same equilibrium constant, K_T .

In a solvent of low relative permittivity, the degree of dissociation of ion pairs, α , is so small that $(1 - \alpha) \approx 1$. Hence, it can be assumed that

$$\alpha = (K_P/c)^{1/2} \quad (4.1.5)$$

where c is the concentration of the electrolyte. The degree of dissociation for the triple ions, α_T , is given by

$$\alpha_T = \frac{(K_P c)^{1/2}}{K_T} \quad (4.1.6)$$

If the limiting molar conductivity of the electrolyte at infinite dilution, Λ^0 , represents the conductivity of a fully dissociated electrolyte solution with no ion-ion interactions, then

$$\Lambda^0 = \lambda_{M^+}^0 + \lambda_{X^-}^0 \quad (4.1.7)$$

where $\lambda_{M^+}^0$ and $\lambda_{X^-}^0$ are the molar conductivities of the cation and anion in the limit of infinite dilution, respectively. The limiting molar conductivity of the triple ions, Λ_T^0 , can similarly be expressed as

$$\Lambda_T^0 = \lambda_{MXM^+}^0 + \lambda_{XMX^-}^0 \quad (4.1.8)$$

The actual molar conductivity is, therefore, given by

$$\Lambda = \alpha\Lambda^0 + \alpha_T\Lambda_T^0 \quad (4.1.9)$$

Substitution of equations (4.1.5) and (4.1.6) into equation (4.1.9) yields

$$\Lambda = \frac{\Lambda^0 K_P^{1/2}}{c^{1/2}} + \frac{\Lambda_T^0 K_P^{1/2} c^{1/2}}{K_T} \quad (4.1.10)$$

The limiting molar conductivity of the electrolyte, Λ^0 , must be known if K_P and K_T are to be calculated through equation (4.1.10). For strong electrolytes in aqueous solution, the Onsager equation can be used to calculate Λ^0 .⁹ In media of low relative permittivity, however, this method of analysis is precluded by the predominance of ion association at even low electrolyte concentrations. Extrapolation of the lowest concentration data to infinite dilution is not acceptable due to both the erroneous nature of this data and the extremely large conductivity range over which a limited number of data must be extrapolated. Investigations in media of low relative permittivity have, therefore, commonly used Walden's rule^{10,11} to determine Λ^0

$$\Lambda^0 \eta = \text{constant} \quad (4.1.11)$$

where η is the viscosity of the solvent. This rule relies on the assumption that Stokes' relation¹ successfully describes the frictional drag on the ion under consideration.

4.1.2 Electrical Conductivity Measurements in Supercritical Media

Early investigations into the electrical conductivity of supercritical media focused on measurements in aqueous solutions. In the 1950s, Franck measured the conductometric properties of a variety of electrolytes in aqueous solution at

temperatures up to 800 °C and at pressures as high as 400 MPa.¹²⁻¹⁴ Marshall and co-workers then made a number of similar measurements.¹⁵⁻²⁷ The limiting molar conductivities of several electrolytes at supercritical conditions were consequently calculated.

If reliable values of the electrical conductance of pure water can be obtained at high temperatures and pressures, conductivity measurements can then be used to estimate ionic impurities present in steam generator water-steam cycles and other industrial applications. Marshall and co-workers, therefore, determined the specific conductance of pure water by an indirect method that applies the ionic product of water, K_w , and the limiting molar conductivities of both the hydrogen ion, $\lambda^0(\text{H}^+)$, and hydroxide ion, $\lambda^0(\text{OH}^-)$.²⁷ K_w was calculated using an equation recognised as an International Association for the Properties of Steam (IAPS) standard.²⁸ According to the law of the independent migration of ions, the limiting molar conductivities of ions are additive.¹ Marshall and colleagues were, therefore, able to calculate the sum of $\lambda^0(\text{H}^+)$ and $\lambda^0(\text{OH}^-)$ by measuring the limiting molar conductivities of a variety of electrolytes, as exemplified in equation (4.1.12).

$$\Lambda^0(\text{H}^+, \text{OH}^-) = \lambda^0(\text{H}^+) + \lambda^0(\text{OH}^-) = \Lambda^0(\text{HCl}) + \Lambda^0(\text{NaOH}) - \Lambda^0(\text{NaCl}) \quad (4.1.12)$$

The resulting conductance data were also used to study the associative behaviour of high temperature aqueous electrolytes. It was shown that at a fixed temperature the limiting molar conductivity of a 1-1 electrolyte varies approximately linearly with density. Furthermore, at supercritical temperatures from 400 to 800 °C, the value of Λ^0 was essentially equal for all of the 1-1 electrolytes studied when extrapolated to zero density.

The conductance of pure water is, however, experimentally very difficult to measure because of interference from the conductances of electrolyte impurities often introduced through corrosion of the containment vessel. Marshall and co-workers, therefore, proposed an equation that describes the specific conductance of water over the temperature range of 0 to 1000 °C and at pressures up to 1000 MPa.²⁷

The electrical conductivities of electrolytes in non-aqueous supercritical media have received relatively little attention in comparison to the aforementioned aqueous measurements. Abbott and Harper measured the conductivity of the hydrophobic electrolyte tetrakis(decyl)ammonium tetraphenylborate (TDATPhB) in supercritical CO₂.²⁹ The low conductivities observed were attributed to pronounced ion association and the low solubility of the electrolyte. TDATPhB, for example, exhibited an electrical conductivity of only approximately 1.5 μS cm⁻¹ at a concentration of 19.2 mM in sc CO₂ at 70 °C and 300 bar. The conductivities measured in the supercritical phase were then compared to those of the same electrolyte in liquid cyclohexane, a medium of very similar relative permittivity to that of sc CO₂. Hence, it was shown that the molar conductivity of an electrolyte can be enhanced in the supercritical phase because the low viscosity of the supercritical medium leads to high ionic mobilities.

Olsen and Tallman measured the conductivity of tetrabutylammonium tetrafluoroborate in the dipolar supercritical fluid, chlorodifluoromethane.³⁰ When electrolyte concentrations of 6 to 12 mM were employed, the molar conductivity of supercritical chlorodifluoromethane increased with the square root of the TBABF₄ concentration at fixed temperature and pressure. It was consequently proposed that triple ions constitute the majority of charge carriers under such conditions, although no mathematical fits of the conductivity data to the Fuoss-Kraus equation were performed.

The current work shows that both liquid and supercritical HFC 134a and HFC 32 can be made conducting via the dissolution of a TBABF₄ electrolyte. The conductivity of this electrolyte is presented in liquid HFC 134a and both liquid and supercritical HFC 32. In particular, the associative behaviour of the electrolyte ions in supercritical HFC 32 is examined.

4.1.3 The Electrical Double Layer

Metals characteristically exhibit high electronic conductivity and, therefore, are unable to support electric fields at equilibrium. This metallic property implies that any excess charge will reside on the surface.³¹ When a potential is applied to a metal electrode in an electrolyte solution, the metallic surface consequently acquires a charge. The solution side of the interface must obtain a charge equal in magnitude but opposite in sign to that at the electrode surface so that overall interfacial electroneutrality is preserved.

Helmholtz proposed that the excess charge in solution also resides at the surface of the metal-solution interface.^{32,33} Here the electrified interface consists of two parallel layers of opposing charge separated by a distance of molecular order. The excess charge on the solution side of the interface is carried by a *compact layer* of solvated ions. This proposal from Helmholtz represents the first model of double layer structure at an electrified interface. The term electrical double layer is now used to denote the distribution of ions, solvent and any other molecules at the electrode-electrolyte interface.

The Helmholtz compact double layer is equivalent to a parallel-plate capacitor, with an interplate spacing equal to the radius of the solvated ion, a . The plate formed

from the centre of charge of the ions is known as the Outer Helmholtz Plane (OHP).

The charge density, σ , stored by a parallel-plate capacitor can be related to the voltage drop, V , between the plates by equation (4.1.13)³¹

$$\sigma = \frac{\epsilon\epsilon_0}{d} V \quad (4.1.13)$$

where d is the interplate separation. The differential capacitance, C_d , of the compact double layer, therefore, is given as

$$C_d = \frac{\partial\sigma}{\partial V} = \frac{\epsilon\epsilon_0}{a} \quad (4.1.14)$$

Hence, the Helmholtz model predicts that the differential capacitance is independent of potential, a relationship that is not observed experimentally. In real systems C_d varies with both potential and electrolyte concentration. The Helmholtz model fails because it ignores the thermal motion of ions, which tends to loosen ions from the compact layer.

Working independently, Gouy and Chapman were the first to propose a model for the double layer that incorporated the effect of ionic thermal motion close to the electrode surface.³³⁻³⁶ In this model, electrostatic forces are able to overcome the randomising effect of thermal motion adjacent to the electrode surface, where the concentration of excess charge is, therefore, at its highest. At distances further away from the electrode surface the forces of electrostatic ordering are overcome by thermal randomising effects, leading to progressively lower concentrations of excess charge. A diffuse layer consequently extends into the bulk solution. The proposed *diffuse double layer* model was described by statistical mechanical means.³³⁻³⁶

The diffuse double layer model, however, is also unable to predict the observed experimental results. The failure of the Gouy-Chapman model can be largely attributed

to the treatment of ions as point charges. At high, polarizations, therefore, the distance between the metallic and solution phase charge zone unrealistically approaches zero.

Stern realised that a combination of the compact layer and diffuse layer models provides a more satisfactory description of the double layer structure.^{33,37} In this model the majority of the potential drop occurs across the compact layer, with the diffuse layer accommodating a much smaller and more gradual change in potential, as shown in figure 4.1.1. The Stern model successfully predicts the gross behavioural features observed in experimental systems.^{38,39}

It was also proposed by Stern that some ions can lose their solvation sheaths, at least in the direction of the electrode surface, and hence approach the electrode-solution interface very closely. Such ions are said to undergo *specific adsorption*. Neutral molecules and ions, especially anions, have been shown by electrocapillary methods to specifically adsorb at electrode surfaces.⁴⁰⁻⁴³ Specifically adsorbed species are tightly bound to the electrode surface and the locus of their centres forms the Inner Helmholtz Plane (IHP). Ions residing in the OHP, such as strongly hydrated cations, retain their solvation sheaths because of strong solvent-ion interactions. These ions experience only long-range interactions with the electrode surface and are said to be *nonspecifically adsorbed*.³³

The compact and diffuse layers of Stern's double layer model can be represented by elements of an electronic circuit. Figure 4.1.1 shows that the total galvanic potential drop ($\Delta\phi$) across the double layer is equal to the sum of the inner ($\Delta\phi_I$) and diffuse ($\Delta\phi_D$) layer components, such that

$$\Delta\phi = \Delta\phi_I + \Delta\phi_D \quad (4.1.15)$$

The double layer is, therefore, electrically equivalent to a pair of capacitors in series.

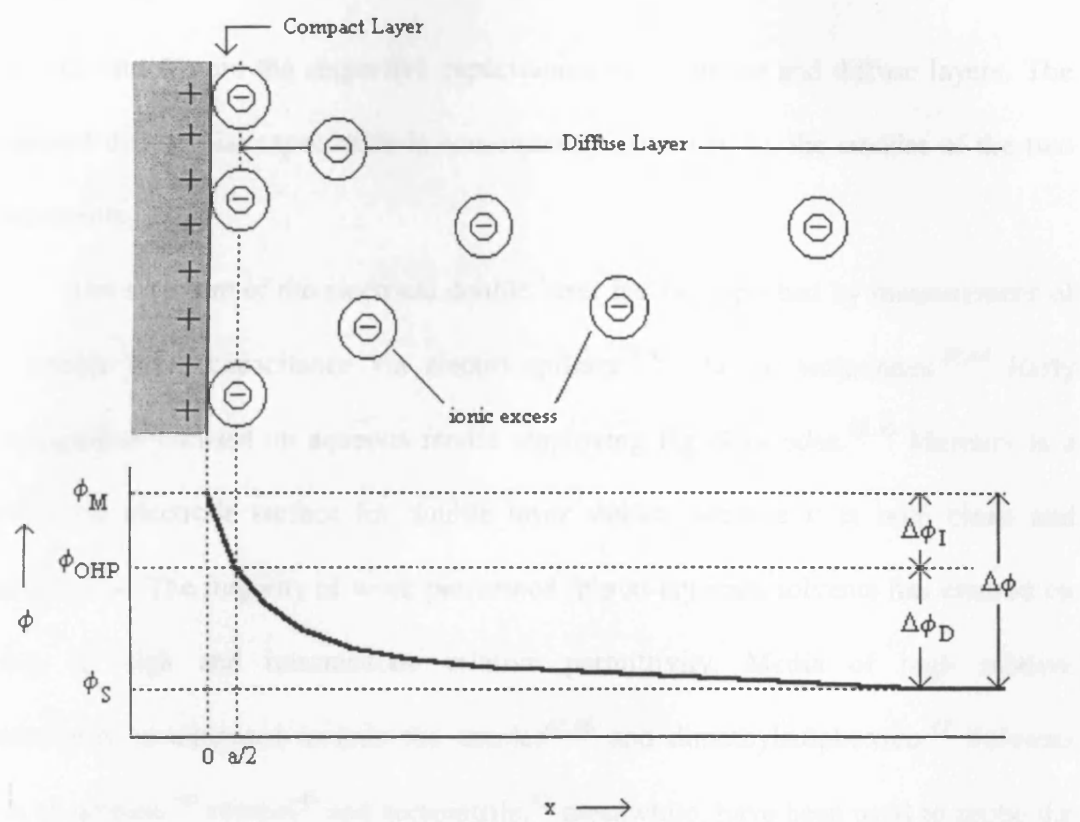


Figure 4.1.1 The electrical double layer

Hence, the total differential capacitance of the double layer is given by

$$\frac{1}{C_d} = \frac{1}{C_I} + \frac{1}{C_D} \quad (4.1.16)$$

where C_I and C_D are the respective capacitances of the inner and diffuse layers. The measured differential capacitance is consequently governed by the smaller of the two components.

The structure of the electrical double layer has been probed by measurement of the double layer capacitance via electrocapillary³⁹⁻⁴³ and ac techniques.^{33,44} Early investigations focused on aqueous media employing Hg electrodes.^{39,40} Mercury is a convenient electrode surface for double layer studies because it is both clean and reproducible. The majority of work performed in non-aqueous solvents has centred on media of high and intermediate relative permittivity. Media of high relative permittivity investigated include the amides^{45,46} and dimethylsulphoxide.⁴⁷ Solvents such as acetone,⁴⁸ ethanol⁴⁹ and acetonitrile,⁴² meanwhile, have been used to probe the metal-solution interface in media of intermediate ($\epsilon = 20-40$) relative permittivity. It has consequently been shown that in solvents of reduced relative permittivity the double layer structure is strongly dependent on ion-pairing effects.

More recent work has concentrated on media of low relative permittivity ($\epsilon < 10$). Tetrahydrofuran and 2-methyltetrahydrofuran were the first solvents to be studied with relative permittivities in this range.⁵⁰ Drogowska and Fawcett used these solvents to probe the mercury electrode-solution interface, and subsequently showed that diffuse layer structure is significantly affected by both ion pair and triple ion formation.

The capacitance of quaternary ammonium-based electrolytes in media of low relative permittivity was first studied by Long.⁵¹ Here tetrabutylammonium

tetrafluoroborate was employed as the electrolyte in solutions of dichloroethane ($\epsilon = 10.27$) and anisole ($\epsilon = 4.33$) whilst using a mercury electrode. Abbott and Harper have presented double layer capacitance data at a platinum electrode for a range of quaternary ammonium electrolytes in dichloroethane, anisole and cyclohexane ($\epsilon = 2.02$).⁴⁴ They investigated the effect of anion and cation size on the measured capacity in these three solvents. A preliminary result in supercritical CO₂ also suggested that the double layer structure differed to that in cyclohexane.⁵²

The aforementioned studies demonstrate that double layer structure in liquid solvents of all types has been thoroughly investigated. This is in stark contrast to the structure of the electrode-supercritical electrolyte interface, which remains basically unexplored. In this work, the structure of the double layer at the platinum electrode-electrolyte interface will be investigated in the case of a polar supercritical HFC solvent employing a tetraalkylammonium electrolyte. The effect of supercritical solvent density on the structure of the double layer will be presented.

4.1.4 Measurement of the Double Layer Capacitance via AC Methods

Electrocapillary techniques have commonly been used to determine the differential capacitance at mercury electrodes in both aqueous and non-aqueous electrolytes. Such techniques are not applicable to solid electrodes and electrolyte solutions at high pressure. AC impedance experiments permit the measurement of the solid electrode-electrolyte solution interfacial capacitance as a function of electrode potential.^{33,53}

In the ac experiment, a small amplitude sinusoidal voltage, E , is applied to the electrochemical cell, typically superimposed on an applied potential, E_{dc} ,

$$E = \Delta E \sin \omega t \quad (4.1.17)$$

where ΔE is the maximum amplitude of the sinusoidal voltage, ω is the angular frequency, which is 2π times the conventional frequency of perturbation in hertz, and t is the time. Although the sinusoidal current response, I , will have a frequency equal to that of the voltage, the amplitude and phase will differ. Hence,

$$I = \Delta I \sin(\omega t + \phi) \quad (4.1.18)$$

where ΔI is the maximum amplitude of the sinusoidal current and ϕ is the phase angle between the sinusoidal current and voltage. If the circuit is equivalent to a pure capacitor, the phase angle will be $-\pi/2$, as in the case of an ideally polarizable interface with negligible solution resistance. The phase angle will be zero, however, if the interphase behaves as a pure resistor. In reality, the electrochemical cell is equivalent to an electrical circuit with resistances and capacitances. Non-zero phases shifts are consequently observed, with $0 \leq \phi \leq -\pi/2$.

The impedance of an electrode reaction, Z , is defined by

$$E = IZ \quad (4.1.19)$$

where Z can be described by the complex quantity

$$Z(\omega) = Z' - jZ'' \quad (4.1.20)$$

where Z' and Z'' are the in-phase (real) and out-of-phase or quadrature (imaginary) components of the impedance, and $j = \sqrt{-1}$. In a typical ac experiment, both components of the cell impedance are measured as a function of the frequency of voltage perturbation by employing a frequency response analyser.

A lone resistor has an impedance equal to the resistance because there is no imaginary component. The impedance of a capacitor, Z_c , however, has no real component and can be described by

$$Z_c = -\frac{j}{\omega C} \quad (4.1.21)$$

where C is the capacitance. The impedance of a capacitor and resistor in series is, therefore, given by

$$Z(\omega) = R - \frac{j}{\omega C} \quad (4.1.22)$$

whereas for a capacitor and resistor in parallel,

$$\frac{1}{Z(\omega)} = \frac{1}{R} - \frac{j\omega C}{1} \quad (4.1.23)$$

In ac impedance experiments, the results are commonly presented as a ‘Nyquist plot’ or ‘Argand diagram’, where Z'' is plotted against Z' over the range of applied frequencies. The magnitude of the impedance, $|Z|$, and the phase angle, ϕ , are then given by

$$|Z| = [(Z')^2 + (Z'')^2]^{1/2} \quad (4.1.24)$$

and

$$\tan \phi = \frac{Z''}{Z'} \quad (4.1.25)$$

The electron transfer reaction of many electrochemical systems can be represented by a series combination of the charge transfer resistance, R_{ct} , and the Warburg impedance, Z_w . The Warburg impedance models the effect of diffusion and is frequency dependent. If $Z_w \ll R_{ct}$, the electrochemical cell can be represented by the equivalent circuit shown in figure 4.1.2. The double layer capacitance is equivalent to a

pure capacitance and is represented by the circuit element C_{dl} . R_u is the uncompensated solution resistance of the electrolyte solution. The impedance of the equivalent circuit displayed in figure 4.1.2 is

$$Z(\omega) = R_u + \frac{R_c}{1 + j\omega C_{dl} R_c} \quad (4.1.26)$$

The real and imaginary components of the impedance can then be separated as follows

$$\begin{aligned} Z(\omega) &= R_u + \frac{R_c}{1 + j\omega C_{dl} R_c} \times \frac{1 - j\omega C_{dl} R_c}{1 - j\omega C_{dl} R_c} \\ &= R_u + \frac{R_c}{1 + (\omega C_{dl} R_c)^2} - j \left[\frac{\omega C_{dl} R_c^2}{1 + (\omega C_{dl} R_c)^2} \right] \end{aligned} \quad (4.1.27)$$

Equation (4.1.27) results in the semi-circular Nyquist plot illustrated in figure 4.1.3.

The double layer capacitance can be derived from the maximum of this plot, where

$$R_c C_{dl} \omega_{max} = 1 \quad (4.1.28)$$

and ω_{max} corresponds to the ac frequency of highest imaginary impedance component.

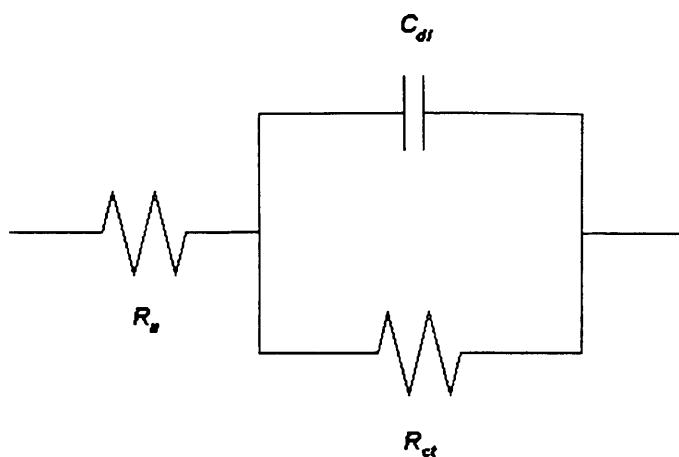


Figure 4.1.2 Equivalent circuit of an electrochemical cell where there is a parallel RC circuit in series with the uncompensated solution resistance, R_u

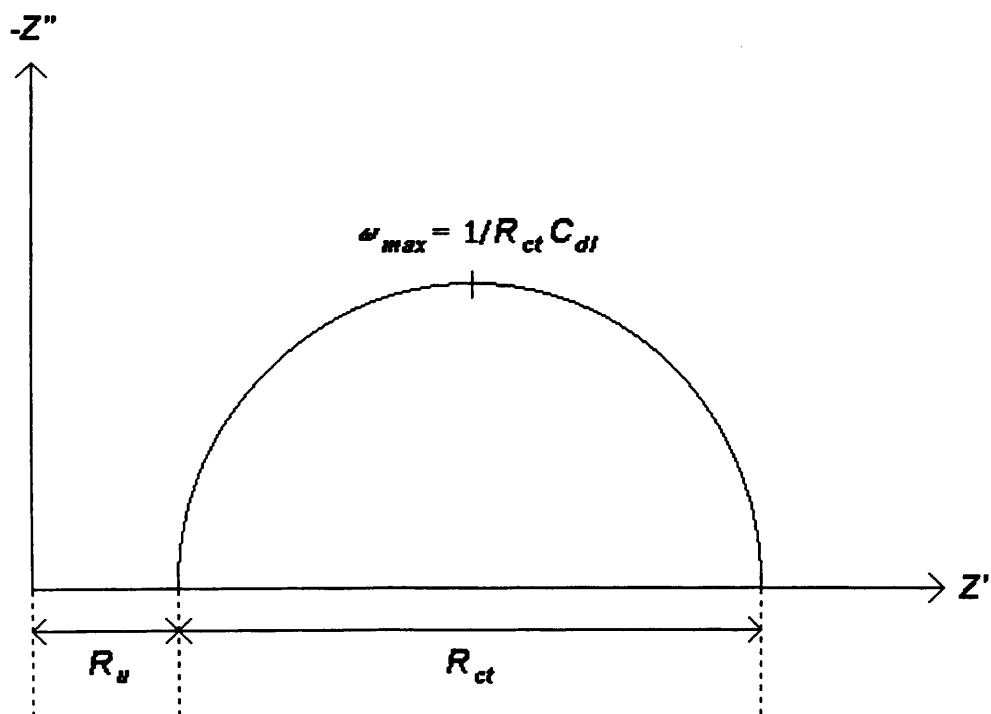


Figure 4.1.3 Nyquist plot for the equivalent circuit of figure 4.1.2

4.2 Results and discussion

4.2.1 Electrical Conductivity of Liquid and Supercritical Hydrofluorocarbons

Figures 4.2.1 and 4.2.2 show the conductivity, κ , of TBABF₄ in liquid HFC 134a and HFC 32 respectively at 30 °C and a range of electrolyte concentrations. The form of both plots is very similar, although the conductivity of TBABF₄ is considerably greater in liquid HFC 32 over the studied concentration range. At a fixed electrolyte concentration in either solvent, the conductivity increases with increasing fluid pressure. This effect can be ascribed to the increase in solvent relative permittivity with increasing pressure and the consequent decrease in the extent of electrolyte ion association.

Figures 4.2.3 and 4.2.4 display the molar conductivity of TBABF₄ in both liquid HFC 134a and HFC 32 as a function of the square root of electrolyte concentration at 30 °C and a variety of fluid pressures. In the absence of ion aggregation, the molar conductivity should decrease linearly with the square root of electrolyte concentration in accordance with Kohlrausch's law.^{1,54} Figure 4.2.3, therefore, signifies that the TBABF₄ electrolyte undergoes ion association in liquid HFC 134a. At each fluid pressure in figure 4.2.3, at a TBABF₄ concentration of approximately 14 mM, there is a minimum in the molar conductivity that corresponds to a change in the dominant charge carriers from single ions to triple ions. The plot also shows that at a constant electrolyte concentration, the molar conductivity increases with increasing fluid pressure. This is in contrast to many non-aqueous liquid electrolytes, where an increase in the pressure results in a decrease in the molar conductivity due to the concomitant increase in fluid viscosity.⁵⁵ This increase in molar

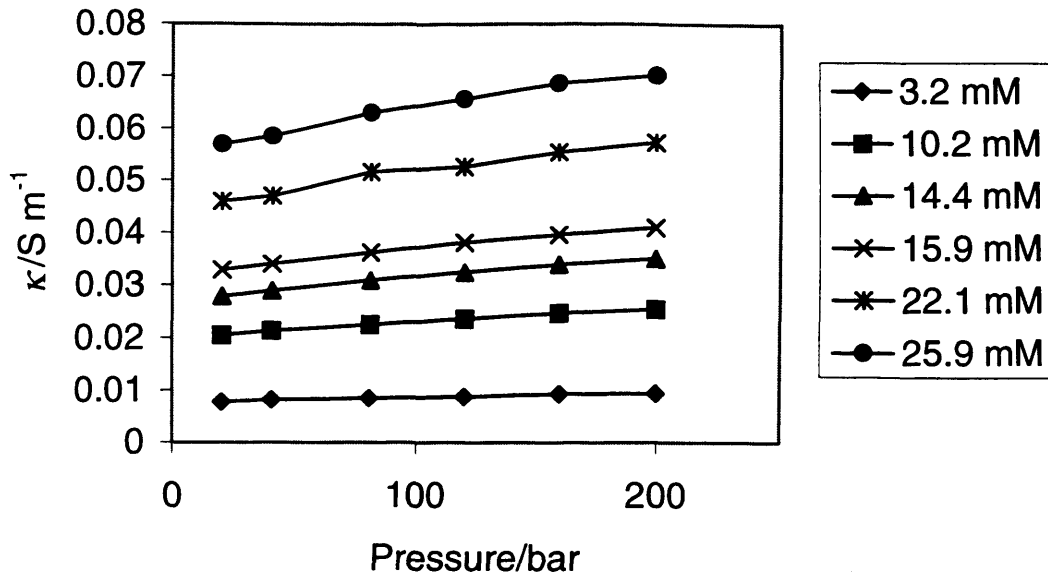


Figure 4.2.1 Conductivity of TBABF₄ in HFC 134a as a function of pressure at 30 °C and a variety of electrolyte concentrations

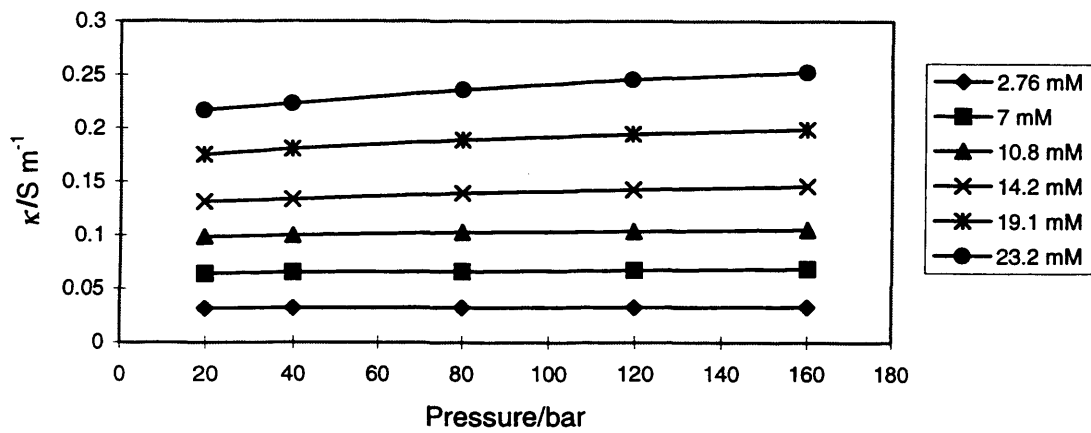


Figure 4.2.2 Conductivity of TBABF₄ in HFC 32 as a function of pressure at 30 °C and a variety of electrolyte concentrations

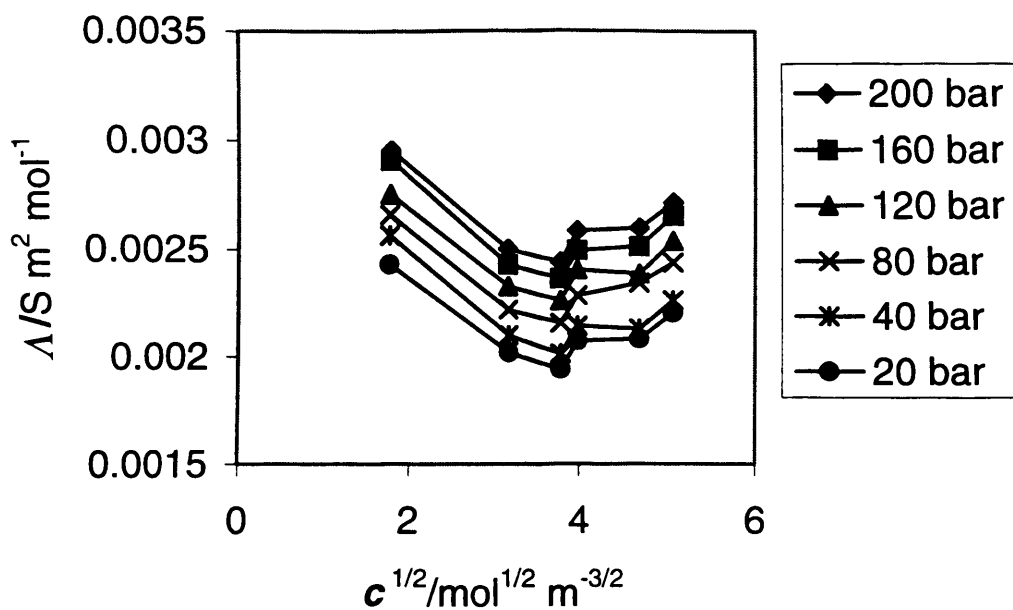


Figure 4.2.3 Molar conductivity of TBABF₄ in HFC 134a as a function of concentration at 30 °C and a variety of fluid pressures

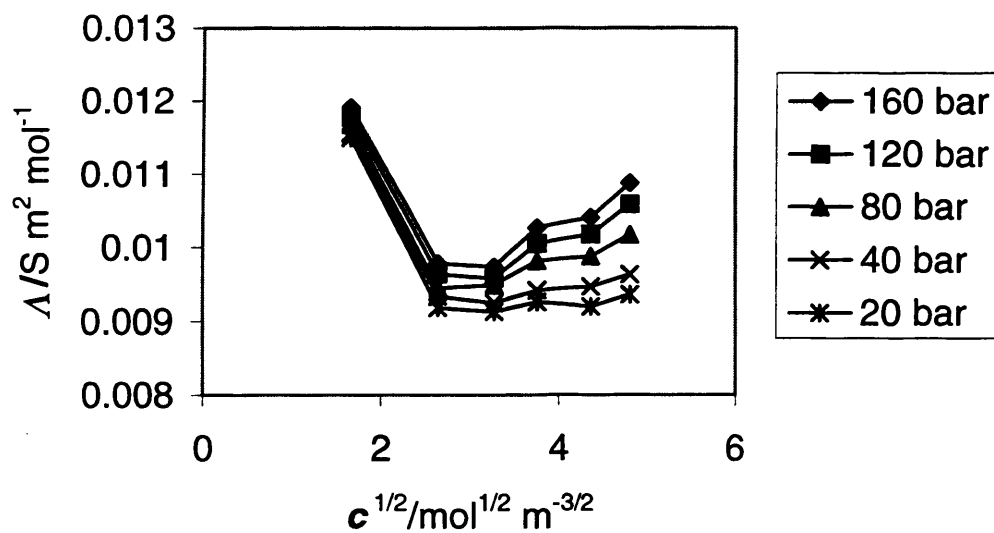


Figure 4.2.4 Molar conductivity of TBABF₄ in HFC 32 as a function of concentration at 30 °C and a variety of fluid pressures

conductivity can be attributed to the increase in fluid relative permittivity with pressure, which decreases the extent of ion-pairing in solution.

When considering TBABF₄ in liquid HFC 32, the plot of figure 4.2.4 also indicates that both single ions and triple ions contribute significantly to the conductivity of the solution at levels governed by the electrolyte concentration and fluid pressure. As for TBABF₄ in liquid HFC 134a, Λ increases with increasing pressure as a consequence of reduced ion aggregation.

The molar conductivity of TBABF₄ in liquid HFC 32 is considerably higher than that in liquid HFC 134a at each electrolyte concentration studied at 30 °C and fixed pressure. This difference can be attributed to the greater relative permittivity (see Appendix) and lower viscosity⁵⁶⁻⁵⁸ of HFC 32 compared to HFC 134a at 30 °C over the studied pressure range, as shown in table 4.2.1. The extent of ion-pairing will, therefore, be smaller in HFC 32 and the charge carriers will also display higher mobilities.

Solvent	ϵ	η/cP	c/mM	$\Lambda \times 10^3/S\ m^2\ mol^{-1}$
HFC 134a	9.7	0.221	14.4	2.26
HFC 32	13.4	0.130	14.2	10.06

Table 4.2.1 A comparison of the molar conductivity of TBABF₄ in liquid HFC 134a and HFC 32 at a similar concentration, c , at 30 °C and 120 bar

If the equilibria between free ions, ion pairs and triple ions can be described by Fuoss-Kraus theory in a liquid electrolyte, a plot of $\Lambda c^{1/2}$ against c should be linear in

accordance with equation (4.1.10). Plots of this type displayed in figures 4.2.5 and 4.2.6 for HFC 134a and HFC 32 at 30 °C show a convincing linear correlation between $\Lambda c^{1/2}$ and c at all the fluid pressures studied. The equilibrium constants for ion pair dissociation, K_P , and triple ion dissociation, K_T , were therefore calculated at a range of fluid pressures by application of equation (4.1.10). Values of the limiting molar conductivity of TBABF₄ in HFC 134a and HFC 32 were calculated using Walden's rule (equation (4.1.11)), where the Walden constant was taken as 4.34×10^{-6} S kg m mol⁻¹ s⁻¹.^{10,11} The viscosity of HFC 134a was calculated from the equation of state of Okubo *et al.*,⁵⁶ whereas that of HFC 32 was computed from the equation of Steil and Thodos⁵⁷ using literature values of the dilute gas viscosity.⁵⁸ The resulting plots of K_P and K_T as a function of pressure are shown in figures 4.2.7, and 4.2.8, respectively, for TBABF₄ in both liquid HFC 134a and HFC 32 at 30 °C.

The K_P values for TBABF₄ in HFC 32 are considerably larger than those in HFC 134a at 30 °C, as expected. Ion-pairing is less favored in HFC 32 because of the higher relative permittivity of the medium. In both solvents, however, K_P increases roughly linearly with pressure. Here the increased relative permittivity will enable the solvent to stabilize the charged species. K_T , however, exhibits a lower sensitivity to pressure than K_P in both the HFC 134a and HFC 32 liquid electrolytes. This phenomenon may result from the lower sensitivity of K_T to changing relative permittivity as has been previously observed for TBABF₄ in liquid media of low relative permittivity.¹¹

K_P and K_T can be used to calculate both the degree of dissociation for the ion pair and triple ion through equations (4.1.5) and (4.1.6) respectively. Over the concentration range studied, the degree of ion pair dissociation, α , in HFC 32 is

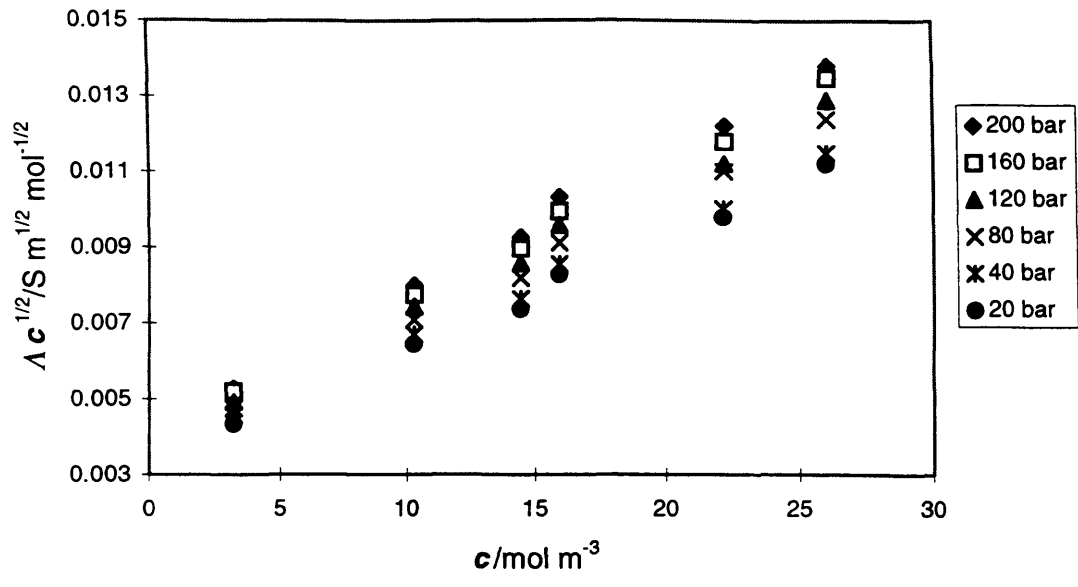


Figure 4.2.5 $\Lambda c^{1/2}$ as a function of TBABF₄ concentration in HFC 134a at 30 °C and a variety of pressures

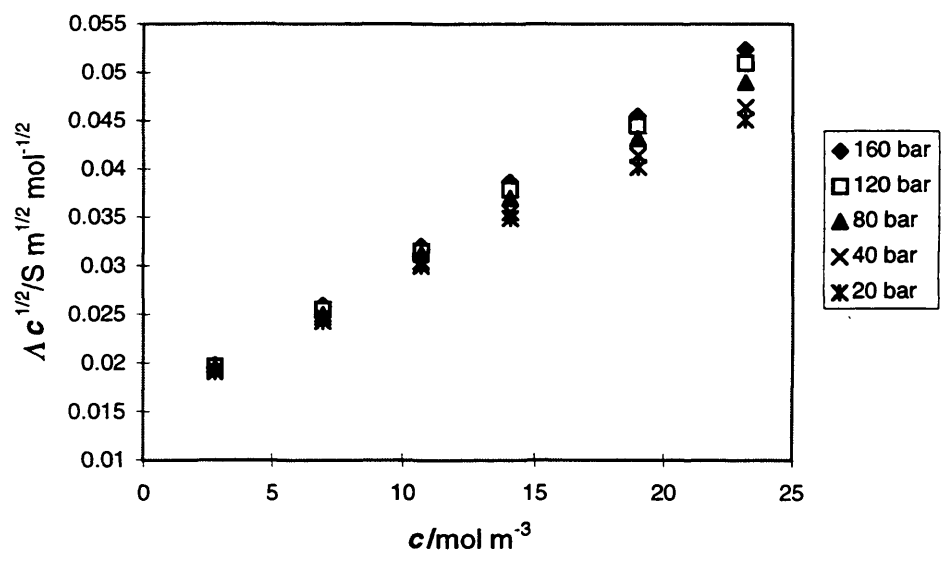


Figure 4.2.6 $\Lambda c^{1/2}$ as a function of TBABF₄ concentration in HFC 32 at 30 °C and a variety of pressures

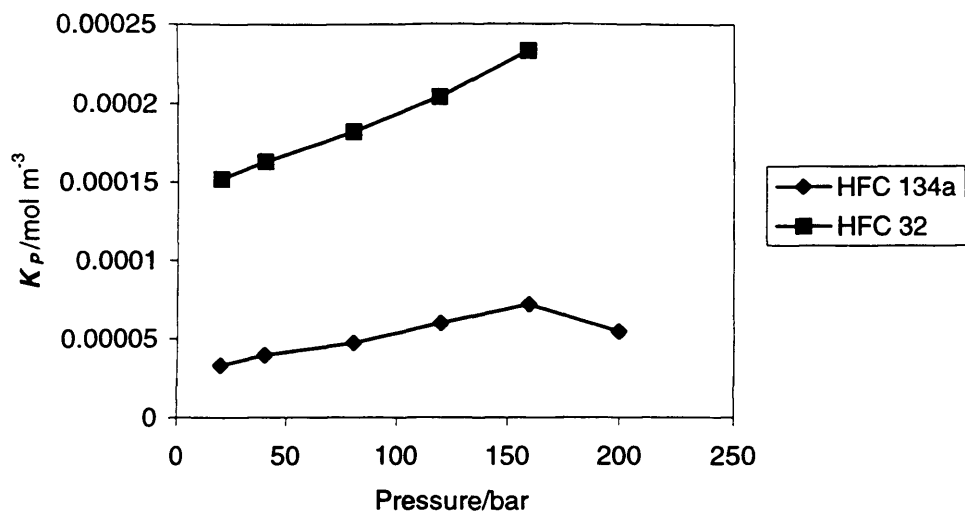


Figure 4.2.7 K_p as a function of pressure for TBABF_4 in HFC 134a and HFC 32 at 30 °C

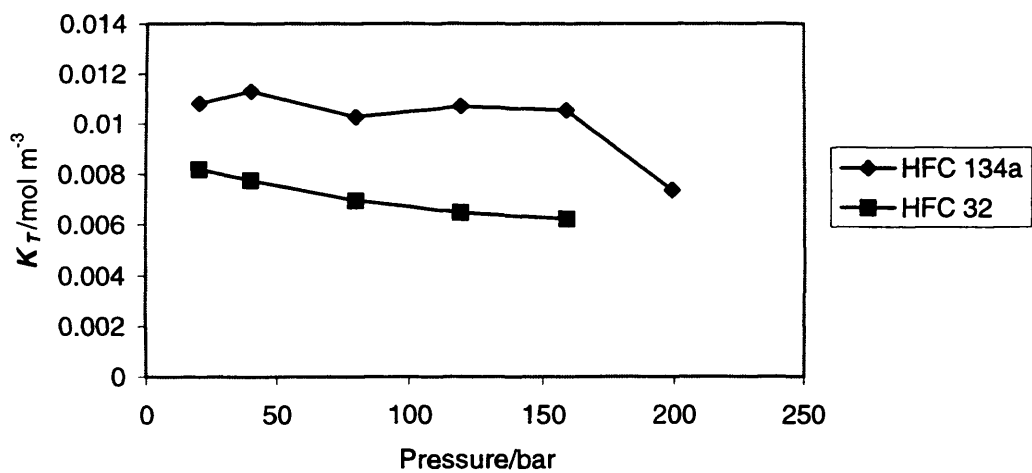


Figure 4.2.8 K_T as a function of pressure for TBABF_4 in HFC 134a and HFC 32 at 30 °C

is approximately double that in HFC 134a at 30 °C, as exemplified in figure 4.2.9 at 160 bar. Figure 4.2.10 compares the degree of dissociation for the triple ions, α_T , at 30 °C and 160 bar in HFC 134a and HFC 32. Comparison of figures 4.2.9 and 4.2.10 illustrates that for HFC 134a triple ions become the major charge carrier in solution at a concentration of around 10 mM, whereas in HFC 32 this transition corresponds to a lower concentration of approximately 6 mM.

The molar conductivity of TBABF₄ has been shown to be far greater in liquid HFC 32 than in liquid HFC 134a at 30 °C. It is, therefore, implied that HFC 32 is the more useful solvent for use in supercritical electrochemistry because it also exhibits a lower critical temperature than HFC 134a. The remainder of this section will consequently focus on the conductivity of TBABF₄ in HFC 32 at temperatures slightly below and above the critical temperature ($T_c = 78.11$ °C).

The conductivity of TBABF₄ in liquid HFC 32 at 70 °C and supercritical HFC 32 at 90 °C is shown in figures 4.2.11 and 4.2.12, respectively, as a function of pressure at various concentrations. The conductivities at both temperatures are of the same order of magnitude as those observed in the liquid phase at 30 °C in figure 4.2.2. It is, therefore, implied the increase in ion mobility expected at higher temperatures is offset by an increase in ion aggregation caused by the reduction in solvent relative permittivity. The pressure dependence of the conductivity is highest in the supercritical phase, where the high compressibility of the fluid leads to large changes in relative permittivity with pressure. The constant electrolyte concentration plots of figure 4.2.12 converge around the critical pressure, where the low relative permittivity of the medium should lead to significant ion pair formation.

Figures 4.2.13 and 4.2.14 show the molar conductivities of TBABF₄ in HFC 32

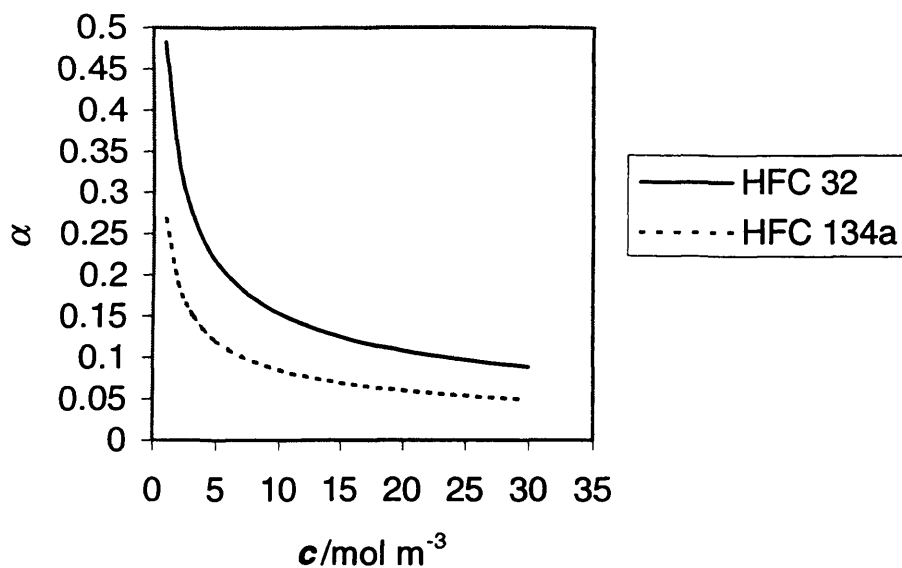


Figure 4.2.9 α as a function of TBABF₄ concentration in both HFC 134a and HFC 32 at 30 °C and 160 bar

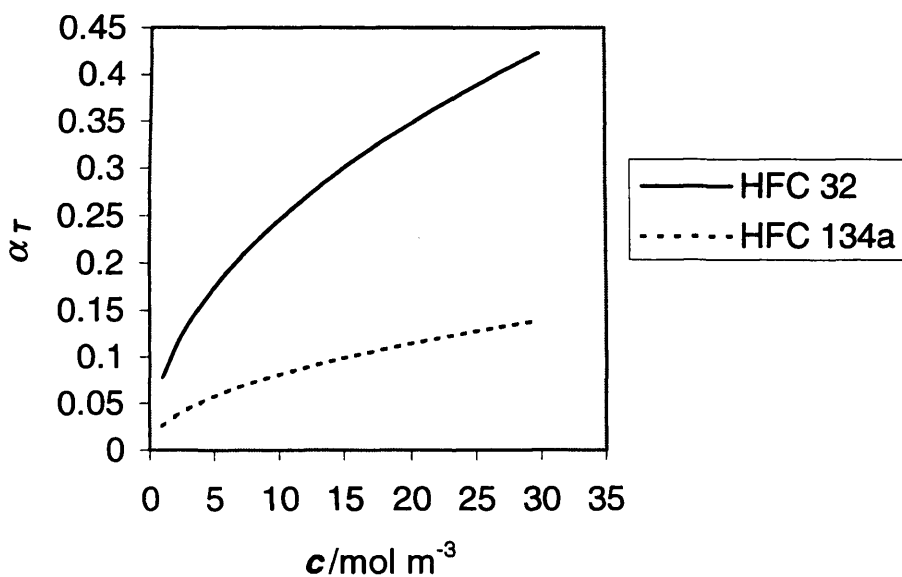


Figure 4.2.10 α_T as a function of TBABF₄ concentration in both HFC 134a and HFC 32 at 30 °C and 160 bar

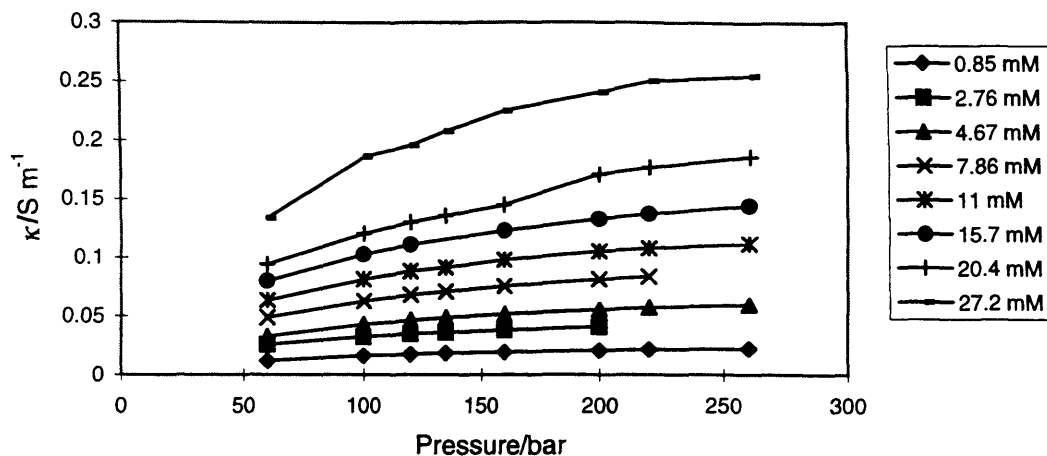


Figure 4.2.11 Conductivity of TBABF₄ in HFC 32 as a function of pressure at 70 °C and a variety of electrolyte concentrations

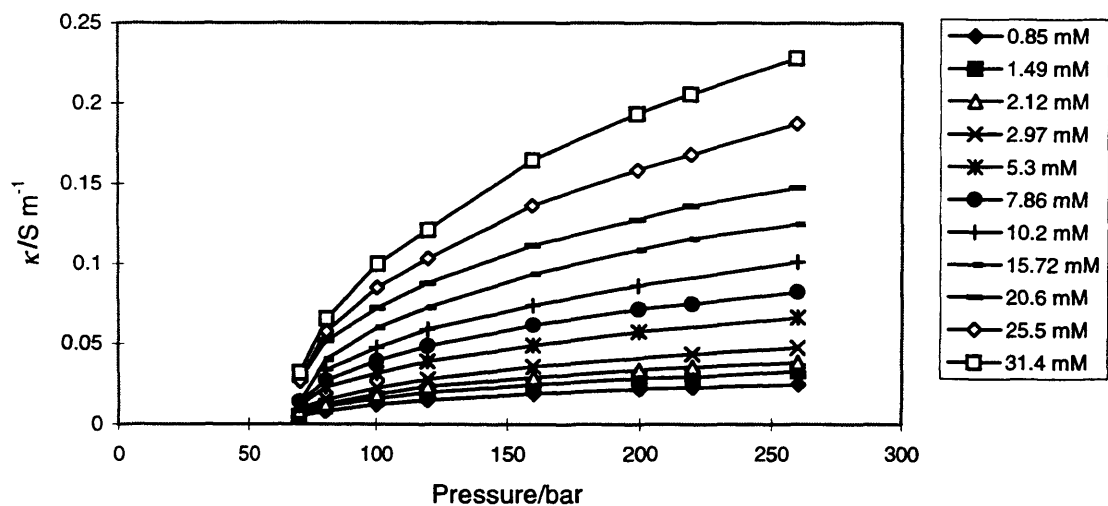


Figure 4.2.12 Conductivity of TBABF₄ in supercritical HFC 32 as a function of pressure at 90 °C and a variety of electrolyte concentrations

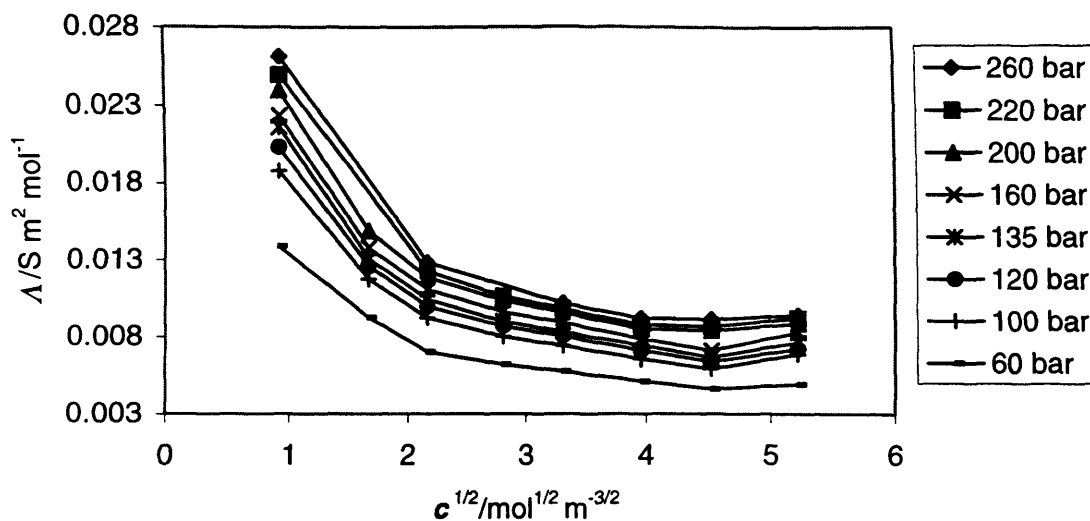


Figure 4.2.13 Molar conductivity of TBABF₄ in HFC 32 as a function of concentration at 70 °C and a variety of fluid pressures

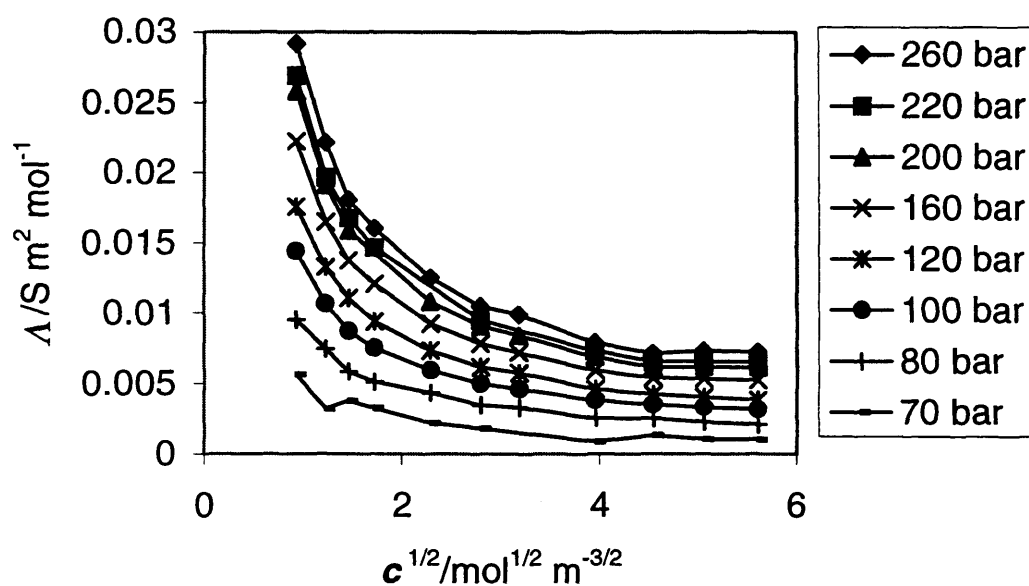


Figure 4.2.14 Molar conductivity of TBABF₄ in supercritical HFC 32 as a function of concentration at 90 °C and a variety of fluid pressures

at 70 °C and 90 °C as a function of the square root of electrolyte concentration. The shape of both sets of plots indicates that ion-pairing is prevalent.

The relatively high molar conductivity of TBABF₄ in supercritical HFC 32 suggests that this solvent-electrolyte system may be particularly suited for use in supercritical electrochemistry. The conductivity of this supercritical medium is far greater than that of the same electrolyte in supercritical chlorodifluoromethane (CDFM), a medium recently recommended for its high electrical conductivity and low critical temperature.³⁰ This difference can be ascribed to the higher relative permittivity and lower viscosity of HFC 32, as shown in table 4.2.2 together with a comparison of the molar conductivities. HFC 32 also holds the advantage of a lower critical temperature than CDFM.

Solvent	$T_c/^\circ\text{C}$	ϵ	$T/^\circ\text{C}$	p/bar	η/cP	c/mM	$\Lambda \times 10^4/\text{S m}^2 \text{mol}^{-1}$
HFC 32	78.11	6.0	90	100	0.0488	10.2	46.3
CDFM	96.15	2.31	115	100	0.0691	10.0	1.89

Table 4.2.2 A comparison of the molar conductivity of TBABF₄ in supercritical HFC 32 and CDFM at similar temperatures and concentrations

The linear correlation observed between $\Lambda c^{1/2}$ and c in figures 4.2.5 and 4.2.6 demonstrated that Fuoss-Kraus theory can be applied to liquid HFC solvent-electrolyte systems. Figure 4.2.15 subsequently shows that Fuoss-Kraus theory can also be used to model ion aggregation equilibria in supercritical HFC 32. Figures 4.2.16 and 4.2.17 display the pressure dependence of K_P and K_T , calculated from equation (4.1.10) for

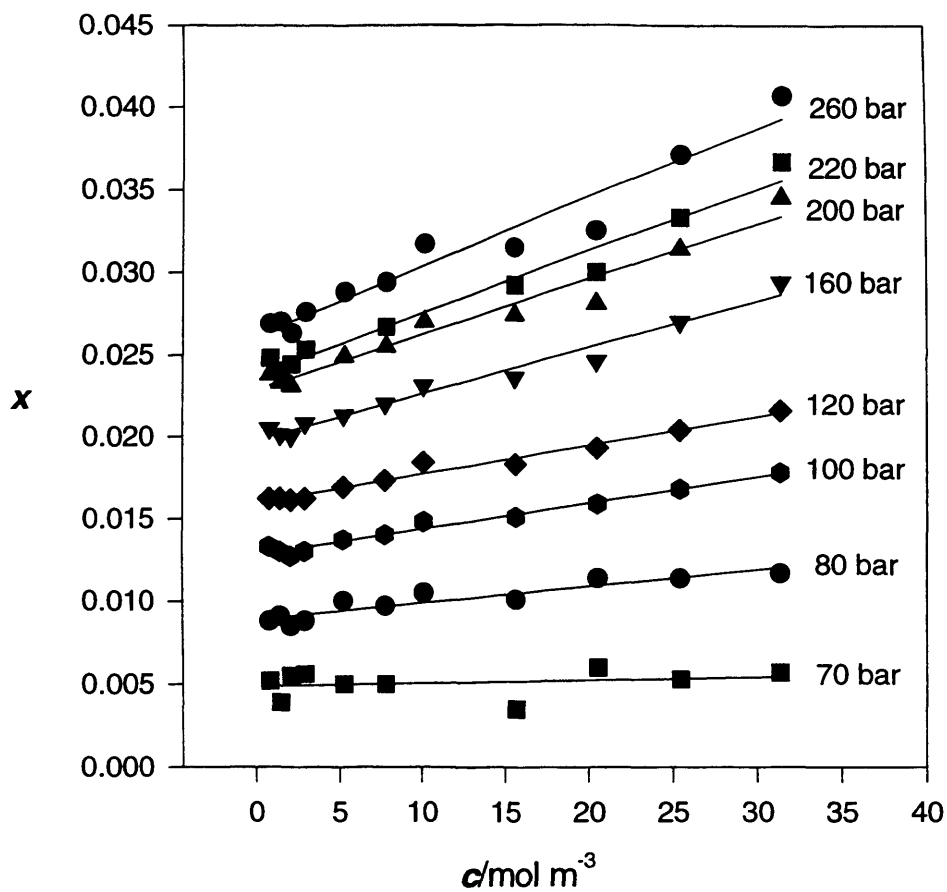


Figure 4.2.15 $\Lambda c^{1/2}$ as a function of TBABF₄ concentration in HFC 32 at 90 °C and a variety of pressures, where $x = \Lambda c^{1/2}/S \text{ m}^{1/2} \text{ mol}^{-1/2}$

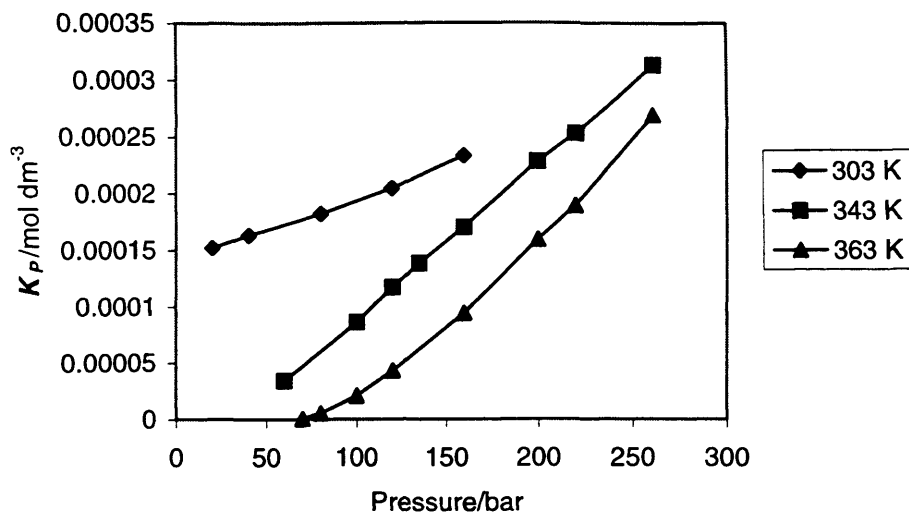


Figure 4.2.16 K_P as a function of pressure for TBABF₄ in HFC 32 at a variety of different temperatures

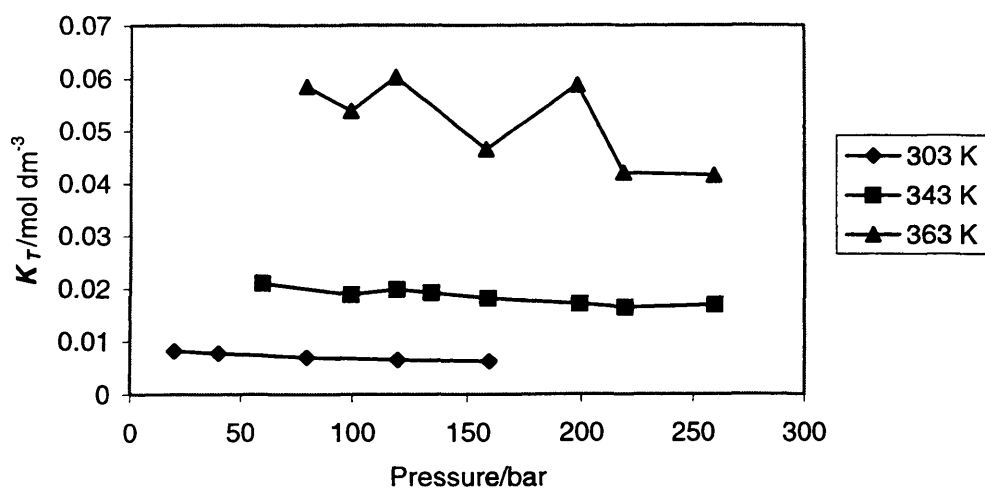


Figure 4.2.17 K_T as a function of pressure for TBABF₄ in HFC 32 at a variety of different temperatures

TBABF₄ in HFC 32 at 30, 70 and 90 °C. At each temperature, K_P increases roughly linearly with increasing pressure. This phenomenon can again be attributed to the increase in the relative permittivity of the medium with increasing pressure. At constant pressure, K_P increases with decreasing temperature. This effect can also be accredited to the change in relative permittivity of the medium.

The degree of dissociation for both the ion pairs and triple ions can be calculated from K_P and K_T using equations (4.1.5) and (4.1.6). Figure 4.2.18 shows the degree of dissociation of TBABF₄ ion pairs as a function of electrolyte concentration in both liquid and supercritical HFC 32 at 160 bar. The plots show that at constant electrolyte concentration, the degree of ion association increases with increasing temperature due to the decrease in relative permittivity. Figure 4.2.19 shows the variation of α_T with electrolyte concentration for TBABF₄ in HFC 32 at conditions equal to those presented in figure 4.2.18. At constant electrolyte concentration, α_T decreases quite dramatically with increasing temperature. It has previously been shown that triple ions become more stable with respect to the single ion as the relative permittivity of the medium decreases at constant temperature.^{11,59} It can, therefore, be assumed that the decrease in α_T with increasing temperature is not a consequence of the decreasing relative permittivity. It has already been shown that K_T increases with increasing temperature in figure 4.2.17. These results, therefore, imply that the process of triple ion dissociation is endothermic in HFC 32.

In solution at constant temperature, the pressure dependence of an equilibrium constant, K , can be expressed by the following thermodynamic relation⁶⁰

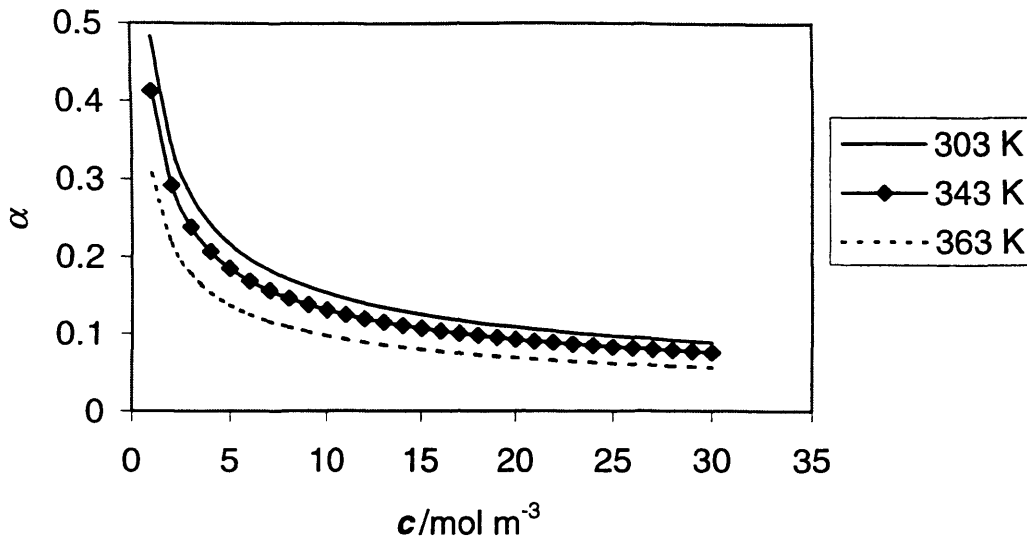


Figure 4.2.18 α as a function of TBABF₄ concentration in HFC 32 at 160 bar and a variety of temperatures

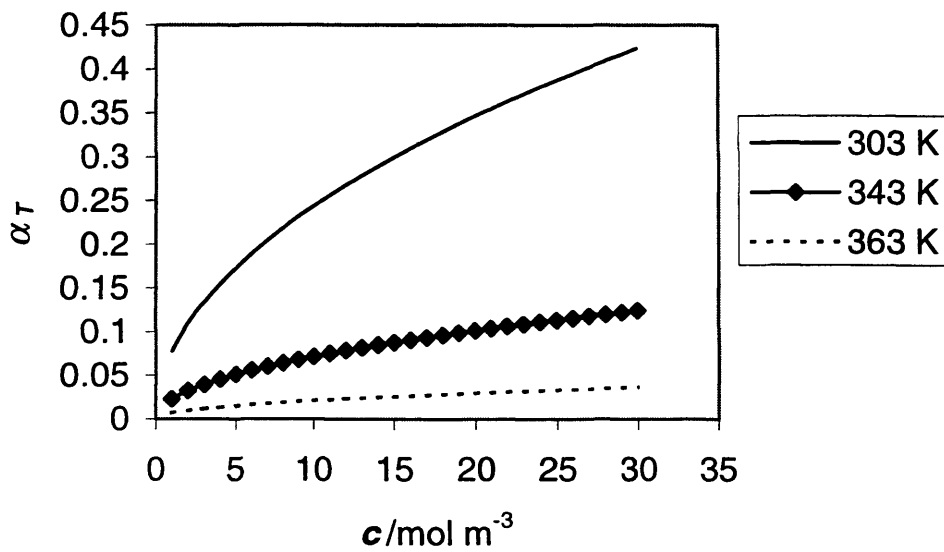


Figure 4.2.19 α_T as a function of TBABF₄ concentration in HFC 32 at 160 bar and a variety of temperatures

$$\left(\frac{\partial \ln K}{\partial p}\right)_T = -\frac{\Delta V^\circ}{RT} \quad (4.2.1)$$

where ΔV° is the standard volume of reaction, the change in volume between the standard states of the reactants and products. The slope of a plot of $\ln K_P$ versus pressure at constant temperature should, therefore, provide the volume of reaction associated with ion pair dissociation. Plots of this type are shown for TBABF₄ in both liquid and supercritical HFC 32 in figure 4.2.20. At 30 °C the plot is linear ($r = 0.999$) over the pressure range studied with a slope yielding a volume of reaction of $-75.3 \text{ cm}^3 \text{ mol}^{-1}$. This value is similar in magnitude to ΔV° values previously calculated for tetrabutylammonium picrate in a variety of media of low relative permittivity.^{61,62} The decrease in ΔV° calculated in the current work can be attributed to the change in ion solvation during ion pair dissociation.⁶³ When the temperature is increased to 70 °C the plot is non-linear implying that the volume change associated with ion pair dissociation becomes less negative with increasing pressure. In the supercritical phase at 90 °C, the curvature of the plot is more pronounced and divergence occurs as the pressure approaches that of the critical point. At first it appears that the volume of the ion pair increases dramatically as the pressure of the supercritical system is lowered, leading to more a negative volume of reaction. It must be noted, however, that the compressibility, $\Delta\beta^\circ$, describes the pressure dependence of ΔV° ⁶⁰

$$\left(\frac{\partial \Delta V^\circ}{\partial p}\right)_T = \Delta\beta^\circ \quad (4.2.2)$$

The divergence exhibited in the supercritical plot of figure 4.2.20 can, therefore, be partially ascribed to the divergence of the compressibility as the pressure tends towards critical. As the temperature of the system is lowered to 303 K, the compressibility of the fluid will decrease dramatically yielding a volume of ion pair dissociation that is

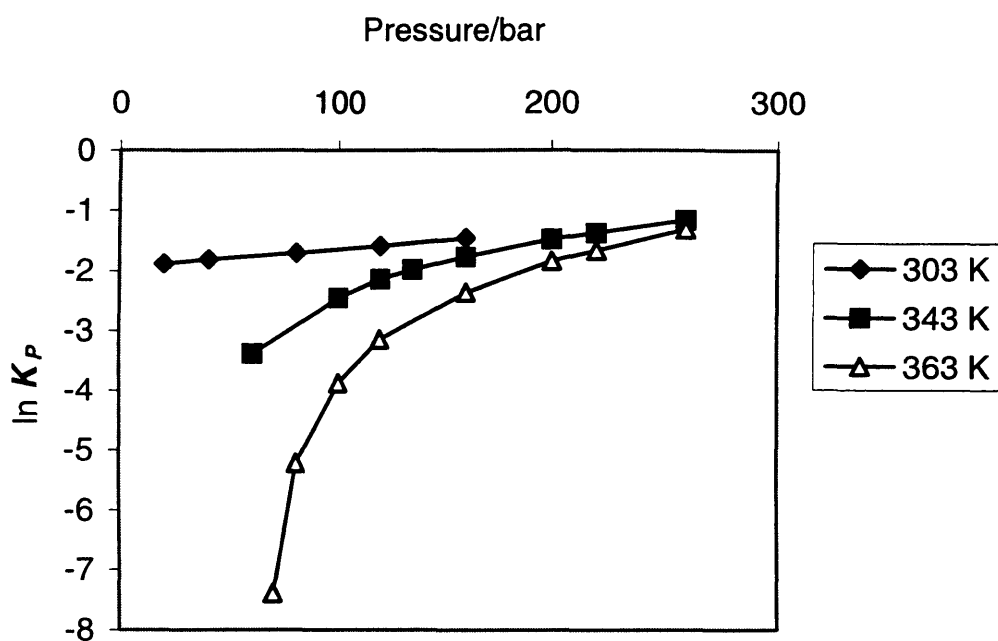


Figure 4.2.20 The pressure dependence of $\ln K_P$ for TBABF₄ in both liquid and supercritical HFC 32

relatively independent of pressure.

Fuoss and Kraus studied ion association in media over a wide range of relative permittivity.⁶ Employing the Bjerrum theory of association, it was shown that the dissociation constant of a non-dipolar 1-1 electrolyte can generally be expressed as

$$\frac{1}{K_p} = A_0 \exp\left(\frac{e^2}{4\pi a \epsilon \epsilon_0 k_B T}\right) \quad (4.2.3)$$

where A_0 is a pre-exponential constant, e is the charge of an electron and a is the distance of closest approach of the two ions. A plot of $\ln(1/K_p)$ versus $1/\epsilon$ should, therefore, be linear for systems that can be described by the thermodynamic approach of Fuoss and Kraus. Figure 4.2.21 shows plots of this type for TBABF₄ in liquid HFC 32 at 30 °C and 70 °C, and in supercritical HFC 32 at 90 °C. Good linear correlations ($r > 0.988$) are observed at each temperature. These results suggest that at each temperature a is independent of pressure over the studied range. At the temperatures of 30, 70 and 90 °C the calculated a values are 11.68, 5.61 and 5.16 Å, respectively. The a values at 70 and 90 °C are in reasonable agreement with those previously published for TBABF₄ in media of low relative permittivity.¹¹ The high a value at 30 °C may be a consequence of the narrow range of ϵ over which K_p values were obtained at this temperature. The strong linear correlation at 90 °C ($r = 0.999$) also suggests that at fixed concentration ion association is purely governed by the temperature and relative permittivity of the medium, independent of whether the conducting phase is liquid or supercritical.

In section 3.2.2, it was shown that local density augmentation can occur in supercritical HFC 32 at 90 °C at densities close to critical. If the critical phenomenon of local density augmentation affects the ion-pairing equilibrium represented in

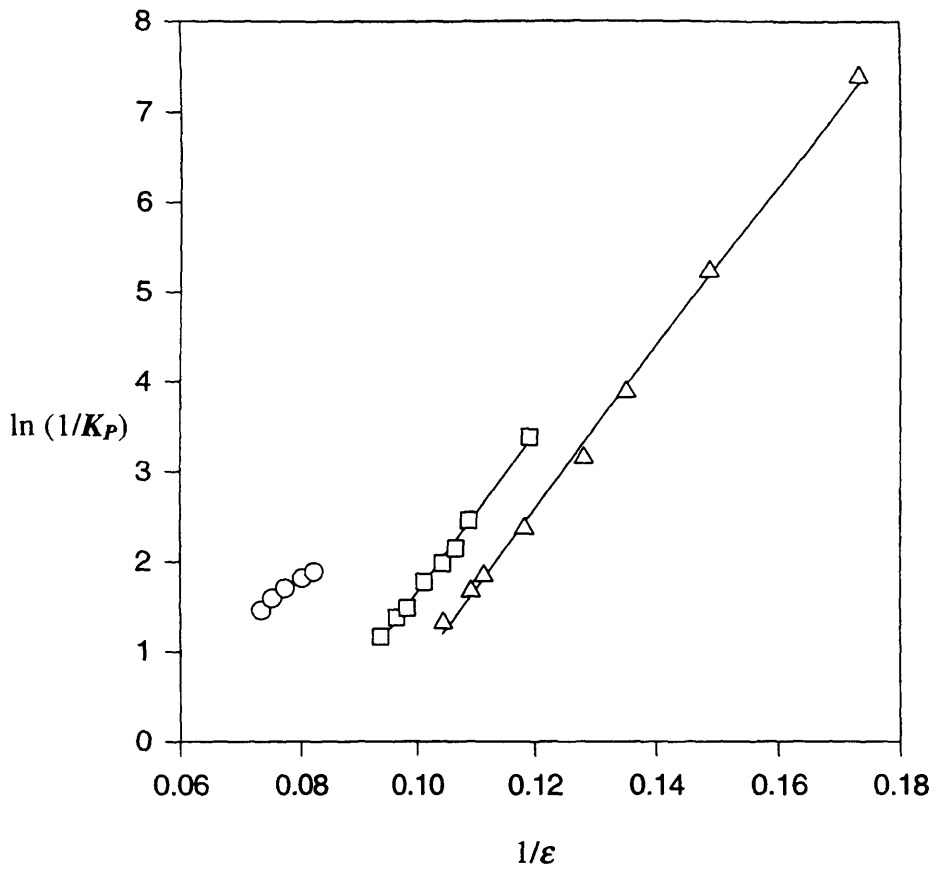


Figure 4.2.21 Variation of $\ln(1/K_p)$ with $1/\epsilon$ for TBABF_4 in HFC 32 at 30 °C (O), 70 °C (□) and 90 °C (Δ)

equation (4.1.2), a plot of $\ln K_p$ against solvent reduced density would be non-linear. Ideally, this plot would display three density regions indicative of solvent density inhomogeneities.⁶⁴ Figure 4.2.22 shows, however, that there is a strong linear correlation ($r = 0.998$) between $\ln K_p$ and reduced density for TBABF₄ in supercritical HFC 32 at 90 °C. It can, therefore, be concluded that it is the bulk relative permittivity, and not the local environment around the solute, that governs the extent of ion association in the supercritical phase.

These studies have shown that highly conducting solutions can be obtained with TBABF₄ in both HFC 134a and HFC 32. Charge is carried by both single and triple ions, the proportions of which are governed by the overall electrolyte concentration and the relative permittivity of the solution in both the liquid and supercritical states.

4.2.2 The Potential Windows of HFC 134a and HFC 32

Although pure HFC 134a and HFC 32 are highly resistive in the liquid state, voltammetry can be performed in these phases when employing a platinum microelectrode. Figure 4.2.23 shows a voltammogram recorded in neat HFC 134a in the liquid state at -78 °C and atmospheric pressure. Separate working electrodes were used for the positive and negative potential scans, with each sweep originating from 0 V. All potential windows presented in the current work were recorded in this manner. The voltammogram in figure 4.2.23 does not exhibit a solvent oxidation limit at potentials up to +10 V, the upper limit of the potentiostat. A reduction limit, however, is observed at -1.75 V, probably due to the reduction of O₂ as has previously been observed in neat chlorodifluoromethane.⁶⁵ Over the potential range of +10 to -1.8 V

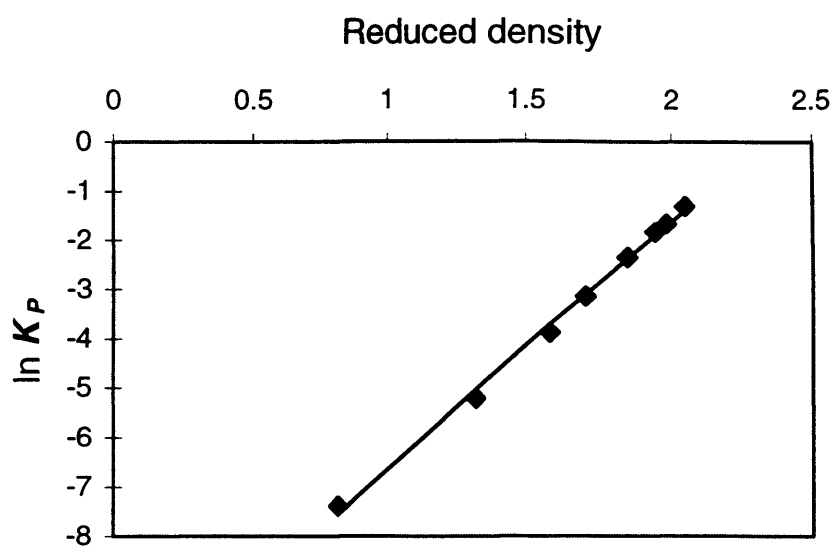


Figure 4.2.22 Variation in $\ln K_P$ with reduced density for TBABF₄ in supercritical HFC 32 at 90 °C

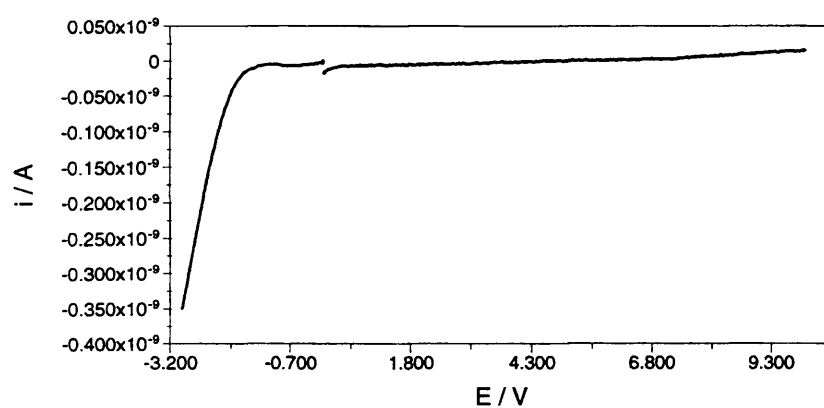


Figure 4.2.23 Voltammogram recorded at a 10 μm diameter Pt disc microelectrode in liquid HFC 134a at -78 °C and atmospheric pressure at a scan rate of 50 mV s^{-1}

the current density is considerably less than 1 mA cm^{-2} . The lack of an anodic potential limit in the studied range demonstrates the great electrochemical stability of the solvent and implies that novel oxidation electrochemistry can be performed in liquid HFC 134a if a suitably stable electrolyte is employed.

As the temperature of liquid HFC 134a is increased, a reduction in the width of the potential window is observed. This trend is illustrated by the linear sweep voltammogram recorded in neat liquid HFC 134a at $25 \text{ }^\circ\text{C}$ and 25 bar in figure 4.2.24. Although the cathodic potential limit of the solvent is relatively similar to that at $-78 \text{ }^\circ\text{C}$, the anodic potential limit is considerably lower at approximately $+7.5 \text{ V}$. As the critical point of HFC 134a was approached only poorly defined voltammograms were observed, probably because of the decreasing relative permittivity of the solvent and increasing fluid resistance.

Similar voltammetric experiments performed in neat liquid HFC 32 showed that the potential window of this medium is significantly lower than that of liquid HFC 134a. Table 4.2.3 compares the potential windows of neat liquid HFC 134a and HFC 32 at similar temperatures and pressures. The electrochemical stability of liquid HFC 32 is also weakened by increasing the temperature.

In order to perform electrochemical investigations in a HFC solvent using macroelectrodes, the medium must be made sufficiently conducting by the addition of a supporting electrolyte. The potential windows of HFC 134a and HFC 32 containing a variety of tetrabutylammonium-based electrolytes were assessed on platinum macroelectrodes via cyclic voltammetry. Figure 4.2.25 shows voltammograms for the two solvent-electrolyte systems investigated with the widest potential windows: TBAClO_4 and TBABF_4 in liquid HFC 134a. The potential windows of a variety of

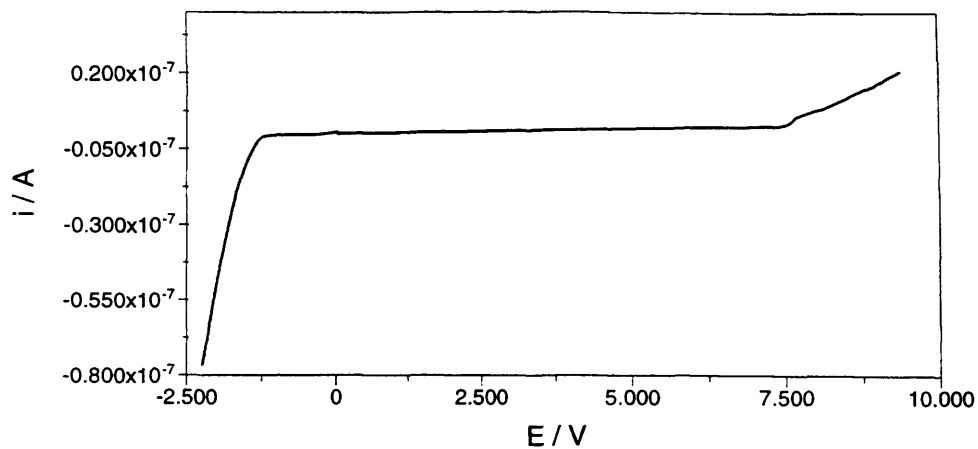


Figure 4.2.24 Voltammogram recorded at a 25 μm diameter Pt disc microelectrode in liquid HFC 134a at 25 $^{\circ}\text{C}$ and 25 bar at a scan rate of 20 mV s^{-1}

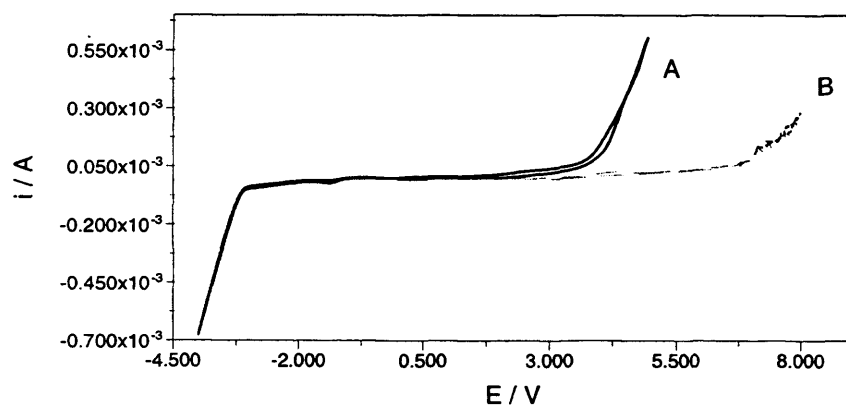


Figure 4.2.25 Cyclic voltammograms recorded at a 1 mm diameter Pt disc electrode in liquid HFC 134a at 25 $^{\circ}\text{C}$ and 10 bar with 0.1 M TBABF_4 (A) and 0.1 M TBAClO_4 (B)

HFC 134a and HFC 32 solvent-electrolyte systems are listed in table 4.2.4.

Solvent	Temperature and pressure	Negative limit/V	Positive limit/V	Potential Window/V
HFC 134a	-78 °C, 1 atm	-1.8	> 10	> 11.8
	25 °C, 25 bar	-1.3	7.5	8.8
HFC 32	-78 °C, 1 atm	-1.8	3.3	5.1
	25 °C, 30 bar	-1.7	3.0	4.7

Table 4.2.3 Potential windows of neat HFC 134a and HFC 32 on a platinum electrode at room and low temperatures

Solvent	Electrolyte	Negative limit/V	Positive limit/V	Potential Window/V
HFC 134a	TBABF ₄	-3.0	3.8	6.8
	TBAClO ₄	-2.9	6.5	9.4
	TBANO ₃	-2.9	2.4	5.3
	TBAPF ₆	-2.9	3.0	5.9
HFC 32	TBABF ₄	-3.0	2.9	5.8
	TBAClO ₄	-3.0	2.9	5.8

Table 4.2.4 Potential windows at a platinum macroelectrode of liquid HFC 134a and HFC 32 at 10 bar and 25 °C containing various electrolytes

The potential window of HFC 134a containing TBAClO₄ is in excess of 9 V, almost twice the largest reported previously.^{33,66} This unprecedented result opens an enormous range of possibilities for novel electrochemical investigations. Previously, few electrochemical studies have been carried out at potentials positive of +3 V because of the instability of the solvent-electrolyte system.

The negative potential limit in all of the cases listed in table 4.2.4 is determined by the reduction of the quaternary ammonium electrolyte. Here the tetrabutylammonium cation is initially reduced to the tetrabutylammonium radical, prior to the immediate decomposition of the short-lived intermediate,⁶⁷ as shown in equations (4.2.4) and (4.2.5).



The anodic limit of the HFC 134a-TBAClO₄ system is lower than that of neat HFC 134a, implying that oxidation of the ClO₄⁻ anion is responsible for the upper limit of the potential window. Similarly, when TBABF₄ is employed as the electrolyte the positive limit is thought to result from the oxidation of the BF₄⁻ anion



The HFC 32 solvent-electrolyte systems listed in table 4.2.4 display positive potential limits that are independent of electrolyte type and are similar to those of neat HFC 32. Thus the upper potential limit of these systems can be attributed to solvent oxidation.

4.2.3 Oxidation Electrochemistry at Extremely Positive Potentials

Figure 4.2.26 shows the oxidation of 18-crown-6 at a platinum macroelectrode in liquid HFC 134a containing 0.1 mol dm^{-3} TBABF₄ at 25 °C and 10 bar. The same figure also shows the oxidation of a [Cs(18-crown-6)]BF₄ complex under the same conditions. In the latter case, the peak on the oxidative sweep at +3.17 V can be attributed to the oxidation of Cs⁺ as no such peak is observed for the uncomplexed crown ether and the solvent and electrolyte are both electro-inactive in the potential range studied. Figure 4.2.27 shows the peak height to be concentration dependent. The oxidation potential of this process appears to be irreversible even at reduced temperatures (-78 °C) but is at a similar potential to that reported by Moock *et al.* (+3.0 V vs. Fc/Fc⁺).⁶⁸ Here it was suggested that the Cs⁺ centre is oxidized to Cs³⁺ because of the highly exothermic nature ($\Delta H = -856 \text{ kJ mol}^{-1}$)⁶⁸ of the following process



Consequently, Cs³⁺ formation is favoured over that of Cs²⁺. Some controversy exists about these earlier results as Jehoulet *et al.* were unable to reproduce this work.⁶⁹ It should, however, be noted that the latter authors did carry out the experiment by a different method, attempting to make the Cs⁺ [crypt] complex *in situ*. Jehoulet *et al.* used SO₂ as a solvent and found the oxidation potential for uncomplexed Cs⁺ to be +4.7 V vs. SCE. The authors also found that a range of Group I metal ions all had very similar oxidation potentials which is clearly counter intuitive. While both results are questionable, the difference in these oxidation potentials (*c.a.* 1.7 V) is not irreconcilable as the cryptand ligand should have a significant effect on the oxidation potential of the alkali metal cation. Uncomplexed cesium salts are almost

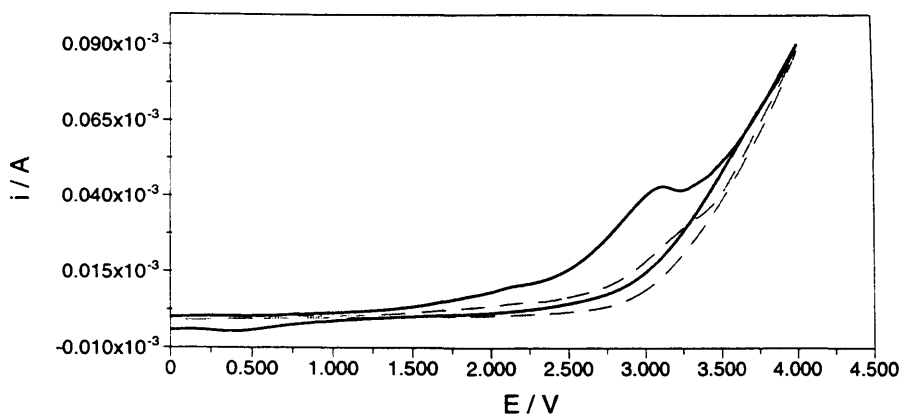


Figure 4.226 Voltammetry of 18-crown-6 (5 mM; dashed line) and [Cs(18-crown-6)]BF₄ (5 mM; solid line) at a 1 mm diameter Pt disc electrode in liquid HFC 134a containing 0.1 mol dm⁻³ TBABF₄ at 25 °C and 10 bar (scan rate = 100 mV s⁻¹)

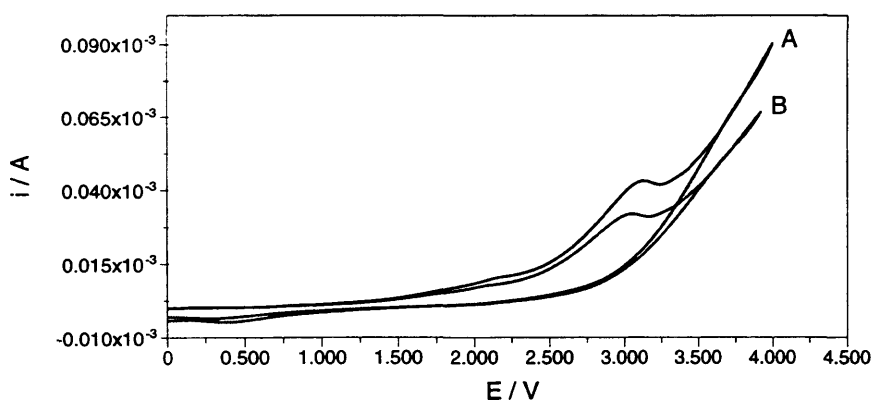
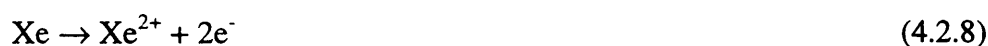


Figure 4.227 Voltammetry of 5 mM (A) and 2.5 mM (B) [Cs(18-crown-6)]BF₄ at a 1 mm diameter Pt disc electrode in liquid HFC 134a containing 0.1 mol dm⁻³ TBABF₄ at 25 °C and 10 bar (scan rate = 100 mV s⁻¹)

totally insoluble in HFC 134a and hence a comparison of Moock and Jehoulet's experiments is not possible.

The above experiment was repeated using the complex [Rb(18-crown-6)]BF₄. Figure 4.2.28 shows the observed irreversible oxidation peak at +3.15 V, corresponding to the oxidation of the Rb⁺ metal centre to Rb³⁺. The similarity in the oxidation potentials of the Cs⁺ and Rb⁺ complexes is probably a consequence of the complexing ability of the crown ether. It should be noted that Jehoulet and Bard found the oxidation potentials of uncomplexed Cs⁺ and Rb⁺ in liquid SO₂ to differ by only 0.06 V.⁶⁹

The oxidation of xenon at a platinum macroelectrode in liquid HFC 134a at 25 °C and 10 bar is shown in figure 4.2.29. A clear oxidation peak, that remains irreversible at higher sweep rates, is observed at approximately +3.5 V. Xe is isoelectronic to the Cs⁺ cation, and so as postulated in the aforementioned case of [Cs(18-crown-6)]BF₄ oxidation, the electrochemical step is thought to involve two electrons



This is the first example of the electrochemical oxidation of a rare earth gas uncomplicated by solvent decomposition and demonstrates the use of HFC 134a for difficult oxidation processes.

4.2.4 Voltammetry of Ferrocene in Liquid and Supercritical HFC 32

In the present study, ferrocene (m.p. = 174 °C) was employed as the test analyte because it is stable at high temperatures. Its electrochemistry has also been studied in a wide variety of liquid^{70,71} and supercritical solvents,^{30,65,72,73} enabling comparison with

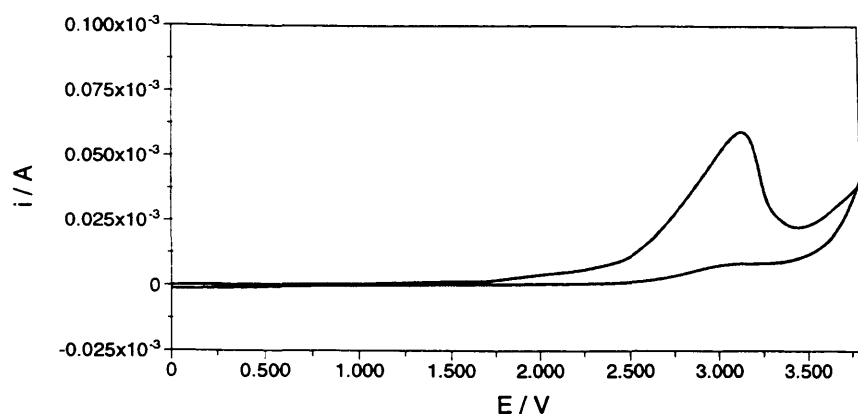


Figure 4.2.28 Voltammetry of 10 mM [Rb(18-crown-6)]BF₄ at a 1 mm diameter Pt disc electrode in liquid HFC 134a containing 0.1 mol dm⁻³ TBABF₄ at 25 °C and 17 bar (scan rate = 100 mV s⁻¹)

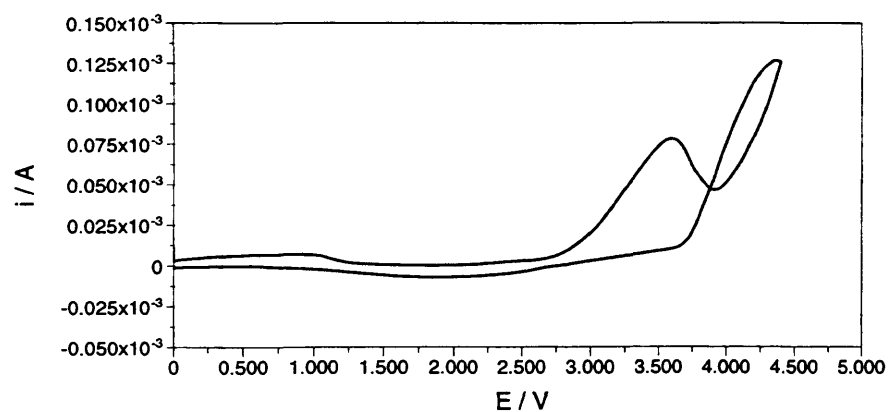


Figure 4.2.29 Voltammetry of xenon (saturated) at a 1 mm diameter Pt disc electrode in liquid HFC 134a containing 0.1 mol dm⁻³ TBABF₄ at 25 °C and 10 bar (scan rate = 100 mV s⁻¹)

results obtained in HFC 32.

Figure 4.2.30 shows a voltammogram of ferrocene recorded at a platinum microelectrode in liquid HFC 32 at 30 °C and 190 bar with a TBABF₄ concentration of 20 mM. A plot of E versus $\ln[(i_d-i)/i]$ for this voltammetric wave yields a line with a slope equal to 0.0261 V. This value is identical to the Nernstian value,³³ confirming that the ferrocene/ferrocinium couple behaves reversibly under normal conditions. The sigmoidal shape of the cyclic voltammogram is a consequence of the control by hemispherical diffusion of ferrocene to the Pt electrode surface. The diffusion coefficient of ferrocene, D , can, therefore, be calculated from the diffusion-limiting current using equation (2.3.5). At 30 °C and 190 bar in HFC 32, ferrocene has a diffusion coefficient of $2.89 \times 10^{-9} \text{ m}^2 \text{ s}^{-1}$.

Figure 4.2.30 also shows linear sweep voltammograms of ferrocene in supercritical HFC 32 at 90 °C as a function of pressure, and compares them to a voltammogram recorded in liquid HFC 32 at 30 °C. It is apparent that the half-wave potential for ferrocene oxidation shifts to considerably more positive values as the temperature of the system is increased from 30 to 90 °C. This shift in potential could result from the entropy change, ΔS , associated with the oxidation of ferrocene. Here the entropy change for the oxidation reaction would have to be positive because⁷⁴

$$\left(\frac{\delta E}{\delta T}\right)_p = \frac{\Delta S}{nF} \quad (4.2.9)$$

A further positive shift is observed in the supercritical phase at 90 °C when the pressure is lowered towards that of the critical point. This potential shift could result from a positive volume of reaction, ΔV , associated with ferrocene oxidation as⁷⁵

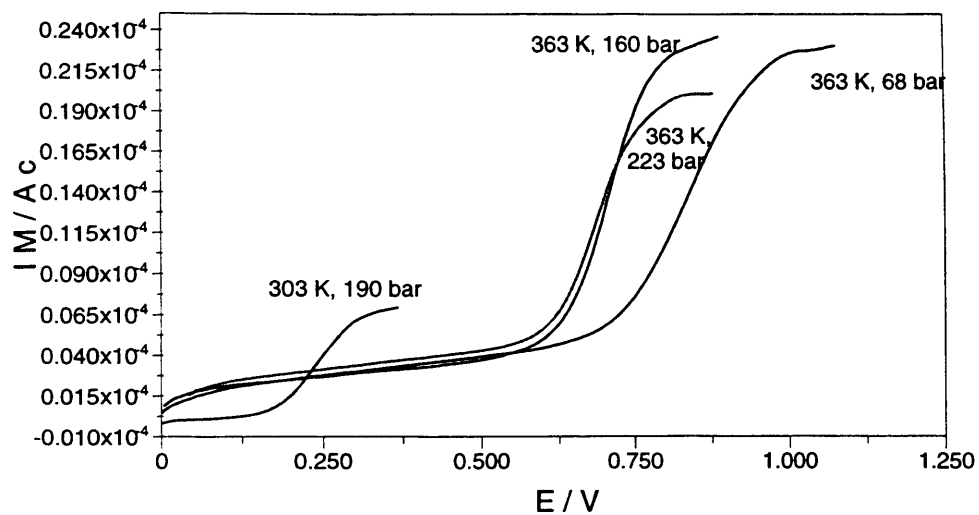


Figure 4.2.30 Voltammetry of ferrocene at a platinum disc microelectrode (diameter = 10 μm) and a scan rate of 10 mV s^{-1} in liquid and supercritical HFC 32 with 20 mM TBABF₄

$$\left(\frac{\delta E}{\delta P}\right)_T = -\frac{\Delta V}{nF} \quad (4.2.10)$$

The entropy and volume changes may also vary with fluid density and thus relative permittivity. The ferrocene/ferrocinium couple, however, is commonly studied because its redox potential is relatively solvent independent.⁷⁶ It is, therefore, suggested that a change in the silver quasi-reference electrode potential with temperature and pressure is predominantly responsible for the observed potential shifts in the voltammetric waves. The silver electrode, however, produces reasonably stable and reproducible reference potentials at a given temperature and pressure, with typical variations within 10 mV.

At 90 °C and 223 bar, conditions at which HFC 32 has a liquid-like density of 844.01 kg m⁻³,⁷⁷ a plot of E versus $\ln[(i_d - i)/i]$ yields a slope of 0.0314 V, compared to the Nernstian value of 0.0313 V. Significant deviations from the expected behaviour are observed, however, when the pressure is lowered towards that of the critical point, as shown in table 4.2.5. Deviations of this type are commonly attributed to ohmic distortion in supercritical fluid electrochemical investigations.^{30,65,78} The uncompensated solution resistance, R_u , can be calculated for a microelectrode from the fluid electrical conductivity. Newman showed that in the case of a disk microelectrode with a remote reference electrode,⁷⁹

$$R_u = \frac{\rho}{4r} = \frac{1}{4\Lambda cr} \quad (4.2.11)$$

where ρ is the fluid resistivity and r is the radius of the microdisk electrode. The data displayed in figure 4.2.14 were consequently used to calculate R_u at a variety of supercritical conditions as shown in table 4.2.5. The values of R_u shown in table 4.2.5 are only sufficient to cause a few millivolts of ohmic distortion when measuring

currents on a scale of 10 nA. Ohmic distortion, therefore, cannot explain the deviations from reversible behaviour observed at low pressures in the supercritical regime.

<i>P</i> /bar	<i>R_u</i> /MΩ	Slope of of <i>E</i> versus ln[(<i>i_d</i> - <i>i</i>)/ <i>i</i>]/mV	
		Experiment	Calculated
223	0.363	314	313
160	0.448	324	313
68	2.01	499	313

Table 4.2.5 Experimentally observed and calculated Nernstian slopes for the voltammograms shown in figure 4.2.30 at 90 °C in HFC 32. *R_u* values were calculated for a TBABF₄ concentration of 20.6 mM.

The diffusion-limited current for ferrocene oxidation increases dramatically as the temperature of the system is increased from 30 to 90 °C. This increase can be attributed to the lower viscosity of supercritical HFC 32 over the pressure range investigated, as shown in table 4.2.6. Also shown in table 4.2.6 are diffusion coefficients for ferrocene in both liquid and supercritical HFC 32, calculated from equation (2.3.5). In supercritical HFC 32, the diffusion coefficient of ferrocene does not increase with decreasing fluid viscosity as predicted by the Stokes-Einstein relation¹

$$D = \frac{k_B T}{6\pi\eta a} \quad (4.2.12)$$

where k_B is Boltzmann's constant and a is the effective radius of the diffusing species.

At 68 bar and 90 °C the calculated diffusion coefficient is actually smaller than that at 160 bar, even though the fluid viscosity is considerably lower.

T/K	P/bar	η/cP	$D \times 10^9/\text{m}^2 \text{ s}^{-1}$
303	190	0.144	2.89
363	223	0.082	7.23
363	160	0.070	8.46
363	68	0.023	8.40

Table 4.2.6 Diffusion coefficients of ferrocene in liquid and supercritical HFC 32

In supercritical chlorodifluoromethane, similar anomalies in the diffusion-limited current of ferrocene oxidation have been reported at pressures close to that of the critical point.⁶⁵ This effect was attributed to the precipitation of a ferrocinium salt on the electrode surface due to the low relative permittivity of the medium.^{70,80} These voltammograms consequently display large stripping peaks upon scan reversal as a result of the ferrocinium film deposited on the electrode surface during the forward sweep. These films can reduce the electrode dimension and consequently cause a decrease in the diffusion-limited current. No evidence of film formation, however, was observed on the reverse scans of cyclic voltammograms recorded in supercritical HFC 32 at 90 °C, even at pressures very close to that of the critical point as shown in figure 4.2.31. This effect can be attributed to the relatively high relative permittivity of supercritical HFC 32 at 90 °C.

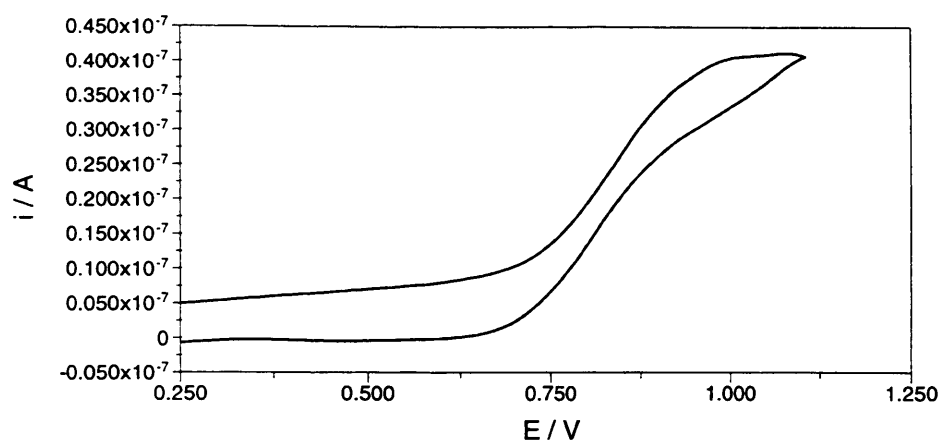


Figure 4.2.31 Voltammetry of ferrocene (1.79 mM) at a platinum disc microelectrode (diameter = 10 μm) and a scan rate of 10 mV s^{-1} in supercritical HFC 32 at $90 \text{ }^\circ\text{C}$ and 68 bar with 20 mM TBABF₄

It has been demonstrated above that the irregularities associated with voltammograms recorded in supercritical HFC 32 at low pressure cannot be ascribed to ohmic distortion or ferrocinium precipitation on the electrode surface. It is, therefore, suggested that the deviations from the expected Nernstian behaviour may result from a change in the double layer structure close to the critical conditions.

4.2.5 Double layer Structure in Liquid and Supercritical HFC 32

The capacitance of liquid HFC 32 at 30 °C and 220 bar ($\epsilon = 14.1$) containing 20 mM TBABF₄ at a platinum electrode as a function of potential is shown in figure 4.2.32. The decrease in capacitance at -0.37 V is indicative of a diffuse layer minimum.³³ In the present study the potential of zero charge (PZC) will be assumed to be close to the capacitance minimum. The shape of this plot is remarkably similar to those observed for NaF in aqueous solutions at low concentrations at 25 °C.⁴⁰ This suggests that the TBA⁺ and BF₄⁻ ions are insignificantly adsorbed at potentials close to the PZC. The capacitance values, however, are much lower than those of NaF in aqueous solution at potentials both positive and negative of the PZC, as expected in view of the reduced relative permittivity. Furthermore, the capacitance values at extreme positive potentials ($E > 0$ V) are less than those at extreme negative potentials ($E < -0.8$ V). The capacitances at these potentials correspond well to a compact layer of ions where the capacitance, C_H , is given by³³

$$C_H = \frac{\epsilon\epsilon_0}{d} \quad (4.2.13)$$

where ϵ_0 is the permittivity of free space (8.854×10^{-12} F m⁻¹) and d is the distance between the centre of the ions and the electrode surface.

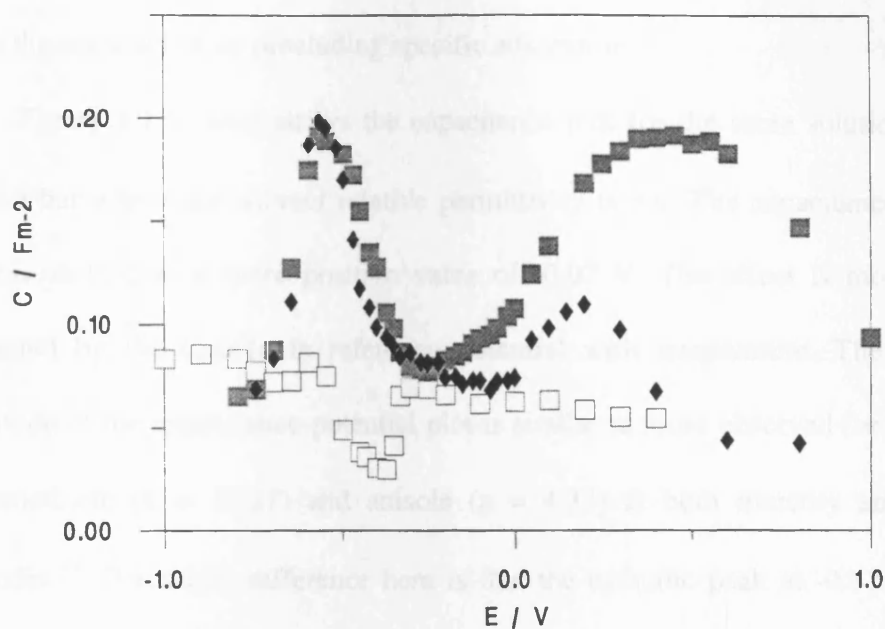


Figure 4.2.32 Double layer capacitance of a Pt electrode in a solution of TBABF₄ (0.02 mol dm⁻³) in liquid and supercritical HFC 32 at 30 °C and 220 bar [□], 70 °C and 135 bar [◆] (both liquid), 90 °C and 260 bar [■] (supercritical)

Assuming that the relative permittivity close to the electrode surface is approximately equal in both cation and anion adsorption, the capacitance values indicate a larger value of d in the latter case. The ionic radii of 0.413 and 0.202 nm for TBA^+ and BF_4^- respectively,⁸¹ therefore, imply that the BF_4^- anion remains solvated within the compact layer precluding specific adsorption.

Figure 4.2.32 also shows the capacitance plot for the same solution at 70 °C and 135 bar where the solvent relative permittivity is 9.6. The capacitance minimum has now shifted to a more positive value of -0.07 V. The effect is most probably dominated by the change in reference potential with temperature. The shape and magnitude of the capacitance-potential plot is similar to those observed for TBABF_4 in dichloroethane ($\epsilon = 10.27$) and anisole ($\epsilon = 4.33$) at both mercury and platinum electrodes.⁴⁴ The major difference here is that the cathodic peak at -0.57 V is larger than the anodic peak at 0.2 V. Such capacitance humps have been observed in both aqueous and non-aqueous media such as dimethylsulphoxide and *N*-methylacetamide.^{46,47} The capacitance humps are generally ascribed to the reorientation of polar solvent molecules adjacent to the electrode surface as a result of the change in surface charge.⁸² Capacitance studies in cyclohexane, however, have also yielded anodic humps and it was suggested that the specific adsorption of ion aggregates and not solvent reorientation, can cause the capacitance hump effect.⁴⁴

Also shown in figure 4.2.32 is the capacitance-potential plot for 20 mM TBABF_4 in supercritical HFC 32 at 90 °C and 260 bar, where the solvent relative permittivity is 9.5. Anodic and cathodic capacitance humps are again observed, on either side of the capacitance minimum at -0.25 V. This is an important result as it shows that the double layer structure is present in supercritical fluids at high pressures.

Voltammetric studies in supercritical HFC 32 at similar conditions described in section 4.2.4 have already shown the ferrocene/ferrocinium couple to behave reversibly at a platinum microelectrode. Ion adsorption, therefore, was not expected at these conditions.

The ionic strength of the solution and hence the cell capacitance will clearly be determined by the relative permittivity of the solution. Extensive ion pairing is prevalent for TBABF₄ in HFC 32 but the capacitance plots at 90 and 70 °C can be compared because the solutions have the same relative permittivity. Indeed both plots are similar, except that at supercritical conditions displays a significantly larger anodic capacitance hump that has a magnitude similar to that of the cathodic hump. Interestingly, both plots display a cathodic capacitance hump peak at -0.57 V.

Figure 4.2.33 shows the effect of pressure on the double layer capacitance plots for a supercritical HFC 32 solution at 90 °C. Upon decreasing the pressure from 260 to 160 bar ($\epsilon = 8.5$) there is a decrease in the height of cathodic capacitance hump and a complete disappearance of the anodic hump. A further reduction in pressure to 135 bar, where the solution relative permittivity is 8.1, leads to a complete removal of the cathodic capacitance hump.

At 135 bar the capacitance-potential plot consists of two roughly linear regions divided at approximately -0.55 V. The capacitance in each region is roughly independent of potential, suggesting that ion adsorption is prevalent. It is understandable, therefore, that at such conditions large deviations from Nernstian behaviour have been observed with voltammetry.

In contrast to the capacitance-potential plot of liquid HFC 32 at 30 °C, the capacitance of the cathodic compact layer is lower than that of the anodic equivalent.

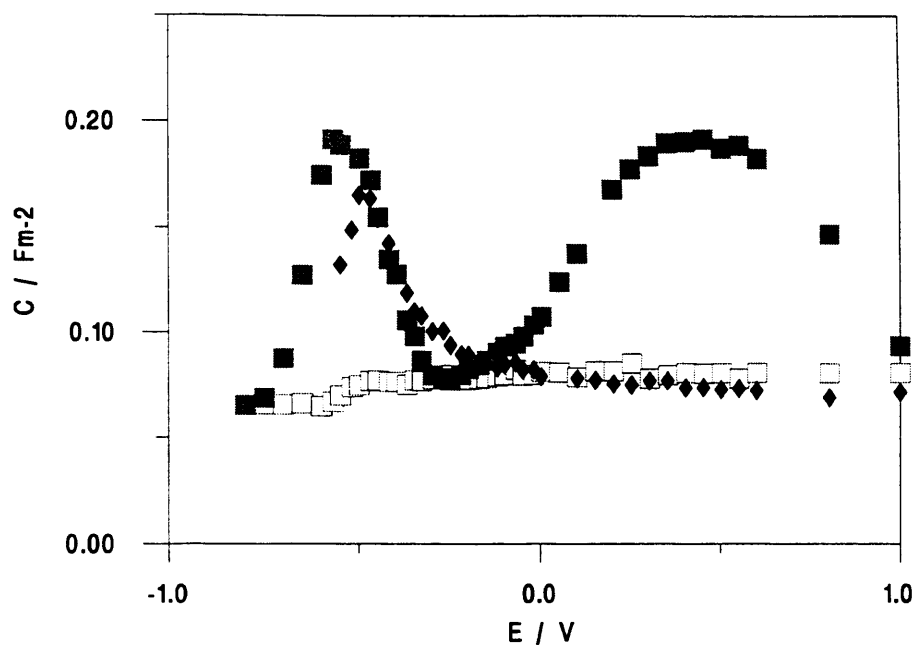


Figure 4.2.33 Double layer capacitance of a Pt electrode in a solution of TBABF_4 (0.02 mol dm^{-3}) in supercritical HFC 32 at $90 \text{ }^\circ\text{C}$ and 135 bar (\square), 160 bar (\blacklozenge) and 260 bar (\blacksquare)

Assuming equation (4.2.13) again holds, it can be inferred that the TBA^+ cations are specifically adsorbed at potentials negative of -0.55 V . It is suggested that at potentials positive of -0.55 V the BF_4^- anions are also specifically adsorbed, as a consequence of the breaking down of the solute-solvent specific interactions implied present in the liquid phase. Hence, the double layer structure can be entirely described by the Helmholtz model.

A decrease of the pressure of the supercritical system at $90\text{ }^\circ\text{C}$ from 260 to 135 bar, therefore, apparently causes a diffuse double layer structure to collapse. It is proposed that the increased thermal motion at lower pressures, a consequence of reduced fluid viscosity, prevents the formation of a diffuse layer. Conversely, the reduced relative permittivity of the medium increasingly favours ion adsorption on the electrode surface, yielding a compact double layer. These results explain the deviations from Nernstian behaviour observed for standard redox couples in fluids close to the critical conditions.

4.3 Conclusion

It has been shown that by the addition of a tetrabutylammonium tetrafluoroborate electrolyte to liquid and supercritical hydrofluorocarbons, the conductivity of the medium is sufficient to allow the study of electrochemistry. Both single ions and triple ions have been shown to be responsible for the transport of charge in liquid and supercritical HFC 32.

The unprecedented electrochemical stability of liquid HFC 134a has allowed the study of oxidation processes at large positive overpotentials. HFC 32 has been shown to be a useful solvent for electrochemical studies in the supercritical phase because of its low critical constants and relatively high polarity. The ferrocene couple was shown to behave reversibly in liquid and supercritical HFC 32 at liquid-like densities.

Deviations from Nernstian behaviour observed by voltammetry at pressures close to critical were ascribed to a change in the double layer structure. Double layer capacitance measurements have confirmed that the double layer structure at a platinum electrode in supercritical HFC 32 is strongly dependent on fluid density. At liquid-like densities the capacitance-potential plots exhibit a diffuse layer minimum, but as the density is lowered towards gas-like values the diffuse layer collapses and a pure Helmholtz response is observed.

4.4 References

- 1) Atkins, P. W. *Physical Chemistry*, 4th edn.; Oxford University Press: Oxford, 1990.
- 2) Bjerrum, N. K. *Dan. Vidensk. Selsk. Mat. Fys. Medd.* **1926**, 9, 7.
- 3) Fuoss, R. M.; Kraus, C. A. *J. Am. Chem. Soc.* **1933**, 55, 21.
- 4) Bockris, J. O'M.; Reddy, A. K. N. *Modern Electrochemistry*; Plenum Press: New York, 1970.
- 5) Fuoss, R. M.; Kraus, C. A. *J. Am. Chem. Soc.* **1933**, 55, 476.
- 6) Fuoss, R. M.; Kraus, C. A. *J. Am. Chem. Soc.* **1957**, 79, 3304.
- 7) Fuoss, R. M. *Chem. Rev.* **1935**, 17, 27.
- 8) Abbott, A. P. *Chem. Soc. Rev.* **1993**, 435.
- 9) Robinson, R. A.; Stokes, R. H. *Electrolyte Solutions*; Butterworths: London, 1959.
- 10) Bein, G. S.; Fuoss, R. M.; Kraus, C. A. *J. Am. Chem. Soc.* **1934**, 56, 1860.
- 11) Abbott, A. P.; Schiffrin, D. J. *J. Chem. Soc. Faraday Trans.* **1990**, 86, 1453.
- 12) Franck, E. U. *Z. Phys. Chem., N. F.* **1956**, 8, 92.
- 13) Franck, E. U. *Z. Phys. Chem., N. F.* **1956**, 8, 107.
- 14) Franck, E. U. *Z. Phys. Chem., N. F.* **1956**, 8, 192.
- 15) Dunn, L. A.; Marshall, W. L. *J. Phys. Chem.* **1969**, 73, 723.
- 16) Dunn, L. A.; Marshall, W. L. *J. Phys. Chem.* **1969**, 73, 2619.
- 17) Frantz, J. D.; Marshall, W. L. *Am. J. Sci.* **1984**, 282, 1666.
- 18) Frantz, J. D.; Marshall, W. L. *Am. J. Sci.* **1984**, 284, 651.
- 19) Quist, A. S.; Marshall, W. L. *J. Phys. Chem.* **1965**, 69, 2984.
- 20) Quist, A. S.; Marshall, W. L. *J. Phys. Chem.* **1966**, 70, 3714.
- 21) Quist, A. S.; Marshall, W. L. *J. Phys. Chem.* **1966**, 72, 684.
- 22) Quist, A. S.; Marshall, W. L. *J. Phys. Chem.* **1966**, 72, 1545.

- 23) Quist, A. S.; Marshall, W. L. *J. Phys. Chem.* **1966**, 72, 2100.
- 24) Quist, A. S.; Marshall, W. L. *J. Phys. Chem.* **1966**, 72, 3122.
- 25) Yeatts, L. B.; Dunn, L. A.; Marshall, W. L. *J. Phys. Chem.* **1971**, 75, 1099.
- 26) Yeatts, L. B.; Marshall, W. L. *J. Phys. Chem.* **1972**, 76, 1053.
- 27) Marshall, W. L. *J. Chem. Eng. Data.* **1987**, 32, 221.
- 28) Marshall, W. L.; Franck, E. U. *J. Phys. Chem. Ref. Data.* **1981**, 10, 295.
- 29) Abbott, A. P.; Harper, J. C. *J. Chem. Soc. Faraday Trans.* **1996**, 92, 3895.
- 30) Olsen, S. A.; Tallman, D. E. *Anal. Chem.* **1996**, 68, 2054.
- 31) Halliday, D.; Resnick, R. *Physics*, 3rd edn.; Wiley: New York, 1978.
- 32) von Helmholtz, H. L. F. *Ann. Physik.* **1853**, 89, 211.
- 33) Bard, A. J.; Faulkner, L. R. *Electrochemical Methods*; Wiley: New York, 1980.
- 34) Gouy, G. *J. Phys. Radium.* **1910**, 9, 457.
- 35) Gouy, G. *Compt. Rend.* **1910**, 149, 654.
- 36) Chapman, D. L. *Phil. Mag.* **1913**, 25, 475.
- 37) Stern, O. *Z. Elektrochem.* **1924**, 30, 508.
- 38) Parsons, R. *Mod. Asp. Electrochem.* **1954**, 1, 103.
- 39) Grahame, D. C. *Ann. Rev. Phys. Chem.* **1955**, 6, 337.
- 40) Grahame, D. C. *Chem. Rev.* **1947**, 41, 441.
- 41) Parsons, R. *Modern Aspects of Electrochemistry*, Vol. 1; Butterworth: London, 1954.
- 42) Gambert, R.; Baumgaertel, H. *J. Electroanal. Chem.* **1985**, 183, 315.
- 43) Gambert, R.; Baumgaertel, H. *J. Electroanal. Chem.* **1985**, 185, 147.
- 44) Abbott, A. P.; Harper, J. C. *J. Chem. Soc. Faraday Trans.* **1996**, 92, 3981.
- 45) Damaskin, B. B.; Ivanova, R. V.; Survila, A. A. *Elektrokhimiya*, **1965**, 1, 767.

- 46) Payne, R. *J. Phys. Chem.* **1969**, *73*, 3598.
- 47) Payne, R. *J. Am. Chem. Soc.* **1967**, *89*, 489.
- 48) Jurkiewicz-Herbich, M. *Pol. J. Chem.* **1978**, *52*, 1063.
- 49) Minc, S.; Jastrzebska, J. *J. Electrochem. Soc.* **1970**, *107*, 135.
- 50) Drogowska, M. A.; Fawcett, W. R. *J. Electroanal. Chem.* **1987**, *222*, 293.
- 51) Long, E. E. *Ph. D. Thesis*, Liverpool University, 1992.
- 52) Harper, J. C. *Ph. D. Thesis*, Leicester University, 1998.
- 53) Gileadi, E. *Electrode Kinetics*; VCH: New York, 1993.
- 54) Onsager, L. *Phys. Z.* **1927**, *28*, 277.
- 55) Glugla, P. G.; Byon, J. H.; Eckert, C. A. *J. Chem. Eng. Data* **1981**, *26*, 80.
- 56) Okubo, T.; Hasuo, T.; Nagashima, A. *Int. J. Thermophys.* **1992**, *13*, 931.
- 57) Steil, L. I.; Thodos, G. *AIChE J.* **1964**, *10*, 275.
- 58) Geller, V. Z.; Paulaitis, M. E.; Bivens, D. B.; Yokozeki, A. *Int. J. Thermophys.* **1996**, *17*, 75.
- 59) Fuoss, R. M.; Kraus, C. A. *J. Am. Chem. Soc.* **1933**, *55*, 2387.
- 60) Blandamer, M. J.; Burgess, J.; Robertson, R. E.; Scott, J. M. W. *Chem. Rev.* **1982**, *82*, 259.
- 61) Everaert, J.; Persoons, A. *J. Phys. Chem.* **1982**, *86*, 546.
- 62) Marcus, Y. *Z. Naturforsch.* **1983**, *38a*, 247.
- 63) Marcus, Y. *Ion Solvation*; Wiley: New York, 1985.
- 64) Tucker, S. C.; Maddox, M. W. *J. Phys. Chem. B* **1998**, *102*, 2437.
- 65) Olsen, S. A.; Tallman, D. E. *Anal. Chem.* **1994**, *66*, 503.
- 66) Mann, C. K. *Electroanal. Chem.* **1969**, *3*, 57.
- 67) Galova, M. *Electrochim. Acta.* **1984**, *29*, 323.

- 68) Moock, K.; Seppelt, K. *Angew. Chem. Int. Ed. Engl.* **1989**, 28, 1676.
- 69) Jehoulet, C.; Bard, A. J. *Angew. Chem. Int. Ed. Engl.* **1991**, 30, 836.
- 70) Daschbach, J.; Blackwood, D.; Pons, J. W.; Pons, S. *J. Electroanal. Chem. Interfacial Electrochem.* **1987**, 237, 269.
- 71) Bond, A. M.; Henderson, T. L. E.; Mann, D. R.; Mann, T. F.; Thormann, W.; Zoski, C. G. *Anal. Chem.* **1988**, 60, 1878.
- 72) Cabrera, C. R.; Bard, A. J. *J. Electroanal. Chem.* **1989**, 273, 147.
- 73) Michael, A. C.; Wightman, R. M. *Anal. Chem.* **1989**, 61, 270.
- 74) Gritzner, G.; Lewandowski, A. *J. Chem. Soc. Faraday Trans.* **1991**, 87, 2599.
- 75) Doine, H.; Whitcombe, T. W.; Swaddle, T. W. *Can. J. Chem.* **1992**, 70, 81.
- 76) Southampton Electrochemistry Group, *Instrumental Methods in Electrochemistry*; Ellis Horwood: Chichester, 1985.
- 77) Tillner-Roth, R.; Yokozeki, A. *J. Phys. Chem. Ref. Data* **1997**, 26, 1273.
- 78) Chong-yang, L.; Snyder, S. R.; Bard, A. J. *J. Phys. Chem. B* **1997**, 101, 1180.
- 79) Newman, J. J. *J. Electrochem. Soc.* **1970**, 117, 198.
- 80) Geng, L.; Ewing, A. G.; Jernigan, J. C.; Murray, R. W. *Anal. Chem.* **1986**, 58, 852.
- 81) Abraham, M. H.; Marcus, Y.; Lawrence, K. G. *J. Chem. Soc. Faraday Trans.* **1988**, 84, 175.
- 82) Payne, R. *J. Phys. Chem.* **1967**, 71, 1548.

CHAPTER V

THE ELECTROCHEMICAL REDUCTION OF CARBON DIOXIDE IN CARBON DIOXIDE/1,1,1,2-TETRAFLUOROETHANE MIXTURES

5.1 Introduction

5.1.1 The Electrochemical Reduction of Carbon Dioxide

5.1.2 The Mechanism of CO₂ Electroreduction

5.1.3 Reduction of CO₂ at Non-ambient Conditions

5.2 Results and Discussion

5.2.1 Voltammetric Measurements

**5.2.2 Bulk Electrolysis in Supercritical Carbon Dioxide/1,1,1,2-Tetrafluoroethane
Mixtures**

5.3 Conclusions

5.4 References

5.1 Introduction

The natural carbon cycle and a range of industrial processes form large quantities of carbon dioxide as a waste product. The reduction of this inexpensive and readily available compound was first investigated in the last century, where the intention was to form a carbon-rich product.¹⁻⁵ Interest in the subject was then largely lost until the 1950s,⁶⁻⁸ when it was recognised that efficient and economical reduction of CO₂ could solve two global problems. Firstly, such a process could reduce the levels of CO₂ present in the upper atmosphere and thus combat against the 'greenhouse effect'.⁹⁻¹¹ Secondly, food products such as glucose could be synthesised from the cheap and accessible raw material CO₂ on a large scale.¹²

On a less momentous scale, CO₂ reduction could also provide a cheap source of materials such as methanol and oxalic acid, which are important to the chemical industries.^{13,14} Other potential applications include the manufacture of synthetic hydrocarbon fuels from the products of CO₂ reduction^{15,16} and the removal of CO₂ from closed environments in life-support systems such as submarines.

5.1.1 The Electrochemical Reduction of Carbon Dioxide

The CO₂ molecule is extremely stable with a free energy of formation of -394.4 kJ mol⁻¹.¹⁷ This stability results from the complete occupation of the bonding and non-bonding molecular orbitals and the very high energy of the lowest unoccupied antibonding orbitals.¹⁸ Hence, it is widely accepted that the initial activation of the CO₂ molecule constitutes the most difficult step of the reduction process. The CO₂ molecule may be activated via electrochemical methods, although reaction with inorganic or organometallic catalysts is a viable alternative.^{11,19-25}

Following the work of Royer in 1870,² the electroreduction of carbon dioxide has been studied at a variety of cathode materials in both aqueous and non-aqueous electrolyte solutions.²⁶⁻²⁹ A variety of organic compounds have been produced accordingly. The most abundant reactions, however, are:



Electroreduction of CO_2 , therefore, commonly produces a mixture of organic compounds. Large overpotentials are required to activate the CO_2 molecule because of its aforementioned stability.³⁰ Thus in aqueous solutions hydrogen evolution always accompanies the reduction of CO_2 .^{31,32} The faradaic yield of each product is therefore a critical parameter used to assess the reaction selectivity.

In aqueous solutions, the majority of organic compounds formed possess a single carbon atom.^{26,33} The nature of the cathode and electrolyte solution largely determines the faradaic yields and composition of the electroreduction products. The metallic cathodes can be generally grouped in accordance with the primary reaction products, as shown in table 5.1.1.²⁶ Note that the classification does not take into account the reaction conditions. Of all the organic products listed above, formic acid is the least desirable. It is difficult to separate from solution and on oxidation to carbon dioxide its energy content is extremely low.

Many studies in aqueous solutions have focused on metal electrodes that require high overpotentials for the cathodic evolution of hydrogen. By employing

Group	Cathode material	Major organic product
I	Hg, Pd, Pb, In, Sn	HCOO ⁻
II	Zn, Au, Ag	CO
III	Mo, Cu, Ru	CH ₄ , CH ₃ OH, C ₂ H ₄ , etc.
IV	Ni, Fe, Pt, Al	CO ₂ does not reduce

Table 5.1.1 Classification of metallic electrodes in the aqueous electrochemical reduction of CO₂.²⁶

cathode materials such as lead, mercury, tin and indium,^{8,31,33-35} hydrogen evolution can be minimised at low overpotentials. Unfortunately, large overpotentials in the range of -1.0 to -1.5 V versus the normal hydrogen electrode (NHE) are generally required to reduce CO₂ on the group I metals listed in table 5.1.1.²⁶ Hence, interference from the competing hydrogen evolution process remains a problem. In addition to this dilemma, the electroreduction of CO₂ on such materials leads to the predominant formation of formate ions at ambient conditions. Teeter and van Rysselberghe, for example, observed faradaic yields close to 100 % for formate production at a mercury electrode in aqueous solution.^{8,36}

More recent investigations have concentrated on the electroreduction of CO₂ in aqueous solutions at a variety of non-metallic cathodes, such as oxide and semiconductor electrodes.³⁷⁻⁴² Bandi demonstrated the electrosynthesis of methanol with a faradaic efficiency of 50-70 % by employing an electrode prepared from mixed oxides of ruthenium and titanium.³⁸ Taniguchi and co-workers also produced methanol

with reasonable faradaic efficiency (44 %) on a p-type GaP cathode in the presence of a crown-ether.⁴⁰ A number of studies have also investigated the electroreduction of CO₂ in aqueous media containing complex catalysts.⁴³⁻⁴⁵

The problems associated with hydrogen evolution in the electrochemical reduction of CO₂ can be completely eradicated by using aprotic solvents. Reactions (5.1.1) to (5.1.4) can then be neglected. Hence, the electroreduction of CO₂ in non-aqueous media promises high yields of oxalate anions. In the first such study in 1967, Haynes and Sawyer investigated CO₂ reduction in dimethylsulphoxide at gold and silver electrodes via a variety of electroanalytical techniques.⁴⁶ On both metals, somewhat unexpectedly, CO and formate were the main reaction products. The electrosynthesis of formate ions on gold, however, was shown to be strongly dependent on the water content of the solvent.

Any adventitious water present in the system acts a proton donor, facilitating reaction (5.1.1) and thus increasing the faradaic efficiency of formate production at the expense of that of oxalate and CO.³³ Subsequent studies in non-aqueous solvents have shown that high yields of oxalate ions can be obtained if the water content of the system is minimised and an appropriate electrode material employed.^{13,14,33,47} In 1972, for example, Baizer *et al.* employed a mercury electrode in dimethylformamide and acquired a faradaic efficiency of approximately 90 % for oxalate production in the absence of water.⁴⁷

The variation in product selectivity achieved with metallic cathodes in aprotic solutions prompted Ito and co-workers to introduce a scheme of electrode classification.³³ The electrodes are grouped in accordance with the faradaic efficiencies observed for oxalate and carbon monoxide production, as shown in table 5.1.2.

Group	Metals	Faradaic efficiency of oxalate formation	Faradaic efficiency of CO formation
I	Hg, Pb, Tl	60-80 %	0-15 %
II	In, Zn, Au, Ag, Cu, Cd, Pt, Pd	< 20 %	50-90 %
III	Fe, Cr, Mo, Ti	10-40 %	10-40 %

Table 5.1.2 Classification of metallic cathodes employed in the electrochemical reduction of CO₂ in aprotic solvents³³

It should also be noted that oxalate ions can be electrosynthesised with high faradaic yields at stainless steel cathodes in aprotic solvents.^{13,48}

5.1.2 The Mechanism of CO₂ Electroreduction

The electroreduction of CO₂ yields a variety of products depending on the nature of the solvent-electrolyte system, electrode material and reaction conditions employed. It is, therefore, insinuated that CO₂ may be electroreduced via a number of reaction pathways. Eyring and co-workers performed some of the earliest mechanistic studies of CO₂ electroreduction in aqueous solution.^{49,50} Using a mercury electrode, they recorded polarization and cathode galvanostatic charging curves in order to probe the complicated mechanism. The polarization curves recorded in neutral solution displayed two linear Tafel regions indicative of a two consecutive step mechanism. Many mechanistic studies in aqueous media ensued⁵¹⁻⁵³ that led to the general acceptance of the reaction pathways given in figure 5.1.1.

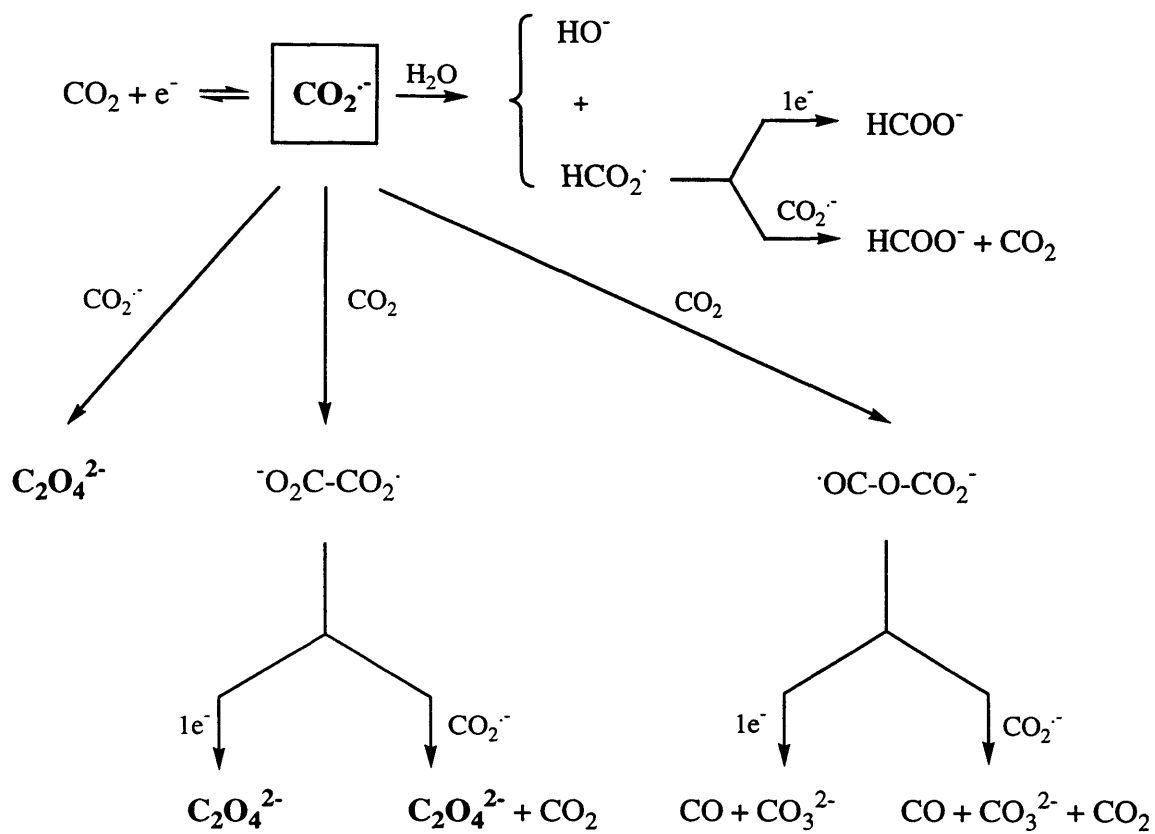


Figure 5.1.1 The electrochemical reduction of CO_2

In aprotic media protonation of the carbon dioxide radical anion is no longer possible. Haynes and Sawyer performed some of the earliest mechanistic studies in non-aqueous media, employing controlled potential coulometry and galvanostatic methods to study the electroreduction of CO₂ at gold and mercury electrodes in dimethylsulphoxide.⁴⁶ They consequently proposed that the reduction of CO₂ to the carbon dioxide radical anion was rate-limiting.

The mechanism of the reaction portrayed in equation (5.1.5) has received considerable interest in aprotic media because of the desirability of the oxalate product. The electroreduction of CO₂ was studied by Aylmer-Kelly and co-workers on lead electrodes in solutions of propylene carbonate and acetonitrile using modulated reflectance spectroscopy.⁵³ The authors showed that two probable mechanisms accounted for the production of oxalate

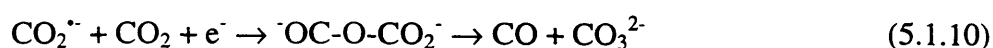


and



Aylmer-Kelly *et al.* were able to show that in addition to CO₂^{•-}, another radical species, assumed to be (COO)₂^{•-}, accumulated on the lead electrode surface. The actual reductive process was also found to be first order with respect to CO₂^{•-}. As a result, it was suggested that oxalate predominantly forms via reactive steps (5.1.8) and (5.1.9), as the dimerisation reaction (5.1.7) is second order in CO₂^{•-}.

Subsequent investigations into the rate-limiting step of oxalate formation, however, were not in accordance with the findings of Aylmer-Kelly and co-workers. Both Gimenez *et al.*⁵⁴ and Amatore *et al.*⁵⁵ studied the effect of a variety of reaction factors on the faradaic yield of a number of reaction products. It was consequently concluded that oxalate is predominantly formed by the dimerisation of CO₂^{•-} radical anions. Although the validity of reaction (5.1.8) was accepted, it was suggested that this reaction would result in the formation of a short-lived addition product that would dissociate to form carbon monoxide and carbonate ions



This process may account for the frequently observed phenomenon of CO formation in aprotic media. Christensen and co-workers, however, believe that carbonate ions are only formed as a result of the interaction between hydroxide ions and CO₂ molecules, where the hydroxide ions are a product of the reduction of trace impurities of water in the aprotic solution.⁵⁶

Vassiliev and co-workers studied the kinetics of CO₂ electroreduction in acetonitrile on mercury, lead, indium and tin electrodes.⁵⁷ The polarisation curves obtained for these four metallic electrodes exhibited two linear regions when plotted in semilogarithmic co-ordinates. It was suggested that the two different Tafel slopes correspond to two different reaction mechanisms. It was proposed that at more positive potentials the reaction rate is determined by the further reduction of CO₂^{•-} radical anions according to reactions (5.1.7), (5.1.8) and (5.1.9). At more negative potentials, however, the rate limiting step is believed to be CO₂^{•-} formation.

It is now generally accepted that following the initial one electron step of CO₂ electroreduction in aprotic media, the CO₂^{•-} radical anion may undergo a number of

possible reactions that are strongly influenced by the nature of the cathodic electrode.⁵⁷

Gressin and co-workers were able to summarize the processes involved in CO₂ electroreduction in figure 5.1.1.⁵⁸

5.1.3 Reduction of CO₂ at non-ambient conditions

The low solubility of CO₂ in both protic and aprotic liquid media commonly limits the rate of the reduction process. The concentration of CO₂ in solution can be raised by increasing the CO₂ pressure. At 25 °C, for example, CO₂ has a solubility in water of only 0.033 mol dm⁻³; a concentration that increases to 1.17 mol dm⁻³ at a CO₂ pressure of 60 atm.⁵⁹ Ito and co-workers investigated the effects of increasing pressure on the electroreduction of CO₂ in aqueous solution at Zn, Pb, In and Sn electrodes.^{35,60} Increasing the CO₂ pressure to approximately 20 atm led to a gain in both the faradaic efficiency and current density of the reductive process. Further investigations have shown that CO₂ can be reduced with relatively high faradaic efficiencies (16-62 %) under high CO₂ pressures (50-60 atm) on Co, Fe, Pt, Pd and Ni electrodes.⁶¹ The electroreduction of CO₂ was negligible, however, when employing the same electrode materials and a CO₂ pressure of 1 atm.

Bandi and co-workers suggested that liquid CO₂, containing a tetraalkylammonium electrolyte, could be employed as the electrochemical solvent in the reduction of CO₂.^{62,63} The problems associated with CO₂ solubility and hydrogen evolution would, therefore, be irradiated. Although CO₂ can be made conducting through the introduction of bulky hydrophobic electrolytes,⁶⁴ the resistivity of the medium is still too high as to make the reduction reaction impractical.

Supercritical media are miscible with gases in all proportions, which facilitates very high CO₂ concentrations. Mass transport of an electroactive species to or from the electrode surface is also rapid in such low viscosity media. Furthermore, CO₂ itself has conveniently low critical constants ($T_c = 31.4\text{ }^\circ\text{C}$; $p_c = 72.3\text{ bar}$). As a result, supercritical CO₂ has been reduced under non-electrochemical conditions using catalysts such as ruthenium (II) complexes.⁶⁵

Abbott and Harper were the first to investigate the electrochemical reduction of CO₂ in the supercritical state.⁶⁶ The reductive process was studied at platinum and lead electrodes in a supercritical CO₂/H₂O solvent mixture. The aqueous component of the mixture acts as a polar modifier, permitting the dissolution of a TBABF₄ electrolyte and hence substantially increasing the conductivity of the medium. At platinum electrodes formate was the only significant product detected, with faradaic efficiencies below 30 %. Oxalate was shown to be the major organic product formed at a lead electrode with a faradaic efficiency of approximately 16 %. The low faradaic efficiencies of the organic products were attributed to competition from the hydrogen evolution process



In this work, HFC 134a rather than water will be employed as a polar modifier in the supercritical mixtures. Reactions (5.1.11) and (5.1.1) can then be completely neglected at negative overpotentials because HFC 134a is aprotic. As a result, the electroreduction of CO₂ should be more efficient and the formate anion cannot form. HFC 134a also has a considerably lower critical temperature than water, leading to relatively mild critical conditions for the solvent mixture.⁶⁷ The current work reports

the product distributions and efficiencies associated with the electroreduction of CO₂ at Pt and Pb electrodes in supercritical CO₂/HFC 134a solvent mixtures.

5.2 Results and Discussion

5.2.1 Voltammetric measurements

A CO₂/HFC 134a mixture with a HFC 134a mole fraction, $x_{\text{HFC 134a}}$, of 0.304 was employed as the solvent in all of the voltammetric experiments presented in the current work. This composition exhibits relatively mild critical constants ($T_c = 57\text{ °C}$; $p_c = 72\text{ bar}$),⁶⁷ whilst simultaneously facilitating the dissolution of a sufficient amount of TBABF₄ electrolyte to support electrochemistry without significant ohmic distortion. All of the CO₂/HFC 134a/TBABF₄ systems employed in the current work were present as a single phase, as confirmed by visual observation using an optical cell.

Figure 5.2.1 shows cathodic voltammograms recorded at a platinum microelectrode in both liquid and supercritical CO₂/HFC 134a mixtures with TBABF₄ concentrations of 20 mM. The cathodic current can be assigned to the reduction of CO₂ because both HFC 134a and TBABF₄ are electroinactive over the potential range investigated. In the liquid phase at 30 °C and 150 bar, CO₂ is electroreduced at potentials negative of approximately $-0.6\text{ V vs. Ag/Ag}^+$. On increasing the temperature to 60 °C the reduction wave is shifted to more positive potentials. Under these supercritical conditions, the potential corresponding to the onset of CO₂ reduction is approximately -0.19 V . Negative shifts in the onset potential of CO₂ reduction are commonly ascribed to the adsorption of intermediates, such as CO, on the electrode surface.⁶⁸⁻⁷¹ It is, therefore, implied that adsorbed species such as CO exhibit a lower surface coverage on the platinum electrode under the supercritical conditions studied. Note that the observed positive shift in potential cannot be attributed to an increase in CO₂ concentration, as described by Ito and co-workers,⁶⁰ because the density of the

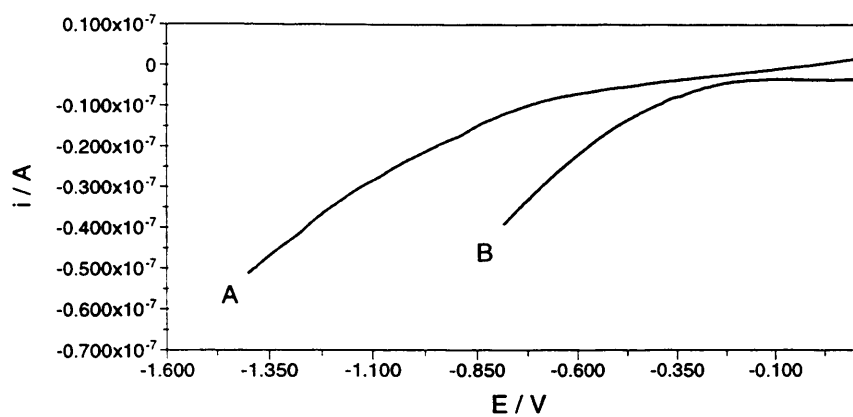


Figure 5.2.1 Voltammograms recorded at a 10 μm diameter Pt disc microelectrode in $\text{CO}_2/\text{HFC 134a}$ ($x_{\text{HFC 134a}} = 0.304$) with 20 mM TBABF_4 ; A = 30 $^\circ\text{C}$ and 150 bar (liquid), B = 60 $^\circ\text{C}$ and 150 bar (supercritical). Scan rate = 20 mV s^{-1}

specified supercritical mixture is lower than that of the liquid mixture studied.

Figure 5.2.1 also shows that the cathodic current associated with CO₂ reduction at a platinum electrode is higher under supercritical conditions. This result implies that the rate of CO₂ reduction is limited by mass transport in the liquid phase at 30 °C and 150 bar. The lower viscosity of supercritical CO₂/HFC 134a will allow any species involved in the electroreduction of CO₂ to diffuse to and from the electrode surface at higher rates than in the liquid.

The potential for the onset of CO₂ reduction is shown in figure 5.2.2 to undergo a slight negative shift to approximately -0.25 V as the pressure of the supercritical fluid is increased from 150 bar to 200 bar at 60 °C. The density of the fluid increases with increasing pressure, suggesting that the negative potential shift is caused by an increase in intermediate adsorption on the electrode surface and not a CO₂ concentration decrease. At the lower pressure of 150 bar, there is also an increase in the cathodic current. This increase can be assigned to the drop in fluid viscosity and consequent increase in the diffusivity of any species involved in the reductive process.

Figure 5.2.3 shows voltammograms recorded in liquid and supercritical CO₂/HFC 134a at a lead microelectrode. At 30 °C and 165 bar the reduction of CO₂ only occurs at potentials approximately negative of -2.15 V. This value is considerably more negative than the corresponding reduction potential on platinum. Vassiliev and co-workers also reported that the overpotential of CO₂ reduction in liquid aprotic solvents is more negative on lead than on platinum.⁵⁷ The large difference in onset potentials reported in this work suggests that there is a change in the major reaction mechanism of CO₂ reduction on replacement of the platinum electrode with lead.

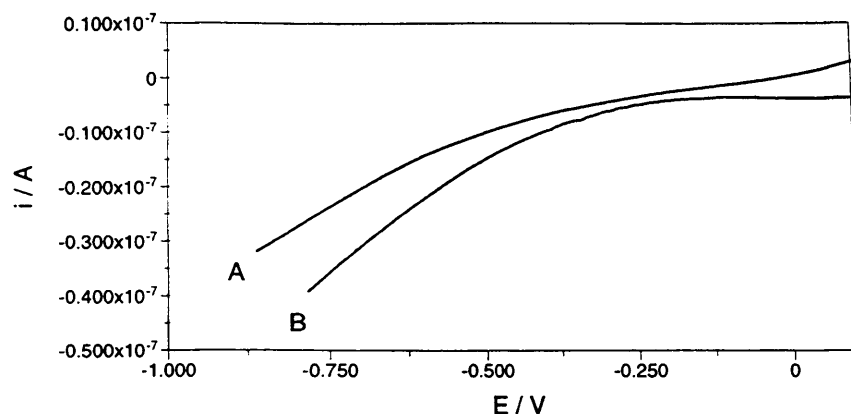


Figure 5.2.2 Voltammograms recorded at a 10 μm diameter Pt disc microelectrode in supercritical $\text{CO}_2/\text{HFC 134a}$ ($x_{\text{HFC 134a}} = 0.304$) at 60 $^\circ\text{C}$ with 20 mM TBABF₄; A = 200 bar, B = 150 bar. Scan rate = 20 mV s^{-1}

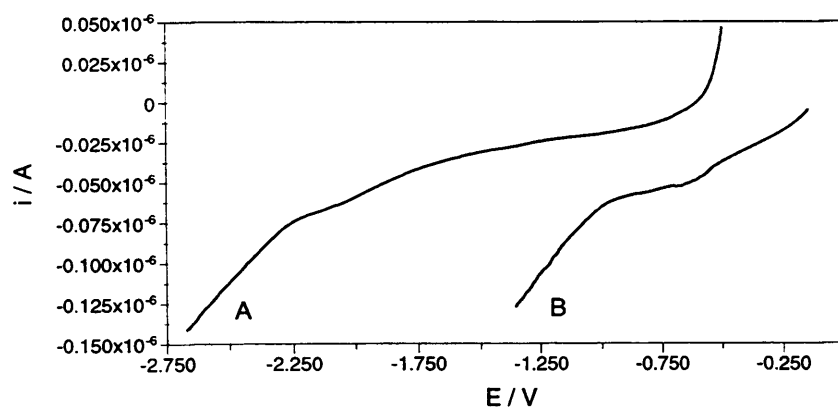


Figure 5.2.3 Voltammograms recorded at a 25 μm diameter Pb disc microelectrode in $\text{CO}_2/\text{HFC 134a}$ ($x_{\text{HFC 134a}} = 0.304$) with 20 mM TBABF₄; A = 30 $^\circ\text{C}$ and 165 bar (liquid), B = 60 $^\circ\text{C}$ and 240 bar (supercritical). Scan rate = 20 mV s^{-1}

At supercritical conditions of 60 °C and 240 bar the reduction wave reported in the liquid phase shifts to more positive potentials by approximately 1.2 V. This shift is larger than that observed on platinum and suggests that intermediates such as CO are adsorbed to a greater extent on lead under the liquid phase conditions specified. The overpotential of CO₂ reduction is, however, still significantly more negative than that on platinum. Electroreduction of CO₂ on platinum is, therefore, a more attractive proposition because it is a more energy efficient process.

5.2.2 Bulk Electrolysis in Supercritical Carbon Dioxide/1,1,1,2-Tetrafluoroethane Mixtures

Bulk electrolysis experiments were performed in supercritical CO₂/HFC 134a mixtures at both platinum and lead electrodes. In each case, a constant potential of -4 V was applied to the working electrode until 100 C of charge were passed. The faradaic efficiencies of the detected products are given in table 5.2.1.

Electrode	<i>T</i> /°C	<i>p</i> /bar	Faradaic efficiency/%		
			(COOH) ₂	CO	HCOOH
Pt	60	260	41.6	14.6	0
	80	260	37.3	16.4	0
Pb	60	260	17.5	42.0	0
	80	260	13.7	42.9	0

Table 5.2.1 Electrochemical reduction products of CO₂ at platinum and lead electrodes in CO₂/HFC 134a (*x*_{HFC 134a} = 0.304) with 0.1 M TBABF₄ (charge passed = 100 C)

The faradaic efficiency of oxalate formation is reasonably high at a platinum electrode at the supercritical conditions listed. In comparison, previous studies in liquid aprotic media have reported faradaic efficiencies no higher than 5 %.³³ In these liquid media CO was the main product with faradaic efficiencies higher than 60 %. It was thus suggested that the $\text{CO}_2^{\cdot-}$ radical anions easily desorb from the Pt surface and are then attacked by CO_2 molecules in the bulk to form CO as shown in figure 5.1.1. In the supercritical $\text{CO}_2/\text{HFC 134a}$ mixture, however, the CO_2 concentration will be much higher at the electrode surface than in the aforementioned liquid bulk electrolysis experiments. There will, therefore, be a higher surface coverage of $\text{CO}_2^{\cdot-}$ radical anions, facilitating dimerisation to the oxalate anion as shown in equation (5.1.7). Consequently, a lower percentage of $\text{CO}_2^{\cdot-}$ radical anions will desorb from the electrode surface to form CO, as exemplified by the low faradaic efficiencies of CO formation in table 5.2.1. The results of table 5.2.1, therefore, show that when very high concentrations of CO_2 are employed the efficiency of oxalate formation is less dependent on the energetics of $\text{CO}_2^{\cdot-}$ adsorption at the electrode surface.

Table 5.2.1 also shows that the faradaic efficiency of oxalate formation actually undergoes a slight decrease when the temperature of the supercritical system is raised from 60 °C to 80 °C. There is also a slight concurrent increase in the faradaic efficiency of CO formation. These changes could result from the lower density of the solvent at 80 °C and the consequent decrease in CO_2 concentration at the electrode surface. At 80 °C there will, therefore, be a lower surface coverage of $\text{CO}_2^{\cdot-}$ radical anions on the electrode surface and a reduced tendency to form oxalate ions.

It is evident from the results in table 5.2.1 that the combined faradaic efficiencies of oxalate and CO formation fall some way short of 100 %. This deficit

can probably be attributed to design of the electrochemical cell, where the anode and cathode are not separated. Voltammetry was performed at a platinum microelectrode in the electrochemical cell subsequent to the bulk electrolysis of CO₂ at 60 °C and 260 bar, as shown in figure 5.2.4. A small anodic peak was observed at approximately +0.55 V, which can probably be ascribed to the oxidation of small amounts of dissolved oxalate. This result may account for the very low faradaic efficiencies associated with the formation of oxalate at lead electrodes in supercritical CO₂/HFC 134a. The kinetics of CO₂ reduction on Pb have been shown to be inferior to those on Pt in sc CO₂/HFC 134a in section 5.2.1. Consequently, oxalate ions will have a much longer time in which to travel to the anode.

An attempt was made to separate the cathode and anode using a medium porosity glass frit. The 3 mm thick frit was placed centrally between two rectangular platinum electrodes (26 × 10 × 0.5 mm), separated by a distance of 8 mm. The anode was then enclosed in teflon so that the anodic compartment was only separated from solution by the glass frit. A bulk electrolysis experiment was then performed at 80 °C and 260 bar in sc CO₂/HFC 134a with 0.1 M TBABF₄ at -4 V. After the passage of 50 C of charge, the faradaic efficiency of oxalate production was 43.0 %. This value is significantly higher than that of 37.3 % observed in the non-separated electrochemical cell, confirming the idea that the faradaic efficiencies listed in table 5.2.1 are affected by the reoxidation of the oxalate ions at the anode. The oxidation of oxalate may be inhibited more efficiently by the employment of an ion exchange membrane. Considering that the experimental conditions in the present study were not optimized, supercritical CO₂/HFC mixtures appear to be extremely promising media for the efficient electrosynthesis of oxalate.

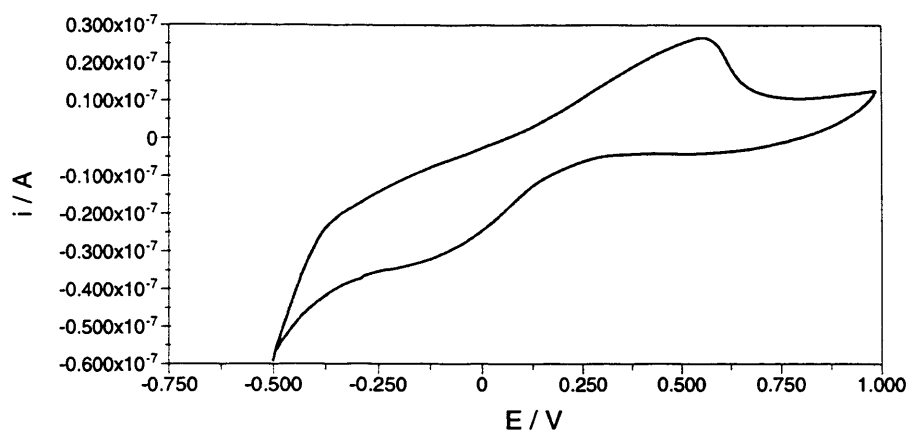


Figure 5.2.4 Cyclic voltammogram recorded at a 10 μm diameter platinum disc microelectrode in $\text{CO}_2/\text{HFC 134a}$ ($x_{\text{HFC 134a}} = 0.304$) at 60 $^\circ\text{C}$ and 260 bar following the completion of a bulk electrolysis experiment. Scan rate = 20 mV s^{-1}

5.3 Conclusion

It has been demonstrated for the first time that CO₂ can be reduced electrochemically in aprotic mixtures in the supercritical phase. Voltammetry has shown that at a platinum electrode in a CO₂/HFC 134a mixture the reduction of CO₂ is under mass transport control. The kinetics of reduction are, therefore, enhanced by employing a supercritical CO₂/HFC 134a mixture.

The nature of the electrode material has been shown to affect both the kinetics and products of CO₂ electroreduction in sc CO₂/HFC 134a. Platinum has been shown to be far superior than lead as a cathode material on which to reduce CO₂ in sc CO₂/HFC 134a mixtures by both voltammetric and bulk electrolysis experiments. By employing a supercritical CO₂/HFC 134a mixture rather than an aprotic liquid as the electrochemical solvent, the faradaic efficiency of oxalate formation at a platinum electrode is dramatically improved. This increase in efficiency can be attributed to the high concentration of CO₂ at the electrode surface in sc CO₂/HFC 134a mixtures.

5.4 References

- 1) Beketov, N. N. *Zh. Russ. Fiz. O-va*, **1869**, 1, 33.
- 2) Royer, E. *C. R. Acad. Sci.* **1870**, 70, 371.
- 3) Klobukov, N. Z. *Prakt. Chem.* **1887**, 34, 64.
- 4) Lieben, A. *Monatsh. Chem.* **1895**, 16, 211.
- 5) Lieben, A. *Monatsh. Chem.* **1895**, 18, 528.
- 6) Müller, O. H. *Proc. 1st Int. Congr. Polarogr.*; Prague, **1951**, 159.
- 7) Vlcek, A. A. *Nature*, **1953**, 172, 861.
- 8) Teeter, T. E.; van Rysselberg, P. J. *Chem. Phys.* **1954**, 22, 759.
- 9) E. T. Sundquist. *Science* **1993**, 259, 934.
- 10) *Carbon Dioxide Chemistry: Environmental Issues*; Paul, J., Pradier, C. –M., Eds.; Royal Society of Chemistry: London, 1994.
- 11) Leitner, W. *Angew. Chem. Int. Ed. Engl.* **1995**, 34, 2207.
- 12) Weliky, N.; Dale, R. J.; Dale, E.; Cale, N.; Sec, E. T.; Silverman, H. P. *Trans. N. Y. Acad. Sci., Ser. 11.* **1972**, 34, 647.
- 13) Kaiser, U.; Heitz, E. *Ber. Bunsenges. Phys. Chem.* **1973**, 77, 818.
- 14) Fischer, J.; Lehmann, Th.; Heitz, E. *J. Appl. Electrochem.* **1981**, 11, 743.
- 15) Steinberg, M. U.S. Pat. No. 3,959,094, 25th May 1976.
- 16) Russel, P. G.; Kovac, N.; Srinivasan, S.; Steinberg, M.; *J. Electrochem. Soc.* **1977**, 124, 1329.
- 17) Atkins, P. W. *Physical Chemistry*, 4th edn.; Oxford University Press: Oxford, 1990.
- 18) Lehmann, Th. Diplomarbeit, Universität Frankfurt, 1974.
- 19) Sneeden, R. P. A. In *Comprehensive Organometallic Chemistry*; Wilkinson, G., Stone, F. G. A., Abel, F. W., Eds.; Pergamon Press: Oxford, **1982**, 8, 225.

- 20) Morgenstern, D. A.; Wittrig, R. E.; Fanwick, P. E.; Kubiak, C. P. *J. Am. Chem. Soc.* **1993**, *115*, 6470.
- 21) Willner, I.; Mandler, D. *J. Am. Chem. Soc.* **1989**, *111*, 1330.
- 22) Ogata, T.; Yanagida, S.; Brunschwig, B. S.; Fujita, E. *J. Am. Chem. Soc.* **1995**, *117*, 6708.
- 23) Collomb-Dunand-Sauthier, M. -N.; Deronzier, A.; Ziessel, R. *J. Organomet. Chem.* **1993**, *444*, 191.
- 24) Kitamura, N.; Tazuke, S. *Chem. Lett.* **1983**, 1109.
- 25) Ishida, H.; Terada, T.; Tanaka, K.; Tanaka, T. *Inorg. Chem.* **1990**, *29*, 905.
- 26) Bagotzky, V. S.; Osetrova, N. V. *Russ. J. Electrochem.* **1995**, *31*, 409.
- 27) Ziessel, R. *Nouv. J. Chim.* **1983**, *7*, 613.
- 28) Taniguchi, I. *Modern Aspects of Electrochemistry*; Bockris, J. O'M., White, R. E., Coway B. E., Eds.; Plenum.: New York, **1989**, *20*, 327.
- 29) *Electrochemical and Electrocatalytic Reactions of Carbon Dioxide*; Sullivan, B. P., Krist, K., Guard, H. E., Eds.; Elsevier: Amsterdam, 1993.
- 30) Lamy, E.; Nadjo, L.; Saveant, J. M. *J. Electroanal. Chem.* **1977**, *78*, 403.
- 31) Udupa, K. S.; Subramanian, G. S.; H. V. K. Udupa. *Electrochim. Acta.* **1971**, *16*, 1593.
- 32) Hori, Y.; Kikuchi, K.; Suzuki, S. *Chem. Lett.* **1985**, 1695.
- 33) Ikeda, S.; Takagi, T.; Ito, K. *Bull. Chem. Soc. Jap.* **1987**, *60*, 2517.
- 34) Ito, K.; Murata, T.; Ikeda, S. *Bull. Nagoya Inst. Tech.* **1975**, *27*, 209.
- 35) Ito, K.; Ikeda, S.; Iida, T.; Niwa, H. *Denki Kagaku*, **1981**, *49*, 106.
- 36) Teeter, T. E.; van Rysselberghe, P. *Abstracts of Papers, 6th Meet. CITCE*; Butterworths: London, 1955, 538.

- 37) Koudelka, M.; Monnier, A.; Augustinski, J. *J. Electrochem. Soc.* **1984**, *131*, 745.
- 38) Bandi, A. *J. Electrochem. Soc.* **1990**, *137*, 2157.
- 39) Bandi, A.; Kühne, H. -M. *J. Electrochem. Soc.* **1992**, *139*, 1605.
- 40) Taniguchi, I.; Yoneyama, H.; Tamura, H. *Bull. Chem. Soc. Jap.* **1982**, *55*, 2305.
- 41) Nogami, G.; Aikoh, Y.; Shiratsuchi, R. *J. Electrochem. Soc.* **1993**, *140*, 1037.
- 42) Aurian-Blajeni, B.; Taniguchi, I.; Bockris, J. O'M. *J. Electroanal. Chem.* **1983**, *149*, 291.
- 43) Ogura, K.; Migita, C. N.; Nagoka, N. *J. Mol. Catal.* **1989**, *56*, 276.
- 44) Fischer, B.; Eissenberg, R. *J. Am. Chem. Soc.* **1980**, *102*, 7361.
- 45) Beley, M.; Collin, J. -P.; Rupert, R.; Sauvage, J. -P. *J. Chem. Soc., Chem. Comm.* **1984**, *19*, 1315.
- 46) Haynes, L. V.; Sawyer, D. T. *Anal. Chem.* **1967**, *39*, 332.
- 47) Tysee, D. A.; Wagenknecht, J. H.; Baizer, M. M.; Chruma, J. L. *Tetrahedron. Lett.* **1972**, *47*, 4809.
- 48) Gambino, S.; Silvestri, G. *Tetrahedron Lett.* **1973**, *32*, 3025.
- 49) Paik, W.; Anderson, T. N.; Eyring, H. *Electrochim. Acta.* **1969**, *14*, 217.
- 50) Ryu, J.; Anderson, T. N.; Eyring, H. *J. Phys. Chem.* **1972**, *76*, 3278.
- 51) Kapusta, S.; Hackerman, N. *J. Electrochem. Soc.* **1983**, *130*, 607.
- 52) Vassiliev, Yu. B.; Bagotzky, V. S.; Osetrova, N. V.; Khazova, O. A.; Mayorova, N. *A. J. Electroanal. Chem.* **1985**, *189*, 271.
- 53) Aylmer-Kelly, A. W.; Bewick, A.; Cantrill, P. R.; Tuxford, A. M. *Faraday Disc. Chem. Soc.* **1974**, 96.
- 54) Gimenez, I.; Maximovitch, S.; Barbier, M. J. *New J. Chem.* **1987**, *11*, 733.
- 55) Amatore, C.; Nadjó, L.; Savéant, J. -M. *Nouv. J. Chim.* **1984**, *8*, 565.

- 56) Christensen, P. A.; Hamnett, A.; Muir, A. V. G.; Freeman, N. A. *J. Electroanal. Chem.* **1990**, 288, 197.
- 57) Vassiliev, Yu. B.; Bagotzky, V. S.; Khazova, O. A.; Mayorova, N. A. *J. Electroanal. Chem.* **1985**, 189, 295.
- 58) Gressin, J. C.; Michelet, D.; Nadjo, L.; Savéant, J. -M. *Nouv. J. Chim.* **1979**, 3, 545.
- 59) Kudo, A.; Nakagawa, S.; Tsuneto, A.; Sakata, T. *J. Electrochem. Soc.* **1993**, 140, 1541.
- 60) Ito, K.; Ikeda, S.; Okabe, M. *Denki Kagaku*, **1980**, 48, 247.
- 61) Nakagawa, S.; Kudo, A.; Azuma, M.; Sakata, T. *J. Electroanal. Chem.* **1991**, 308, 339.
- 62) Maier, C. U.; Bandi, A. *Abstracts 42nd ISE Meet.*, Montreux. **1991**, Abstr. 7-020.
- 63) Bandi, A.; Maier, C. U.; Bloss, W. H. FRG Patent 4126349, C25B 3/04.
- 64) Abbott, A. P.; Harper, J. C.; *J. Chem. Soc., Faraday Trans.* **1996**, 92, 3895.
- 65) Jessop, P. G.; Ikariya, T. Noyori, R. *Nature*, **1994**, 368, 231.
- 66) Harper, J. C. *Ph. D Thesis*, Leicester University, 1998.
- 67) Kordikowski, A.; Robertson, D. G.; AguiarRicardo, A. I.; Popov, V. K.; Howdle, S. M.; Poliakoff, M. *J. Phys. Chem.* **1996**, 100, 9522.
- 68) Hori, Y.; Murata, A.; Takahashi, R. *J. Chem. Soc. Faraday Trans.* **1989**, 85, 2309.
- 69) Hori, Y.; Murata, A. *Electrochim. Acta.* **1990**, 35, 1777.
- 70) Hori, Y.; Murata, A.; Yoshinami, Y. *J. Chem. Soc. Faraday Trans.* **1991**, 87, 125.
- 71) Taguchi, S.; Aramata, A.; Enyo, M. *J. Electroanal. Chem.* **1994**, 372, 161.

CHAPTER VI

SUMMARY AND FUTURE WORK

6.1 Summary

6.1.1 Solvent Properties

6.1.2 Conductivity, Electrochemistry and Double Layer Structure

6.1.3 Electrochemical Reduction of Carbon Dioxide

6.2 Future Work

6.2.1 Solvation in Supercritical Media

6.2.2 Electrochemistry and Double layer Structure

6.2.3 Bulk Electrolysis of Carbon Dioxide at Supercritical Conditions

6.1 Summary

This study has shown that HFC 134a, HFC 32 and HFC 125 are polar fluids with solvent properties that can be markedly changed by alteration of the temperature and pressure. All three solvents display potential for use in supercritical fluid applications such as extraction and chromatography because of their relatively high dipolarity/polarizability in the supercritical state and accessible critical conditions. The conductivity of a tetraalkylammonium electrolyte in supercritical HFC 32 has been shown to be high because of the relatively high relative permittivity and low viscosity of the medium. The high electrochemical stability of HFC 134a has been illustrated and enabled the investigation of a variety of novel oxidation processes. The first double layer capacitance measurements performed in a polar supercritical fluid have shown the double layer structure to be density dependent. The ability of HFCs to act as polar modifiers in supercritical media has also been demonstrated by the first example of CO₂ electroreduction in an aprotic supercritical mixture.

6.1.1 Solvent Properties

The relative permittivity of HFC 134a, HFC 32 and HFC 125 has been measured as a function of temperature and pressure in both the liquid and supercritical states. The fluid dipole moments have been calculated by the application of a polar liquid molecular theory. The dipolarity/polarizability parameter, π^* , has also been measured in the three HFCs as a function of temperature and pressure. The relatively high dipolarity/polarizability of each HFC in the supercritical state demonstrates that the fluids are particularly suited to extraction and chromatographic processes where the analyte is polar.

Analysis of the π^* data has shown that local density augmentation occurs in all of the HFC fluids studied and that the fluid density around the solute at a fixed T_r varies similarly for a variety of solvents. A hard sphere approximation model has successfully been applied to all of the measured π^* data in both the liquid and supercritical states.

6.1.2 Conductivity, Electrochemistry and Double Layer Structure

It has been demonstrated that both liquid HFC 134a and liquid and supercritical HFC 32 can be made electrically conducting by the addition of a tetrabutylammonium tetrafluoroborate electrolyte. Conductivity measurements have shown that in the liquid and supercritical phases charge is carried by both single ions and triple ions at levels predominantly governed by the bulk relative permittivity of the medium and the concentration of the electrolyte.

The unprecedented electrochemical stability of HFC 134a has been illustrated, and it is often the stability of the supporting electrolyte that determines the width of the potential window. HFC 134a was, therefore, used to study electrochemical processes at large positive overpotentials, such as the first reported case of the electro-oxidation of a rare earth gas uncomplicated by solvent decomposition.

This work has shown that HFC 32 is a convenient solvent for electrochemical investigations in the supercritical phase. The relatively high polarity of this medium in the supercritical state circumvents many of the problems associated with solubility, conductivity and ion adsorption on the electrode surface observed with other supercritical media. Voltammetry demonstrated that the ferrocene couple behaves reversibly in both liquid and supercritical HFC 32 at liquid-like densities. Deviations

from the expected Nernstian behaviour were observed in the supercritical state at pressures close to that of the critical point. These anomalies were attributed to a change in the double layer structure, as confirmed by double layer capacitance measurements. The capacitance of a TBABF₄ electrolyte in supercritical HFC 32 at a platinum electrode was shown to be strongly dependent on fluid density. At high pressures the capacitance-potential plots exhibit a diffuse layer minimum, but as the pressure is lowered towards the critical value the diffuse layer collapses and a pure Helmholtz response is observed.

6.1.3 Electrochemical Reduction of Carbon Dioxide

The electrochemical reduction of CO₂ was performed in CO₂/HFC 134a supercritical mixtures at platinum and lead electrodes. Voltammetry showed that the onset of CO₂ reduction occurred at significantly more positive potentials at a platinum electrode. The process of CO₂ reduction at a platinum electrode was also shown to be diffusion controlled at 60 °C. At both electrodes oxalate and carbon monoxide were the major reaction products. Platinum proved to be the superior electrode surface for oxalate production at supercritical conditions, with the corresponding faradaic yields much higher than previously observed with platinum electrodes in aprotic liquid media.

6.2 Future Work

6.2.1 Solvation in Supercritical Media

If the dipolarity/polarizability parameter, π^* , could be determined for HFC 134a, HFC 32 and HFC 125 using an indicator molecule incapable of forming hydrogen bonds (a and $b = 0$), the hydrogen bonding characteristics of the three liquid and supercritical HFCs could then be determined by comparison with the data presented in this work. This indicator solute would also need to be soluble in the HFCs over a wide solvent density range and display a large susceptibility constant.

The hydrofluorocarbons are also a particularly promising class of solvents for use as polar modifiers in supercritical media. In comparison to pure supercritical media, the field of solvation in binary supercritical mixtures is relatively poorly understood. Solvatochromic shift measurements in supercritical solvent mixtures such as CO₂/HFC 134a could offer an interesting insight into this area on a microscopic level through comparison with similar data recorded in the respective pure fluids.

In its current form the mean sphere approximation utilized in chapter 3 does not take into account the polarizability of the solute molecule. Future modifications to equation 3.2.11 would incorporate the solute polarizability and subsequently account for dispersion and solvent Stark effects.

6.2.2 Electrochemistry and Double layer Structure

The high electrochemical stability of HFC 134a offers exciting possibilities in the field of oxidation electrochemistry. Future experiments may also focus on the characterization of oxidation products at the electrode surface, employing *in situ* techniques such as IR spectroscopy. Investigations of this type would be technically

challenging due to the short lifetime of any species formed at very high overpotentials. The experiments would also have to be performed at high pressure or low temperature to ensure the presence of liquid HFC 134a.

The pressure and temperature dependences of the silver pseudo-reference potential require clarification. Comparison of the shifts in redox potential of two reference couples with temperature and pressure may prove useful in this respect.

Future studies into double layer structure in a supercritical fluid could concentrate on the effects of different electrode materials and electrolytes. A more ambitious project, however, would be to determine the extent of ion adsorption at the electrode-electrolyte interface via the employment of the electrochemical quartz crystal microbalance (EQCM).

6.2.3 Bulk Electrolysis of Carbon Dioxide at Supercritical Conditions

The investigation into the electroreduction of CO₂ reported in the present work has demonstrated that oxalate can be formed at a reasonable yield in supercritical CO₂/HFC 134a mixtures. Future research should focus on the optimization of the experimental conditions to give as high a faradaic yield of oxalate as possible at a reasonable rate. A suitable separator, such as an ion exchange membrane, should also be sought. Reduction of CO₂ on other electrode materials could also be studied. The conductivity results in chapter 4 suggest that a mixture of CO₂ and HFC 32 may provide a more highly conducting supercritical medium than CO₂/HFC 134a when employing a TBABF₄ electrolyte. This mixture also conveniently displays a lower critical temperature.

APPENDIX

Table 1. Relative Permittivity Values for HFC 134a at 303 K

p/MPa	$\rho/\text{kg m}^{-3}$	ϵ
3.0	1202	9.21
6.0	1218	9.39
9.0	1233	9.58
14.0	1254	9.78
20.0	1276	9.94
24.0	1289	10.11
28.1	1301	10.23
32.7	1315	10.47

Table 2. Relative Permittivity Values for HFC 134a at 313 K

p/MPa	$\rho/\text{kg m}^{-3}$	ϵ
2.0	1155	8.36
4.0	1169	8.52
6.0	1182	8.69
8.0	1194	8.87
12.0	1215	9.06
16.0	1233	9.25
34.1	1295	9.84

Table 3. Relative Permittivity Values for HFC 134a at 323 K

p/MPa	$\rho/\text{kg m}^{-3}$	ϵ
2.0	1110	7.73
4.0	1128	7.94
6.0	1144	8.07
8.0	1158	8.18
12.0	1182	8.45
16.0	1203	8.68
20.0	1221	8.81
24.1	1237	8.99
28.9	1254	9.23

Table 4. Relative Permittivity Values for HFC 134a at 333 K

p/MPa	$\rho/\text{kg m}^{-3}$	ϵ
2.0	1058	7.15
4.0	1082	7.32
6.0	1103	7.48
8.1	1120	7.67
12.0	1148	7.88
16.0	1172	8.06
19.8	1192	8.26
24.0	1210	8.46
26.0	1218	8.58
30.0	1233	8.79

Table 5. Relative Permittivity Values for HFC 134a at 343 K

p/MPa	$\rho/\text{kg m}^{-3}$	ϵ
4.0	1030	6.84
6.0	1057	7.02
8.0	1079	7.20
12.0	1113	7.43
15.9	1140	7.64
20.0	1162	7.85
24.0	1182	7.97
26.0	1190	8.02
27.2	1195	8.18
27.9	1199	8.13

Table 6. Relative Permittivity Values for HFC 134a at 353 K

p/MPa	$\rho/\text{kg m}^{-3}$	ϵ
4.0	967	6.19
6.0	1005	6.41
8.0	1033	6.59
11.9	1075	6.86
15.8	1107	7.12
18.0	1120	7.30
19.9	1132	7.41
22.0	1144	7.48
25.9	1164	7.67
28.2	1173	7.76

Table 7. Relative Permittivity Values for HFC 134a at 363 K

p/MPa	$\rho/\text{kg m}^{-3}$	ϵ
6.0	945	5.93
10.0	1012	6.34
14.0	1055	6.63
18.0	1087	6.87
22.0	1114	7.16
27.2	1142	7.38

Table 8. Relative Permittivity Values for HFC 134a at 373 K

p/MPa	$\rho/\text{kg m}^{-3}$	ϵ
4.9	822	5.25
5.9	869	5.41
8.0	926	5.71
10.0	963	5.91
11.9	992	6.09
15.8	1036	6.34
18.0	1054	6.53
22.0	1069	6.77
26.0	1108	6.99

Table 9. Relative Permittivity Values for HFC 134a at 383 K

p/MPa	$\rho/\text{kg m}^{-3}$	ϵ
3.0	137	1.14
3.4	168	1.48
5.0	608	4.55
6.0	765	4.78
7.0	822	5.05
8.0	859	5.23
10.0	910	5.46
11.9	946	5.66
13.9	975	5.84
15.8	998	6.02
20.0	1037	6.29
24.0	1067	6.47
26.0	1080	6.57

Table 10. Relative Permittivity Values for HFC 134a at 393 K

p/MPa	$\rho/\text{kg m}^{-3}$	ϵ
3.5	159	1.26
4.1	210	1.78
4.5	255	2.59
5.0	335	3.67
5.5	463	3.98
6.0	591	4.18
7.0	717	4.52
8.0	779	4.75
10.0	851	5.02
11.9	897	5.24
13.9	932	5.38
15.7	959	5.55
20.0	1003	5.90
24.0	1037	6.11
26.1	1052	6.26

Table 11. Relative Permittivity Values for HFC 134a at 403 K

p/MPa	$\rho/\text{kg m}^{-3}$	ϵ
3.4	141	1.09
5.0	270	2.32
7.0	583	3.84
8.0	682	4.19
9.0	743	4.35
10.0	785	4.60
11.9	844	4.81
12.9	867	4.93
13.9	886	5.06
15.6	919	5.24
18.0	946	5.42
22.0	989	5.68
26.1	1022	5.94

Table 12. Relative Permittivity Values for HFC 32 at 303 K

p/MPa	$\rho/\text{kg m}^{-3}$	ϵ
4.0	955	12.51
5.9	967	12.79
8.0	978	12.97
12.0	997	13.35
16.0	1014	13.67
20.0	1029	13.92
24.0	1042	14.20
26.0	1048	14.29
26.9	1050	14.40

Table 13. Relative Permittivity Values for HFC 32 at 363 K

p/MPa	$\rho/\text{kg m}^{-3}$	ϵ
4.9	132	1.54
5.5	164	2.02
6.0	200	3.09
7.0	347	5.78
8.1	564	6.71
9.0	632	7.10
10.0	674	7.39
12.0	725	7.80
16.0	786	8.46
20.1	826	8.99
24.0	857	9.36
26.1	870	9.59
28.1	882	9.72

Table 14. Relative Permittivity Values for HFC 125 at 303 K

p/MPa	$\rho/\text{kg m}^{-3}$	ϵ
4.0	1197	4.48
5.9	1221	4.58
7.9	1241	4.66
10.0	1259	4.73
14.0	1288	4.90
18.0	1313	5.01
22.0	1334	5.13
25.8	1353	5.24

Table 15. Relative Permittivity Values for HFC 125 at 353 K

p/MPa	$\rho/\text{kg m}^{-3}$	ϵ
6.0	828	2.97
8.0	941	3.22
10.2	1000	3.44
12.0	1042	3.54
16.0	1102	3.73
20.0	1145	3.86
24.0	1180	4.03
26.0	1195	4.11
28.0	1209	4.17